IGNEOUS AND METAMORPHIC PETROLOGY OF LAVAS AND DYKES OF THE MACQUARIE ISLAND OPHIOLITE COMPLEX.

by

Brendon John Griffin

Submitted in fulfilment of the requirements
for the degree of Doctor of Philosophy.

University of Tasmania

HOBART

1982
(conferred March '83)

This thesis contains no material which has been accepted for the award of any other degree or diploma in any university, and to the best of my knowledge and belief, contains no copy or paraphrase of material previously published or written by another person, except where due reference is made in the text of this thesis.

B. J. Griffin

University of Tasmania,
May, 1982.

CONTENTS

Contents cont.

Contents cont.

Contents cont.

Contents cont.

List of Figures

Contents cont.

Contents cont.

Contents cont.

List of Tables

Contents cont.

Contents cont. page

List of Plates

Contents cont.

ABSTRACT

Macquarie Island is an emergent part of the Macquarie Ridge, which runs south from New Zealand to join the Indian-Pacific ridge system, and marks the boundary between the Indian-Australian and the Pacific plates.

Most of Macquarie Island is composed of fault-bounded blocks of volcanic rocks that are commonly basaltic pillow lavas with rarer massive flows and minor sediments. The sediments range from *Globigerina* oozes and red siltstones through coarser lithic wackes to agglomerates. Dolerite dyke swarms, gabbroic masses including a layered complex, and serpentinized peridotites also occur in the northern part of the island, where an oceanic lithosphere section has been recognized.

The basalts and dolerites are usually porphyritic, carrying plagioclase (An_{87}-An_{80}) as the dominant phenocryst phase with less abundant olivine (Fo_{89}-Fo_{85}), chrome spinel and rarely clinopyroxene ($Ca_{45}Mg_{50}Fe_5$-$Ca_{38}Mg_{50}Fe_{12}$). Normatively the rocks range from ne- to Q-bearing, with most falling near the critical plane of normative silica undersaturation. Dykes tend to be more iron-rich than lavas, and include the more di-poor rocks. The rocks also range in composition from typical ocean-floor basalts through varieties relatively enriched in some incompatible trace elements, particularly Nb (20-73 ppm) and the light rare earth elements, that otherwise retain ocean-floor basalt phenocryst assemblages, major element compositions and Ti, Ni, Cr and Zr contents. These latter varieties closely resemble the ocean-floor basalts from the "abnormal" ridge segments near 45°N and 36°N (FAMOUS) on the Mid-Atlantic Ridge.

Mixing calculations using phenocryst and rock compositions suggest that much of the compositional variation in the volcanics could have arisen by low-pressure crystal fractionation. However, low-pressure fractionation processes cannot alone account for all of the variations in concentration in the incompatible elements: some may also arise from different degrees of partial melting of a possibly inhomogeneous source.

Four grades of alteration and metamorphism have been distinguished in the lavas and dykes. The lowest grade of alteration produced smectite-carbonate dominated assemblages, principally affecting olivine and glass. Lavas that have suffered this ocean-floor weathering alteration have been shown to retain the magnetic properties of typical oceanic crust, and were probably at the top of the pile, in the uppermost 200 m. Underlying these is a complex zone of zeolite alteration defined by the development of Ca and Na zeolites, principally natrolite, thomsonite, analcite, wairakite and at the bottom of the zone, laumontite. The degree of alteration is variable: fresh glass has been found within a few metres of intensely zeolitized lavas. Beneath these zeolite facies assemblages are albite-chlorite-epidote-sphene assemblages of the lower greenschist facies, present at the base of the lava pile where up to half of the outcrop is composed of basaltic dykes. In contrast, the dykes of the dyke swarms have suffered a distinctive actinolite amphibole alteration and replacement of the primary mafic minerals that has left the plagioclase little altered. This "uralitization" reflects the attainment of conditions of the upper greenschist facies grade of metamorphism, and sporadically at the base of the dyke swarm unit, where veins of hornblende are present, the lower amphibolite facies grade of metamorphism.

It is argued that the observed progression of secondary assemblages arose from hydrothermal alteration under varying temperature and pressure conditions, which affected the oceanic crust section to the base of the dyke swarm unit. Field relationships suggest that on Macquarie Island

this corresponds to a depth of approximately three kilometres. Preliminary oxygen and carbon isotope studies show that sea water was the initial fluid and that the fluid became substantially modified with depth through rock interaction. Fluid movement was concentrated along fracture systems in the lavas.

The major effects of geochemical alteration of the massive rocks, away from the fracture zones, are increases in the H_2O^+ content and Fe^{3+}/Fe^{2+} ratio. The magnitude of the changes is dependent on stratigraphic position: both decrease with depth. Gypsum deposits, containing minor amounts of sulphides, are present in the top of the dyke swarm unit. Pyrite-dominated sulphide-quartz-carbonate assemblages are present in veins in the base of the lava pile and upper part of the dyke swarm unit. A large stockwork deposit, with the same mineralogy, is also present in the base of the lava section. It is suggested that the gypsum-rich deposits reflect temperature-induced sulphate saturation of the descending fluid whereas the sulphide-bearing vein assemblages have been precipitated from cooling upwelling fluids.

Chapter 1

INTRODUCTION

1.1 INTRODUCTION

The Macquarie Ridge is a narrow arcuate system of submarine ridges that runs south from New Zealand to join the Indian-Pacific ridge system, and marks the boundary between the Indian-Australian and the Pacific plates. The crest of the Macquarie Ridge is at water depths of less than 200 m in several places, and near 54°S 159°E has emerged to form Macquarie Island (Cullen, 1969; Hayes & Talwani, 1972).

Linear east-west trending marine magnetic anomalies south of Australia have been traced across the ridge to the Macquarie Trough east of Macquarie Island. Geophysical data show that the island represents oceanic crust produced during Tertiary sea-floor spreading at the Indian-Pacific ridge system, which was later uplifted during marginal interactions between the Indian-Australian plate moving north and the Pacific plate moving west (Williamson, 1974, 1979). Magnetic properties of pillow lavas from the island correspond well with those of ocean floor basalts (Butler *et al.*, 1976) and the island is recognized to have the highest potential of known ophiolites for modelling the magnetic layer of the oceanic lithosphere (Levi *et al.*, 1978).

Macquarie Island therefore provides the opportunity to examine oceanic crust, using the same methodology and at the same scale as land-based studies of ophiolite complexes. The island is the connecting link between the ophiolites of continental environments, and the *in situ* oceanic crust studied by dredge, drill and submersible.

Previous geological studies (Mawson, 1943; Varne & Rubenach, 1972, 1973) indicate, within the pillow lava layer, a range from unmetamorphosed, but oxidized assemblages, through zeolite facies grade assemblages, to lower greenschist facies assemblages in samples possibly from deep in the

oceanic pillow lava layer. The dolerite dyke swarms have been metamorphosed under conditions of upper greenschist and varying grades of amphibolite facies metamorphism. Dykes intruding the pillow lava layer are noted to contain metamorphic assemblages similar to the enclosing lavas. The plutonic rocks present have been variably serpentinized, prehnitized and partially or completely metamorphosed. Similar grades and variations in metamorphism have been reported from modern ocean-floor rocks (Cann, 1971) and ophiolites found in continents (Smewing, 1975; Coleman, 1977; Coish, 1977).

This thesis presents an investigation of the style and nature of the ocean floor metamorphism in the pillow lava and dyke swarm units of the oceanic lithosphere exposed on Macquarie Island. A summary of background studies, logistics and instrument development associated with this project is given in the following chapter. The field relationships and macroscopic features of the lavas and dykes are described in Chapter 3. The primary phase mineralogy and petrological nature of the lavas and dykes are presented in Chapter 4 as a background to the integrated petrographic, electron micro-analytic and isotopic study of the metamorphism of these rocks, given in Chapter 5. Effects of the alteration and metamorphism on the primary geochemistry of selected lavas and dykes are discussed in Chapter 6. The geochemical characterization of oceanic crust, based on the Macquarie Island data, is also considered in Chapter 6; together with a preliminary discussion of the petrogenesis of the samples. The major conclusions of this thesis are summarized and recommendations for further study are made in Chapter 7.

1.2 ACKNOWLEDGEMENTS

I must first thank my supervisor, Dr R. Varne, for his assistance in all aspects of this study and with other problems that inevitably appear during Ph.D. studies. Professor D.H. Green is also gratefully acknowledged for his help and support.

Many people helped with this project through their willingness to listen and advise and I would particularly like to thank Dr R. Berry, Dr C.F. Burrett, Dr A. Bush, Dr C.J. Eastoe, Dr D.J. Ellis, R.J. Ford, Dr J. Foden, S. Harley, G.A. Jenner, Dr M. Solomon, Dr J.C. van Moort, and Dr J.L. Walshe.

Technical problems I encountered were greatly eased by help from W. Doran, R. Lincolme, Dr A. McKee, Dr C. Nuckolds and N.G. Ware. Ms J. Pongratz is thanked for typing and supervising the publication of this thesis.

The project was funded by research grants from the University of Tasmania and the Australian Research Grants Committee. The Macquarie Island Advisory Committee, the National Parks and Wildlife Service of Tasmania and the Antarctic Division of the Australian Department of Science and the Environment generously provided transport to and logistic support on Macquarie Island. I was supported in part by research scholarships from the Department of Education of the Commonwealth of Australia and the Esso Oil Company Pty Ltd, to whom I am grateful.

Chapter 2

LOGISTICS AND TECHNICAL DEVELOPMENTS

2.1 LOCATION AND TECTONIC SETTING OF MACQUARIE ISLAND

Sub-Antarctic Macquarie Island (54°30'S; 159°E) lies in the South Pacific Ocean, 1280 km southeast of Hobart, Tasmania, and 1440 km north of the Antarctic continent (Figure 2.1). It is a subaerial exposure of the Macquarie Ridge. The island is about 37 km long by 4.8 km wide and consists of a hilly plateau at about 300 m altitude; the highest point is 433 m.

The Macquarie Ridge is a narrow, arcuate ridge that runs south from New Zealand to join the Indian-Pacific ridge system. It has a rugged and complicated topography and in some places has a double crest separated by a deep and narrow depression (Summerhayes, 1974). The ridge is locally topped by a flat platform about 160 m below sea level to mark where it may have been exposed in the Pliocene. A subsidiary ridge occurs east of the main ridge in the Macquarie Island region, separted from it by a narrow but deep trench, the Macquarie Trench. This trench contains undeformed sediments (Hayes & Talwani, 1972).

The ridge is seismically active, and is generally considered to mark the boundary between the Indian-Australian and the Pacific plates. Earthquakes are shallow, and first motion analyses imply that the ridge is associated with normal, thrust and strike-slip faulting. Plate tectonic analyses suggest that the predominant motion along the ridge is right-lateral strike-slip (Hayes & Talwani, 1972). Nevertheless, different parts of the ridge are probably also governed by extensional and compressional regimes as a consequence of the closeness of the ridge to the Pacific-Indian pole of relative motion. Marginal interactions between the plates associated with rapid, recent motions of this pole (Le Pichon *et al.*, 1973; Griffiths & Varne, 1972) have probably contributed to the

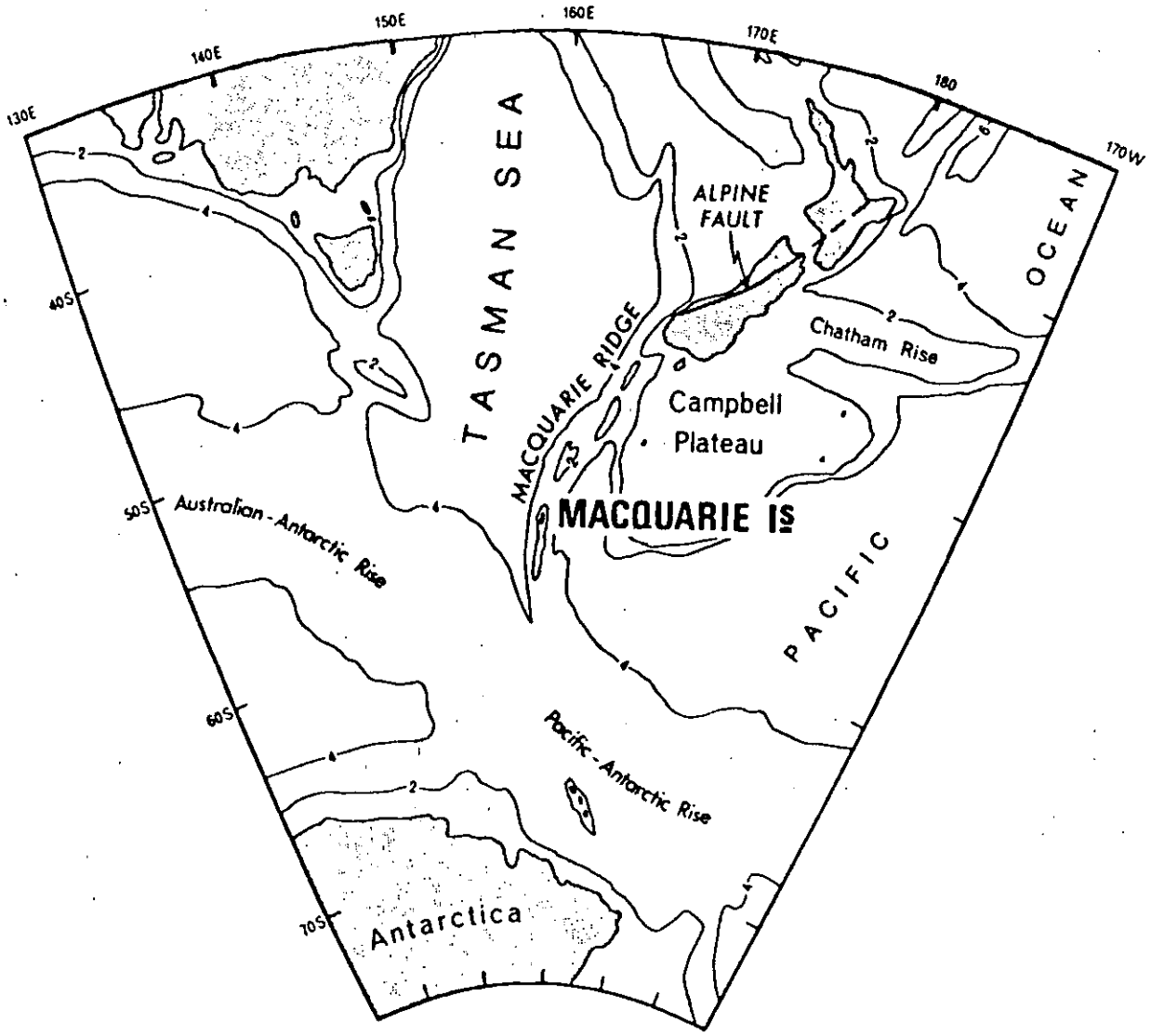

Figure 2.1 Locality map. Isobaths at 2, 4, and 6 km.

complex structural development of the ridge, and incidentally to the exposure of part of it to form Macquarie Island.

Locally, radiometric ^{14}C ages of *Aptenodytes patagonica* (Miller) in uplifted terraces suggest the actual emergence of Macquarie Island in the early Pleistocene, with an average uplift age of the island between 1.5 m and 4.5 m per 1000 years (Colhoun & Goede, 1973).

2.2 ACCESS AND FIELD CONDITIONS

Macquarie Island is a Tasmanian State Reserve and is also classified as an Antarctic base. Its status as a reserve requires that permission to work on and sample the island be obtained from the National Parks and Wildlife Service of Tasmania. Its classification as an Antarctic base means that access is generally limited to personnel of expeditions of the Antarctic Division of the Australian Department of Science and the Environment. Access is normally only possible by sea and the three field trips I made during this study involved 4-6 day voyages (each way) on the M.V. *Nella Dan*, or M.V. *Thala Dan*. The field trips were for the four-month 1975/76 summer season, and two five-day visits during the 1876 and 1979 Spring Relief expeditions. These enabled the completion of mapping and sampling projects initiated by earlier workers (Varne *et al.*, 1969; Varne & Rubenach, 1972, 1973).

The outcrop on Macquarie Island varies. It is generally good along the coast although the rapid emergence of the island has left some large fossil beach deposits where the recognition of *in situ* material can be difficult. On the plateau there is less outcrop and weathering has affected the rocks, the metamorphosed material being particularly susceptible.

Temperatures normally range, at sea level, from 0° to 5°C and with average wind speeds of 28 knots and continuous heavy mist, working conditions are difficult. All movement on the island, except in the

immediate vicinity of the base camp, is on foot. Small field huts are spaced at approximately four-hour walking intervals down the east coast of the island, with only one hut on the west coast at Bauer Bay.

2.3 ELECTRON MICROPROBE DEVELOPMENT AND CALIBRATION

An integral part of this research project was the development of software and hardware necessary for calibration and routine operation of an energy dispersive micro-analytical system for accurate quantitative analyses of geological materials. The system is an EDAX EDS system attached to a JEOL JXA-50A scanning electron microprobe in the Central Science Laboratory, University of Tasmania. The software and operating procedures developed for this system are described in detail by Griffin (1979), Appendix 8 of this thesis.

The initial development of this system by myself required one year, and thus comprises a significant proportion of the study. This was essential to the project as the fine-grained nature of both primary and secondary features of the samples excluded normal identification techniques. Subsequent calibration and updating of correction routines were performed independently of this study, as a consultant. The system currently provides up to 20 analyses per hour of normal silicate and oxide minerals.

Chapter 3

GEOLOGY OF MACQUARIE ISLAND

3.1 INTRODUCTION

The general geology of Macquarie Island has been described by Mawson (1943) and Varne & Rubenach (1972). The results of fieldwork associated with this thesis generally corroborated the work by Varne *et al.* (1969) and Varne & Rubenach (1972), in particular supporting their recognition of the "Older Basic Group" (Mawson, 1943) as dyke swarm units, and therefore this chapter is only a short summary of these earlier studies, mainly drawn from Griffin & Varne (1980) (Appendix 7). However it has proved possible to distinguish stratigraphic relationships between different volcanic blocks, and this aspect of the fieldwork is described in Chapter 5. These field relationships form the basis for the recognition of several partial sections through the volcanic sequence, that eluded the previous workers, based on the spatial distribution of the various secondary assemblages and new structural information.

3.2 GENERAL GEOLOGY

Fault-bounded blocks of volcanics and dyke swarms compose about 80% of the outcrop of Macquarie Island (Figure 3.1). An intrusive complex of dyke swarms, massive and layered gabbros, and serpentinized peridotites located at the northern end of the island (Figure 3.2) constitute the remainder.

The volcanic blocks are mainly pillow lavas, together with varying proportions of rare massive lava flows, basaltic dykes and various sediments. These sediments include calcareous *Globigerina* ooze and volcaniclastic sediments. The ooze forms thin coatings on lava surfaces

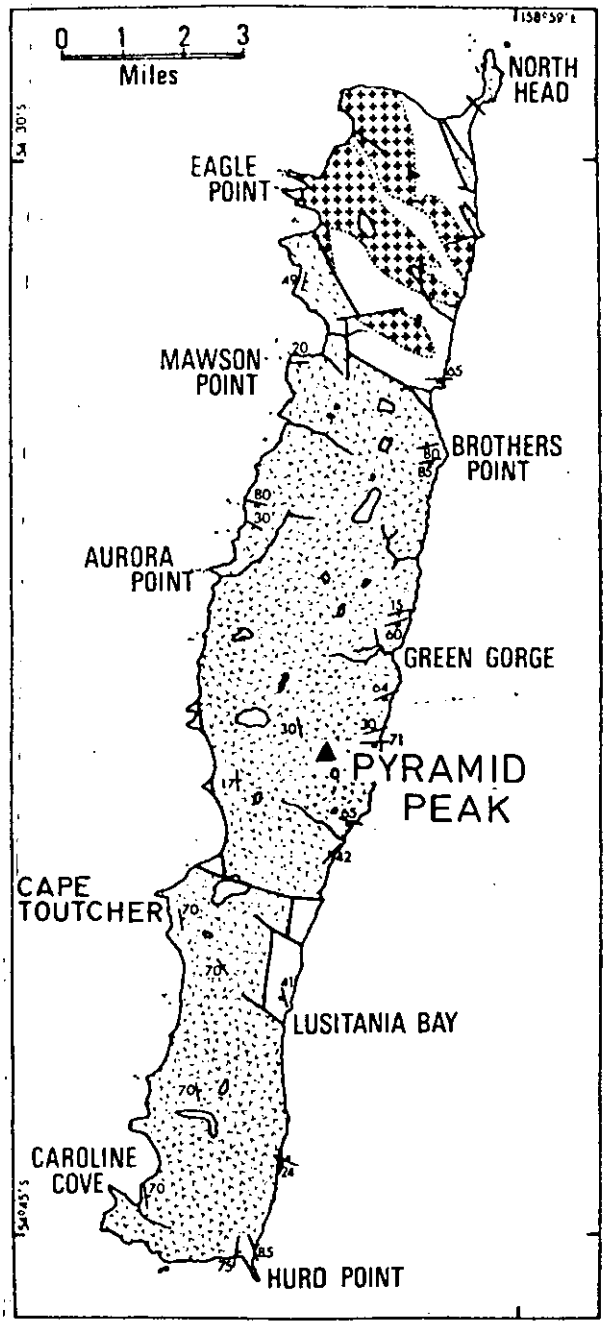

Figure 3.1 Generalized geologic map of Macquarie Island with superficial deposits omitted. Serpentinized peridotite and gabbro masses are marked by crosses; extrusive volcanic rocks and associated sediments are marked by vees; dyke swarms are blank. Strikes on lavas are shown with a single tick, and strikes on dykes are shown with a double tick. Faulted contacts are drawn as heavy lines, and gradational or uncertain contacts are drawn as dotted lines. (From Varne & Rubenach, 1972.)

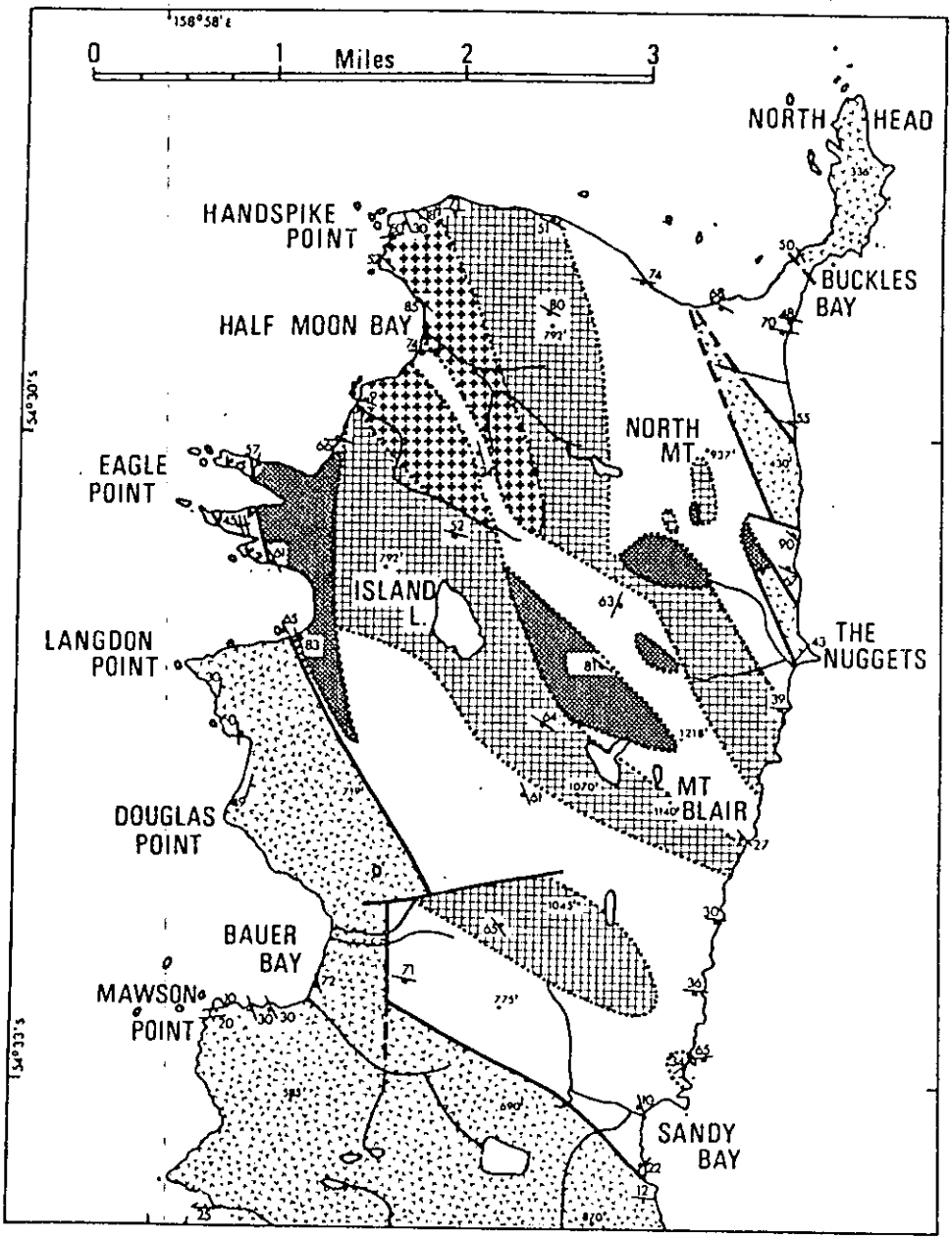

Figure 3.2 Geological map of the northern part of Macquarie Island, with superficial deposits omitted (from Varne & Rubenach, 1972). Serpentinized peridotite bodies are marked by heavy diagonal cross-hatching; layered gabbro complex is marked by crosses; other gabbro masses are marked by light cross-hatching; extrusive volcanic rocks and associated sediments are marked by vees; dyke swarms are blank. Strikes on lavas are shown with a single tick, and strikes on dykes are shown with a double tick. Faulted contacts are drawn as heavy lines, and gradational or uncertain contacts are drawn as dotted lines. Spot heights in feet above sea level.

and irregular, thin, lensoid accumulations interstitial to the pillow lavas, up to 8 cm in thickness. It is usually recrystallized and/or silicified. Poorly preserved coccoliths in this ooze have been interpreted to yield an Early, or perhaps Middle, Miocene age (Quilty *et al.*, 1973).

The volcaniclastic sediments range from siltstones to volcanic breccias. All are reddish-brown, due to a high proportion of iron oxides in the matrix cement. The finer-grained sediments occur in small lenses, up to 2 m thick, intercalated with the lava flows. Their lateral extent is difficult to estimate. One lens is exposed for about 60 m at Mawson Point, on the northwestern coast of Macquarie Island (Figure 3.1). These lenses commonly contain graded beds, from siltstone to lithicwackes, and rarely include truncated, convoluted laminae. The volcanic breccia deposits are lenses ranging from 2-3 m up to 15 m in thickness, again well exposed at Mawson Point. These are unstratified rocks with angular clasts varying up to 15 cm (in maximum section) from a silt-sized matrix and with a highly variable degree of packing. Hyaloclastite breccias occur interstitially to lava pillows and as small lenses.

Varne *et al.* (1969) have noted that the association of pillow lava with interstitial *Globigerina* ooze, hyaloclastite and lithiwacke is characteristic of ocean-floor deposition and probably occurred at water depths between 2000 m and 4000 m. The range of sediment types, including small turbidite flows, reflects a variety of depositonal environments, from low to high energy. The volcanic breccias closely resemble talus-slope and rubble deposits observed at various places on the Mid-Atlantic Ridge.

The dolerite dyke swarms are a notable geological feature, and occur as fault-bounded blocks almost entirely composed of series of narrow dykes lying parallel to sub-parallel to one another to form a

sheeted dyke complex. Screens of massive gabbros, serpentinized peridotites and volcanics are present. Although multiple intrusions, evidenced by series of similarly facing chilled edges, make estimates of thickness difficult, the average dyke thickness is about 1 m, with rare examples ranging to 3 metres.

Rocks of the layered gabbro complex around Half-Moon Bay (Figure 3.2) include wehrlite, plagioclase wehrlite, troctolite, olivine gabbor and gabbro. The rocks are mineralogically simple. They mainly consist of olivine, plagioclase and clinopyroxene. Spinel is a rare but widespread accessory mineral, and orthopyroxene occurs very rarely as thin rims around olivine or as tiny relict grains within clinopyroxene. Cumulate phenocryst phases are olivine, plagioclase and spinel. Clinopyroxene is always postcumulus; plagioclase is also postcumulus in some olivine-rich rocks.

The massive gabbros exposed on the east coast, and to the northeast of the layered gabbro complex (Figure 3.2) possess complicated intrusive contacts, contain inclusions of other gabbros, are in places deformed, and are also cut by dykes. Their bulk chemical compositions are similar to those of some of the lavas and dykes (Griffin & Varne, 1980) and they range in texture from gabbroic to doleritic. A zone of massive gabbros that have undergone high-temperature sub-solidus recrystallization occurs around Island Lake and north of Eagle Point (Figure 3.2). This zone separates the wehrlites of the layered gabbro complex from a harzburgite at Eagle Point, and the gabbros are essentially composed of clinopyroxene and plagioclase, with lesser amounts of olivine, and minor amounts of orthopyroxene, hornblende and spinel.

3.3 STRUCTURAL GEOLOGY

The complex structure of Macquarie Island is a result of the widespread faulting, probably on all scales, and tilting of the fault-bounded blocks. Dips measured on sediments range from near-horizontal to 45° and for pillowed lava units to 80° (Figure 3.3). These latter measurements are less reliable but are supported by good agreement where outcrops allow measurements from both lavas and sediments (Table 3.1). Two strike directions are common, about 150° and 230°. It has been argued that the tilting of the volcanic rocks occurred in two stages: the first stage involved tilting around axes that were near-horizontal and parallel to dyke-bedding plane intersections and therefore only caused variations in dip; the second was a later rotation about vertical axes of the tilted rocks that caused the variations in strike (Varne & Rubenach, 1972). This interpretation is supported by palaeomagnetic studies (Williamson, 1979).

Angular relationships between lavas and dykes measured at 14 localities range from 46° to 86° (Table 3.2). The mean angle is 72° and at 11 of the 14 localities the angle is greater than 60°, supporting a model where the lavas have been intruded by near-vertical or vertical dykes. The deviations of the angular relationships from 90° may in part result from non-horizontal attitudes of the lavas at the time of intrusion. The dykes seem to have been intruded originally striking east-southeast. This orientation corresponds very well with the inferred orientation of the spreading axis of the Indian-Pacific ridge during Anomaly 7 time, as preserved by the present orientation of the linear marine magnetic anomalies in the region (Weissel & Hayes, 1972; Williamson, 1974).

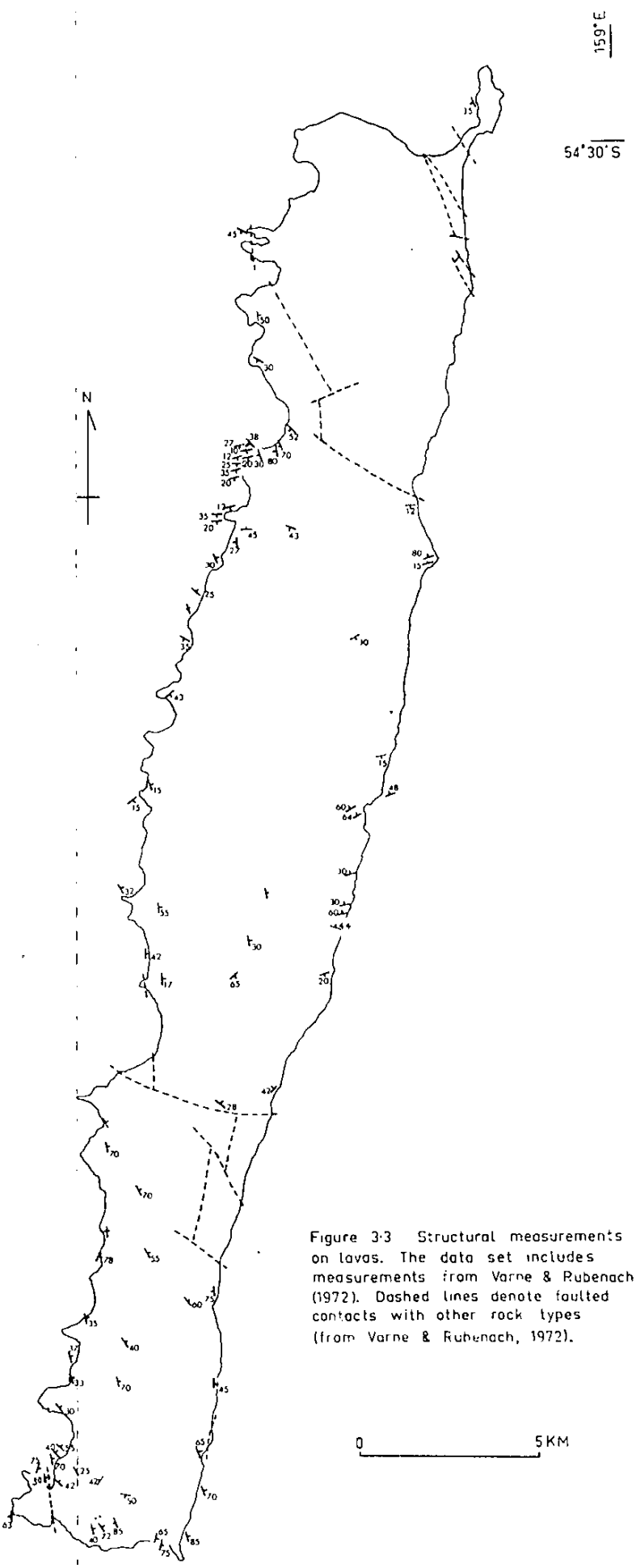

Figure 3·3 Structural measurements on lavas. The data set includes measurements from Varne & Rubenach (1972). Dashed lines denote faulted contacts with other rock types (from Varne & Rubenach, 1972).

Table 3.1

STRUCTURAL MEASUREMENTS FROM PILLOW LAVAS AND SEDIMENTS AT THE SAME LOCALITY

Locality	Lava	Sediment
11/12	219.48	209.60
57	050.25	050.30
59/60	064.25	071.25
213/214	297.40	321.35

*Measurements given using a clockwise convention, e.g.

$\overset{\uparrow}{\vdash}$ 090.45 = $\overset{\vdash}{45}$ and 270.45 = $\underset{\vdash}{45}$

Table 3.2

ANGULAR RELATIONSHIPS BETWEEN LAVAS AND INTRUDING DYKES

Locality	Angle (°)*
12	58
19	86
45	75
52	49
64	85
114	65
128	78
204	76
208	86
220	86
231	46
Bishop Is.	82
414	64
426	72

Average = 72°

Range = 86°-46°

* True angles were obtained by standard stereographic projection techniques.

Rotations of the crustal blocks of the island therefore apparently occurred first about horizontal axes parallel to the spreading axis, probably as an integral part of the spreading process (Ballard & Van Andel, 1977). Later rotations about vertical axes could have been caused by recent strike-slip movements along the Macquarie Ridge.

3.4 AGE

Coccoliths present in the *Globigerina* oozes, interstitial to the pillow lavas, indicate an age of Early, or perhaps Middle, Miocene (Quilty *et al.*, 1973). This is a range of about 11-22 Ma in absolute terms. The correlation of marine magnetic Anomaly 7 across Macquarie Island (Williamson, 1974) suggests an age of about 27 Ma using the Heirtzler *et al.* (1968) magnetostratigraphic time scale, or 25.5 Ma using the more recent time scale of La Brecque *et al.* (1977). Thus the general age appears well constrained, but a specific age determination awaits completion of a geochronological study currently in progress.

Chapter 4

PETROGRAPHY AND PRIMARY PHASE MINERALOGY

4.1 GENERAL PETROGRAPHY OF THE LAVAS AND DYKES

The lavas range from glassy to medium grained crystalline lavas, and from aphyric to strongly porphyritic varieties. Plagioclase is the most abundant phenocryst phase followed by olivine, spinel and rarely clinopyroxene. Dykes intruding the lavas show similar petrographic variations but are coarser grained.

Dyke swarm rocks range from fine to coarse grained, again with both aphyric and strongly porphyritic variants. Plagioclase is more abundant in these rocks than it is in the lavas and associated dykes, as has been noted by Varne & Rubenach (1972).

All of the samples examined have been altered or metamorphosed to some extent but the primary igneous textures have not been significantly disrupted. This is a general feature of the alteration of mafic rocks from ophiolites (Coleman, 1977) and from the ocean floor (Cann, 1971). The mineralogical changes imposed on these rocks during the various metamorphic events are discussed in detail in Chapter 5.

Cameron *et al.* (1979) have recognized three types of basalts from Macquarie Island in the Australian National University collection. *Type-1* basalts are plagioclase-phyric (An_{92-70}) with sub-variolitic textures and contain euhedral olivine phenocrysts (Fo_{90-88}) and, rarely, clinopyroxene. The plagioclase phenocrysts contain glassy inclusions and sometimes tiny euhedral spinels and are not strongly zoned. *Type-2* basalts contain microphenocrysts of altered olivine, elongate laths of plagioclase feldspar and dark areas of mesostasis which are largely clinopyroxene. Reddish chrome spinel is present as tiny euhedra

in altered olivine or as megacrysts up to 0.6 mm. *Type-3* basalts contain primary kaersutite as discrete groundmass crystals or as rims on colourless augite and microphenocrysts of plagioclase, clinopyroxene and chrome spinel.

Type-1 basalts dominate the A.N.U. collection and, with *type-2* basalts, are noted to be texturally and mineralogically similar to basalts generated at mid-ocean ridges or in marginal basins. The amphibole-bearing *type-3* basalt is suggested to have no ocean-floor equivalent and possibly to represent the type of vulcanism that eventually forms seamounts (Cameron *et al.*, 1980) although this seems unlikely from the field relationships.

The study reported here is the first made on a comprehensive collection from Macquarie Island and involved the petrographic examination of 198 lava samples and 41 dyke samples. Three major petrographic variations are present in the sample; in the degree of crystallinity, porphyritic nature and, in the coarser variants, groundmass mineralogy.

The majority of the samples is porphyritic, and relative proportions and assemblages of phenocrysts are given in Table 4.1, based on the initial sample set (129 lava samples: Appendix 9). The major feature shown by Table 4.1 (1) is the predominance of plagioclase amongst the phenocryst phases. It is present in 91% of the phyric lavas, followed by olivine (47%), clinopyroxene (27.5%) and spinel (26.5%). The various phenocryst assemblages present are listed in Table 4.1 (2), together with their relative frequencies of occurrence.

The lavas vary in degree of crystallinity from glassy pillow-selvedge material and spalled glass fragments in interstitial hyaloclastite breccias (e.g., as commonly exposed in the North Head and Pyramid Peak areas) to medium grained holocrystalline rocks in the central zones of the occasional massive lava flows, as exposed at

Table 4.1

PHENOCRYST ASSEMBLAGES AND ABUNDANCES IN LAVAS

(129 samples)

	No.	%
Aphyric samples	27	20.9
Porphyritic samples	102	79.1
PORPHYRITIC SAMPLES		
1. Individual phase occurrences		
plagioclase is contained by	93*	91.2
cpx "	28*	27.5
olivine "	48*	47.1
spinel "	27*	26.5
2. Phenocryst assemblage occurrences		
plag	37	36.3
ol	3	2.9
sp	1	1.0
plag + cpx	10	9.8
plag + ol	13	12.7
plag + sp	5	4.9
cpx + sp	1	1.0
ol + sp	4	3.9
plag + ol + cpx	12	11.8
plag + ol + sp	11	10.8
plag + ol + cpx + sp	5	4.9
	102	

* Many samples contain >1 phenocryst phase and these values include the occurrence of a phase together with other phases.

Mawson Point. A complete variation exists between these two extremes. Many of the glasses contain quenched crystallites, commonly of olivine. These crystallites may contain two-phase inclusions of glass and vapour (Plate 4.1). More slowly-cooled samples contain granular plumes of clinopyroxene with the development of sub-variolitic textures (Plate 4.2).

The groundmass mineralogy of the holocrystalline lavas and dykes exhibits a wide variation. At one extreme the lavas have subophitic to ophitic textures (Plate 4.6) with equant subhedral plagioclase partially or completely enclosed by granular to subhedral augite together with titanomagnetite and glass. In coarser grained examples the augitic clinopyroxenes may have thin purplish titanaugite rims and in rare late-stage segregation veins kaersutitic amphibole, together with apatite rods and skeletal ilmenite, may also be present as a late growth on the clinopyroxene, but not as discrete grains. Olivine is not present as a groundmass phase. Such rocks are not true tholeiites in that they lack pigeonite or orthopyroxene as a groundmass phase (Joplin, 1971). As Carmichael *et al.*(1974) have remarked, ocean-floor basalts have alkaline basalt mineralogy but tholeiitic chemistry. However, as noted by Cameron *et al.* (1980), petrographically these rocks are identical to modern ocean-floor basalts or "abyssal tholeiites" (Cann, 1971). In the following text these variants are consequently referred to as the tholeiitic variants.

At the other extreme the lavas are characterised by purplish titanaugites generally developed as sheaves of tabular, elongate crystals oriented perpendicular to randomly-oriented, elongate laths of plagioclase, forming an intersertal texture (Plate 4.3). The pyroxenes are uniform in colour, and this distinguishable from the late stage overgrowths found in the tholeiitic variants. Euhedral to subhedral

Plate 4.1 Quenched olivine crystallite in glass containing symmetric glass and glass + vapour inclusions (sample 46). Scale: 1 cm = 10 microns.

Plate 4.2 Subvariolitic texture in chilled lava pillow rim (sample 156E). Scale: 1 cm = 10 microns.

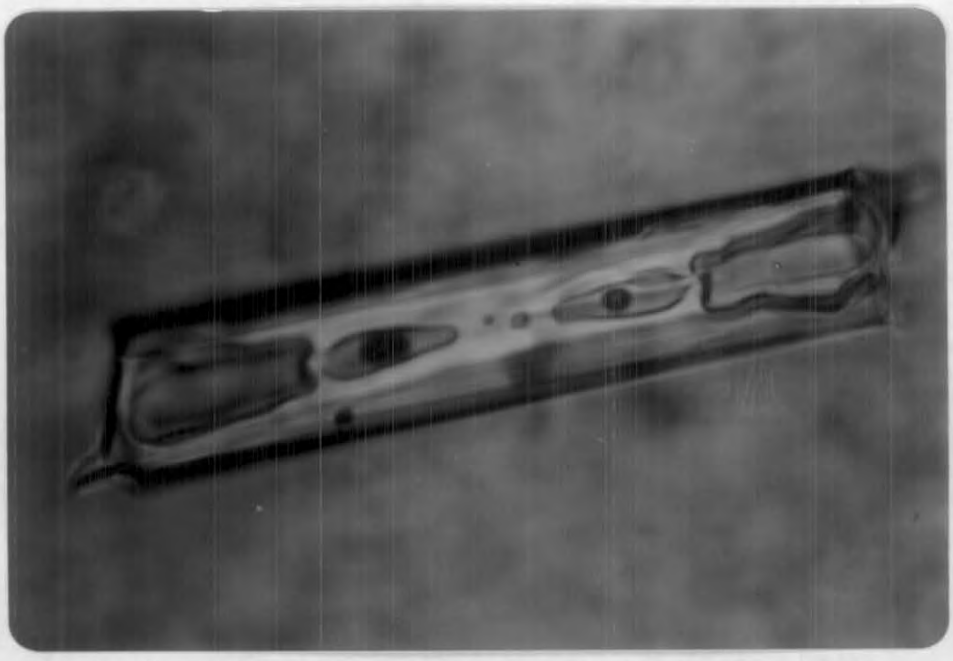

Plate 4.3 Intersertal texture in alkaline basalt (sample 38391). Scale: 1 cm = 800 microns

Plate 4.4 Reddish-brown kaersutitic amphibole as discrete crystals and rims on zoned titaniferous augites in an alkali olivine basalt (sample 3A). Scale: 1 cm = 1000 microns.

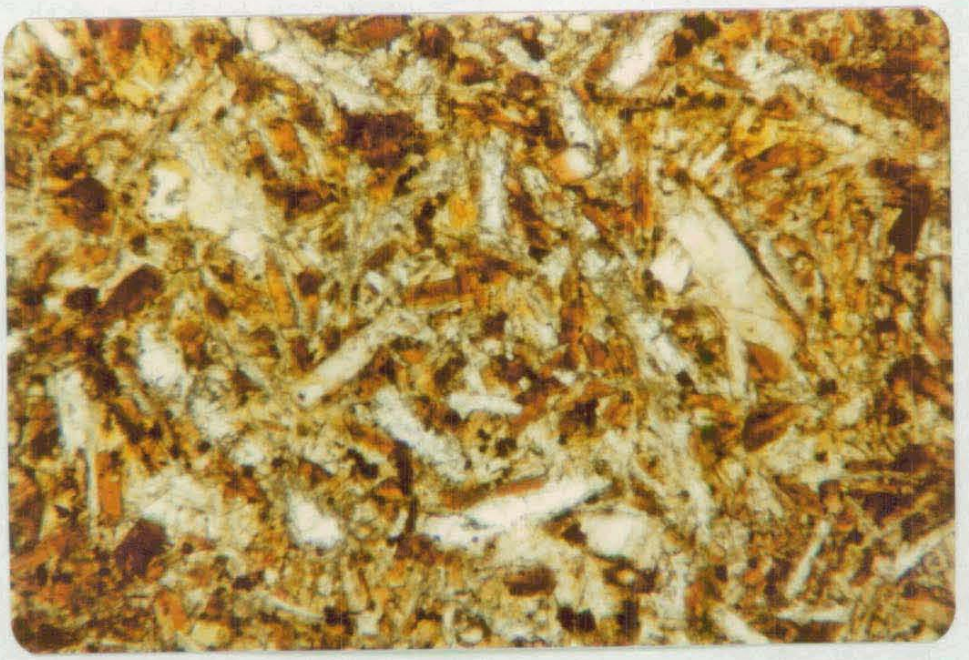

olivine is common as a groundmass phase but is usually replaced by smectites or chlorites, depending upon the grade of metamorphism. It is largely unaltered in samples 38265 and 38392. Kaersutitic amphibole is present in most samples as rims on the titanaugite, and as discrete groundmass crystals in the most extreme variants (e.g. samples 3A and 64D, Plate 4.4). Titanmagnetite is a minor component of the groundmass as skeletal and bladed forms. Interstitial glass is rare. A notable feature of these samples is the presence of spherical aggregates of amphibole and minor titanmagnetite where exsolved hydrous phases appear to have concentrated in the late stages of cooling; a vapour phase being absent (Plate 4.5). These aggregates grade from the spherules to thin rims around vesicles where a vapour phase was present. Petrographically many of these rocks are classifiable as alkali olivine basalts and are subsequently referred to as the alkaline variants.

The alkaline and tholeiitic variants described previously are the end members of a petrographic and chemical (Chapter 6) *spectrum* of lavas and dolerites present on Macquarie Island. The differentiation of the lavas into three types by Cameron *et al.* (1980) is not supported by the observations made in this study.

A major question that arises from the recognition of this petrographic variation of the lavas and dykes is whether or not a systematic distribution of any particular lava (or lavas) exists on the island. This problem is made more difficult by two features. Firstly, the quenched nature of many samples prevented any diagnostic groundmass mineral growth, and secondly, the distinction between olivine as a groundmass or microphenocryst phase is often difficult and subjective. For these reasons, a third group termed intermediate rocks has been recognised in the samples.

Plate 4.5 Sections through spheroidal hydrous segregation zones in an alkaline lava. The largest zone is 0.25 mm in diameter (sample 211).

Plate 4.6 Subophitic texture in a medium grained tholeiitic basalt (sample 56H) from a massive flow.
Scale: 1 cm = 0.1 mm.

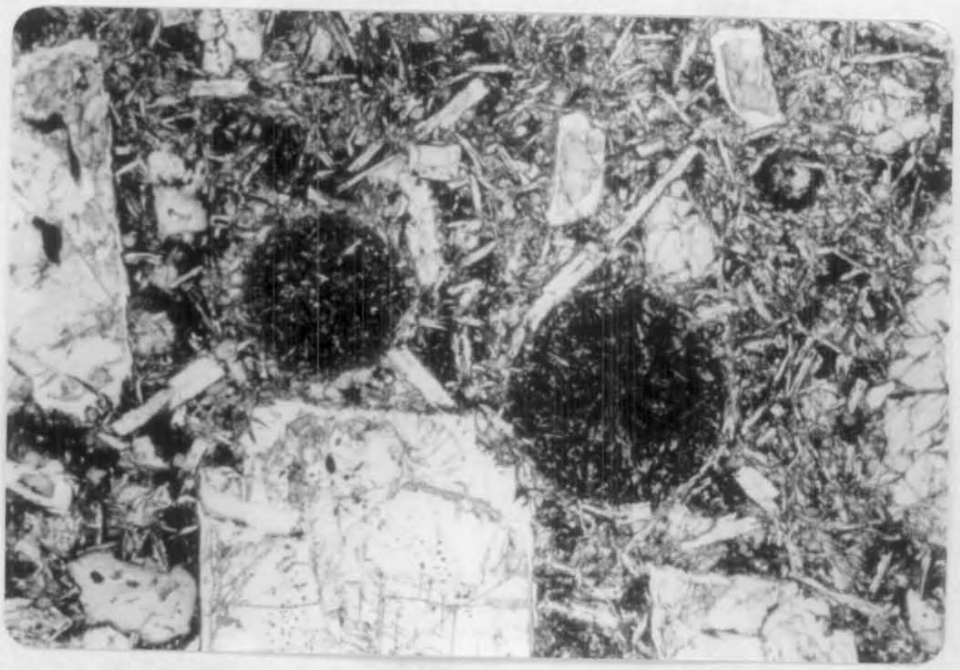

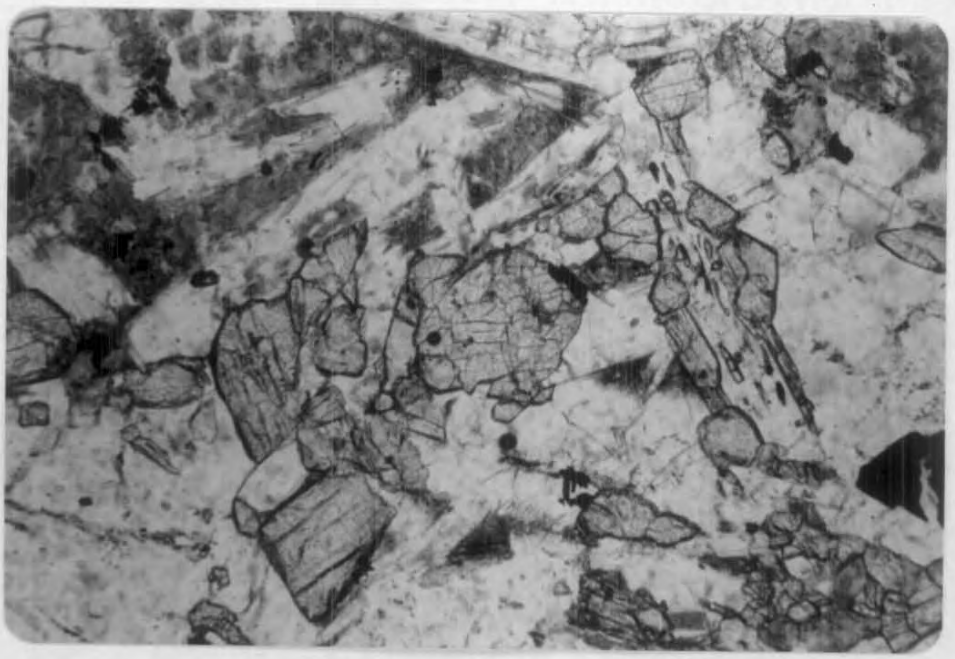

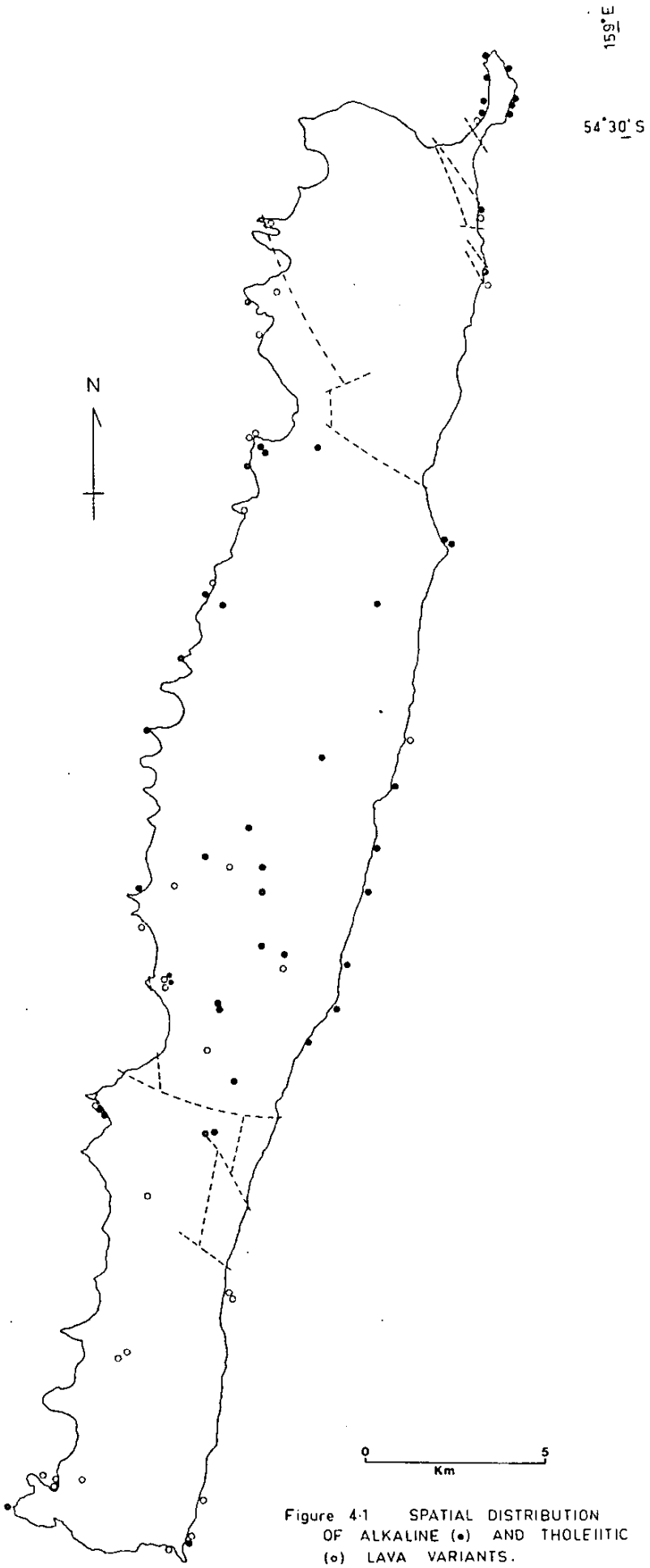

Figure 4·1 SPATIAL DISTRIBUTION OF ALKALINE (•) AND THOLEIITIC (o) LAVA VARIANTS.

The spatial distribution of alkaline and tholeiitic samples is shown in Figure 4.1. The alkaline rocks are relatively more abundant in the North Head volcanic block and in the middle section of the island, but are present in all the volcanic sequences. Metamorphic studies give a zonation which can be correlated with this distribution (Chapter 5; Figure 5.14). The alkaline varieties are most abundant where the lower grades of alteration (zeolite facies grade metamorphism and below) are also observed. If the metamorphic zonation of ocean-floor weathering - zeolite facies - lower greenschist facies is related to depth in the volcanic sequence, as is argued in detail in Chapter 5, then the observed distribution of the various lavas suggests that the magmas became more alkaline with development of the Macquarie Island ocean crust segment. This question is considered in more detail using the geochemistry of the lavas and the possible petrogenetic models in Chapter 6.

4.2 PHENOCRYST DISTRIBUTION AND MINERAL CHEMISTRY

Data on the relative abundances of phenocryst species have been subdivided on the basis of the groundmass mineralogy of the lavas and are presented in Table 4.2. The alkaline lavas have a higher proportion of aphyric samples (43.5%) than the tholeiitic lavas (9.1%). Plagioclase is the most frequent phenocryst phase in both variants although more frequent in the tholeiitic samples. Olivine and spinel occur more often in the alkaline lavas than in the tholeiitic lavas; the reverse is observed for clinopyroxenes. These variations in phenocryst distribution do not correspond with any differentiation between the variants recognized from the groundmass mineralogical studies.

Table 4.2

PHENOCRYST ASSEMBLAGES AND ABUNDANCES

IN ALKALINE AND THOLEIITIC LAVAS

(123 samples)

	Alkalic		Abyssal tholeiitic	
	No.	%	No.	%
Aphyric samples	20	43.5	7	9.1
Porphyritic samples	26	56.5	70	90.9
	46		77	
1. Porphyritic samples				
plagioclase	19	73.1	68	97.1
olivine	15	57.7	32	45.7
cpx	3	11.5	23	32.9
spinel	8	30.8	18	25.7
2. Phenocryst assemblages				
plag	9	34.6	23	32.9
ol	2	7.7	1	1.4
sp	-	-	1	1.4
plag + cpx	-	-	10	14.3
plag + ol	4	15.4	9	12.9
plag + sp	1	3.8	4	5.7
cpx + sp	1	3.8	-	-
ol + sp	4	15.4	-	-
plag + ol + cpx	3	11.5	9	12.9
plag + ol + sp	2	7.7	9	12.9
plag + ol + cpx + sp	-	-	4	5.7
	26		70	

The chemical composition of the primary phases, as determined by electron microanalysis, is discussed in the following sections (Sections 4.2.1 to 4.2.4). Data on both phenocryst and groundmass phases are presented.

4.2.1 Plagioclase feldspar

Plagioclase feldspar is the most abundant phenocryst phase, both in its frequency of occurrence and in its amount within the samples. It ranges in abundance up to a maximum of 50 vol.% (sample 112) and makes up 25-30 vol.% of many rocks. The size of the phenocrysts varies widely from 2-3 mm up to a maximum of 30 mm (sample 159). Most phenocrysts are in the range 2 to 6 mm (Figure 4.2). Size distribution within particular samples is variable: some possess a complete range from the groundmass crystals to the largest phenocryst, whereas others contain uniformly sized phenocrysts. Phenocrysts larger than 15 mm are only present in the alkaline lavas (Figure 4.2).

The plagioclase is present as tabular, euhedral to subhedral crystals. Glomerocrysts are not uncommon, and many crystals are apparently fragments of larger phenocrysts. Zoning is a general feature, often truncated in fractured crystals. Rims are emphasized by the almost ubiquitous corrosion of the more calcic cores of the phenocrysts (Plate 4.7). This corrosion is variable; in extreme cases only skeletal remains of the original crystal have survived. Corrosion is initiated along cleavage planes in the crystals and produces aligned, tabular glassy inclusions within the cores of the slightly reacted phenocrysts (Plate 4.7). In the more extreme cases the inclusions are indistinguishable from the groundmass of the sample. Small spinel phenocrysts (to 0.2 mm) are also present as inclusions.

Plagioclase phenocrysts and groundmass crystals in 20 samples have been thoroughly analysed using electron microprobe techniques. These samples include both alkaline and tholeiitic variants as well as

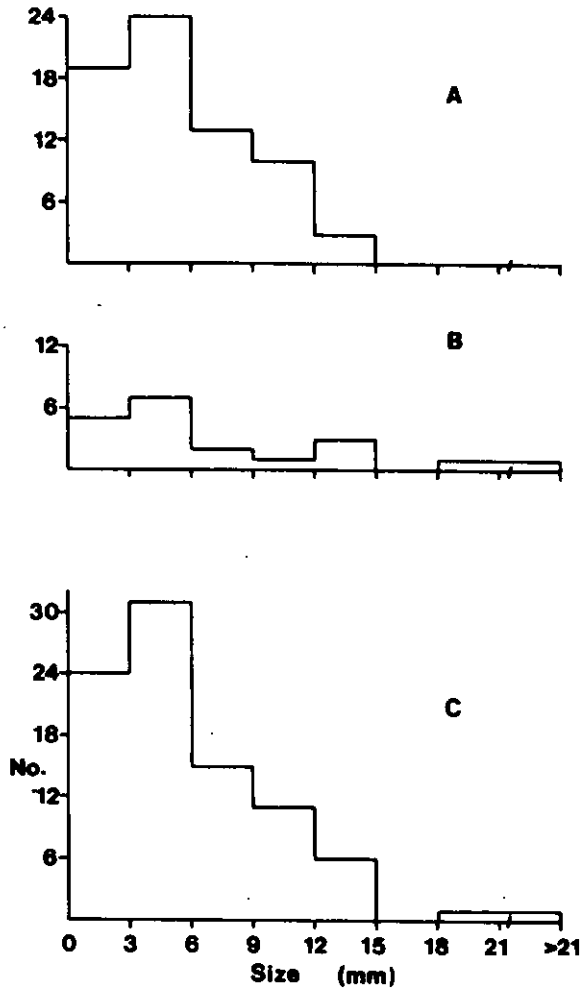

Figure 4.2 Size distribution of plagioclase phenocrysts between tholeiitic (A) and alkaline (B) lava variants and for the lavas as a group (C). Size values represent the largest phenocryst observed in each section.

Plate 4.7 Plagioclase phenocrysts with corroded calcic core (sample 3A). The replacement material is turbid glass The crystal is 0.6 mm long.

Plate 4.8 Rounded and embayed augite phenocryst (sample 43B). The phenocryst is 0.85 mm long.

fresh glasses, and covered the size range of the phenocrysts. Core compositions from within one sample (211, Figure 4.3) cover the entire compositional range (An_{87-72}) that is found in both tholeiitic and alkaline lavas (Figure 4.4). Mid-crystal and rim analyses of phenocrysts span the range of microphenocryst and groundmass plagioclase compositions and range down to An_{43}; but generally fall in the range An_{50-70}. Representative analyses are given in Table 4.3 and the full data set is included in Appendix 3.

4.2.2 Clinopyroxene

Clinopyroxene phenocrysts are relatively rare and form about 1-2% by volume of most pyroxene-phyric lavas, although rare it ranges up to 5% by volume (samples 38439 and 38392). The largest phenocrysts are up to 6 mm in maximum section (211), but generally are in the 1-3 mm size range. Their principal feature is an ubiquitous rounded and embayed form (Plate 4.8). Zoning is common and in most cases is conformable with the present rounded forms. Simple twinning is present in some crystals.

All pyroxene phenocrysts are augitic in composition. Core analyses have a restricted range of major element chemistry (Figure 4.5; Table 4.4A) They are magnesium-rich, reaching Mg/Mg+Fe values of 0.91 and the range in Ca, Mg and Fe is $Ca_{45}Mg_{50}Fe_5$ to $Ca_{38}Mg_{48}Fe_{14}$. Minor elements show considerable variations within and between samples. The clinopyroxenes with Mg/Mg+Fe ~ 0.88 have a variable chromium content, ranging to 1.8 wt.% Cr_2O_3 (Table 4.4; Figure 4.6). Within individual samples the chromium content decreases with decreasing Mg/Mg+Fe, whereas TiO_2 increases (Figure 4.6). In all cases the Cr_2O_3 content is positively correlated with the Al_2O_3 content (Figure 4.7).

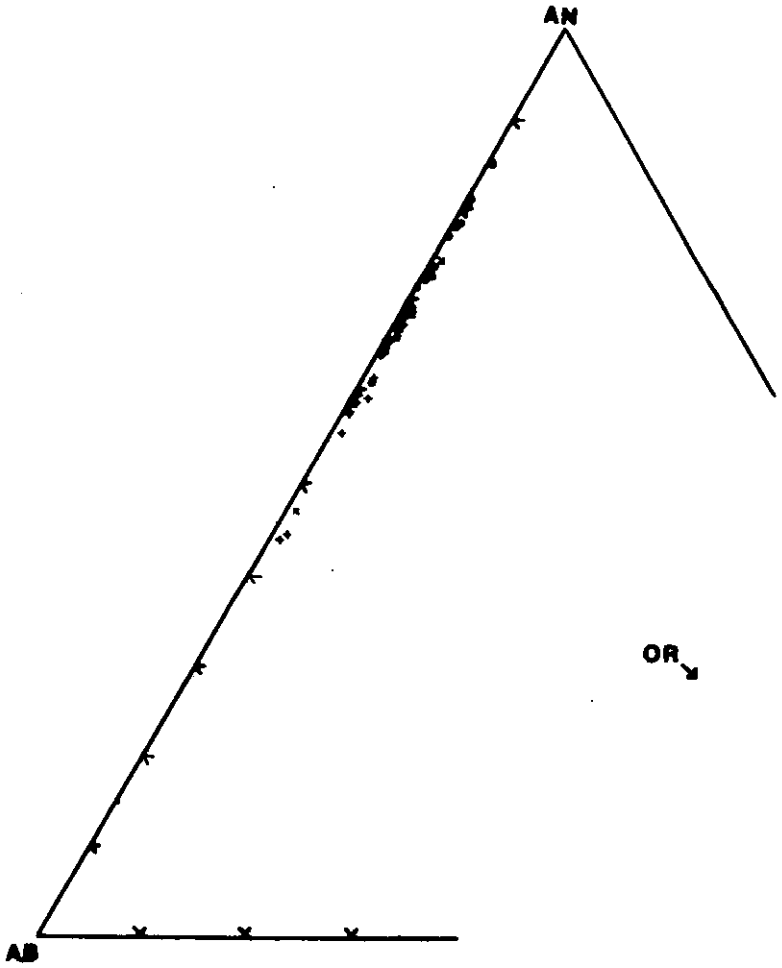

Figure 4.3 Plagioclase compositions in sample 211. Key: Phenocryst cores (o), phenocryst rims (●), microphenocrysts (x), groundmass crystals (+).

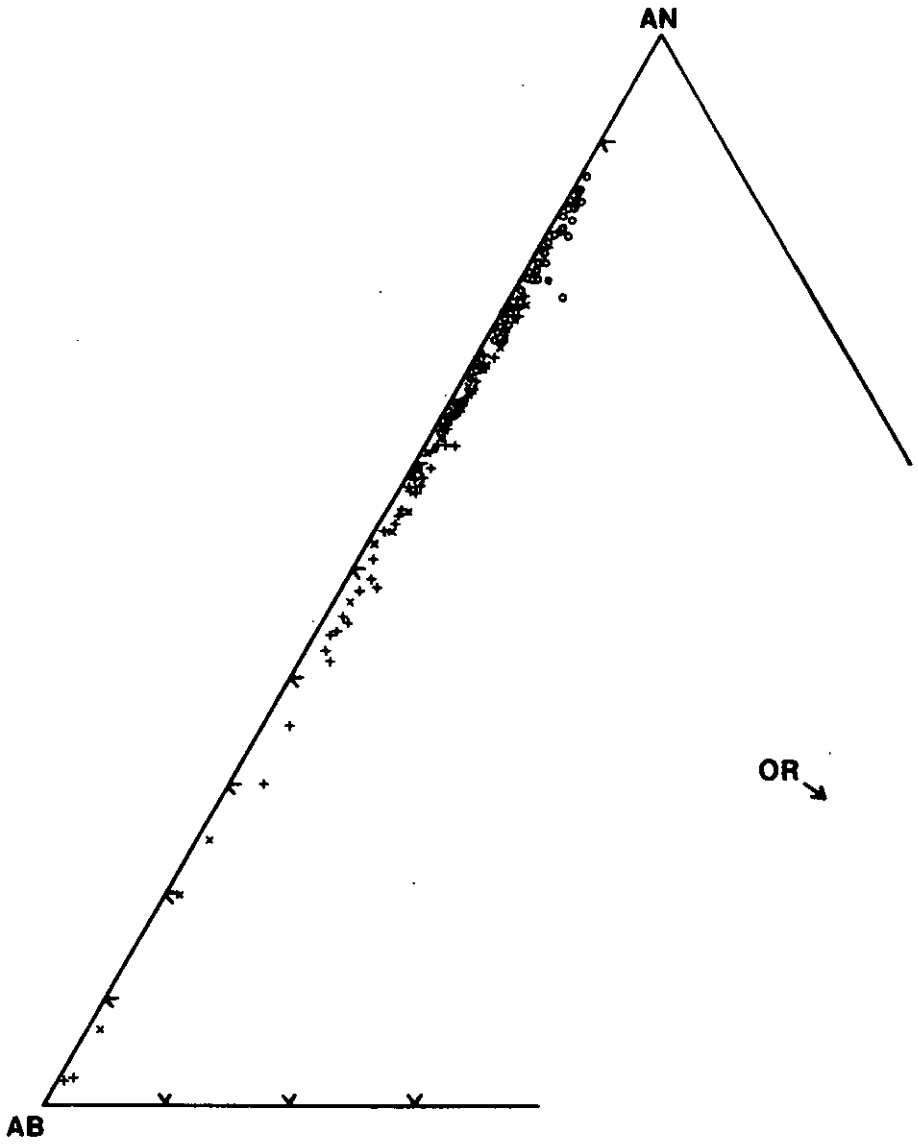

Figure 4.4 Plagioclase compositions in the lavas and dykes. The sodic analyses ($\leq An_{10}$) are of secondary feldspars. Key for symbols is as for Figure 4.3.

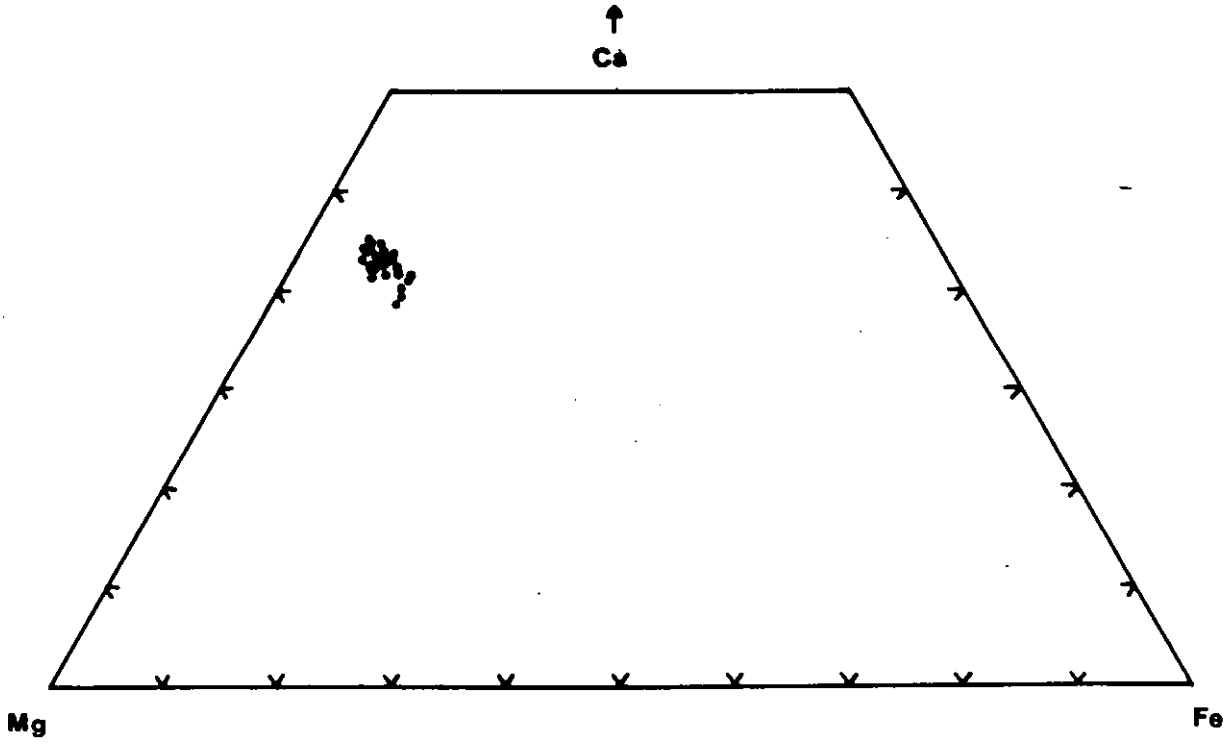

Figure 4.5 Microprobe analyses of cores of clinopyroxene phenocrysts plotted in the system $CaSiO_3$-$MgSiO_3$-$FeSiO_3$.

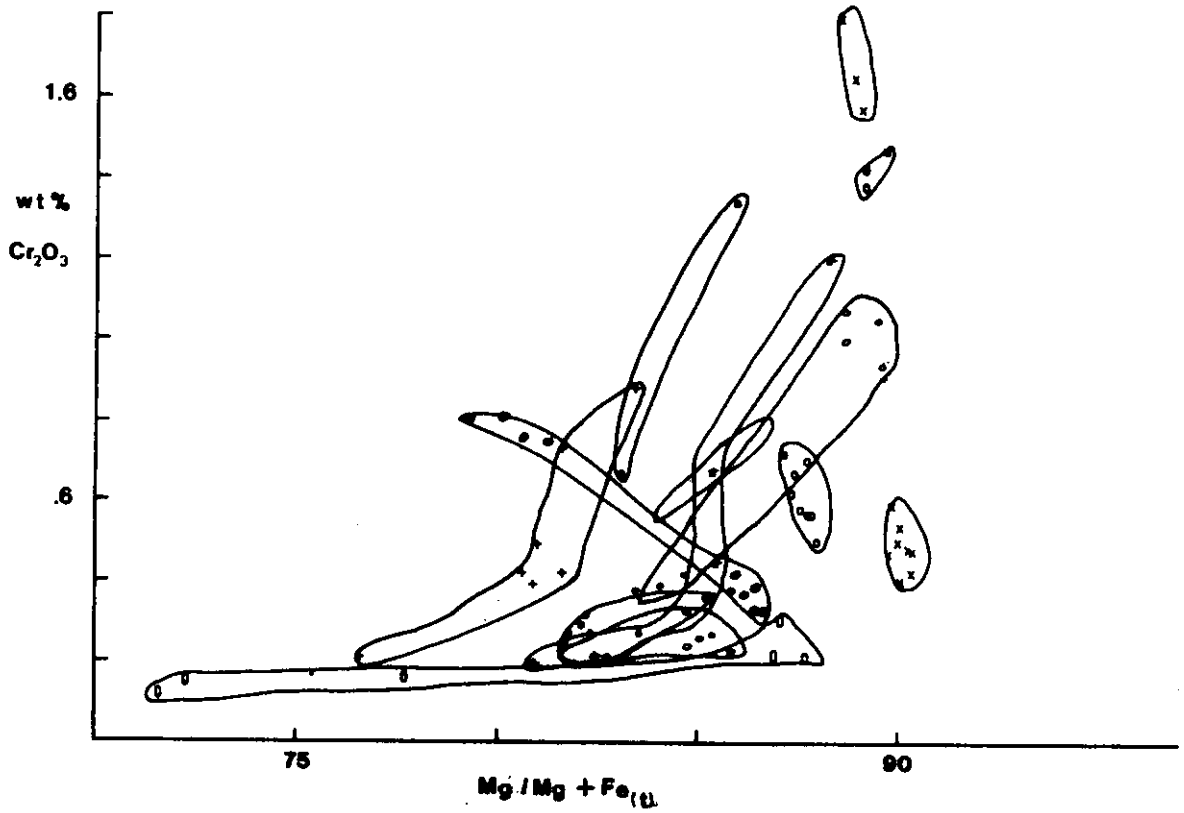

Figure 4.6 Cr_2O_3-Mg/Mg+Fe variations in clinopyroxene phenocrysts. Each surrounded set of data points is from clinopyroxenes in a single lava.

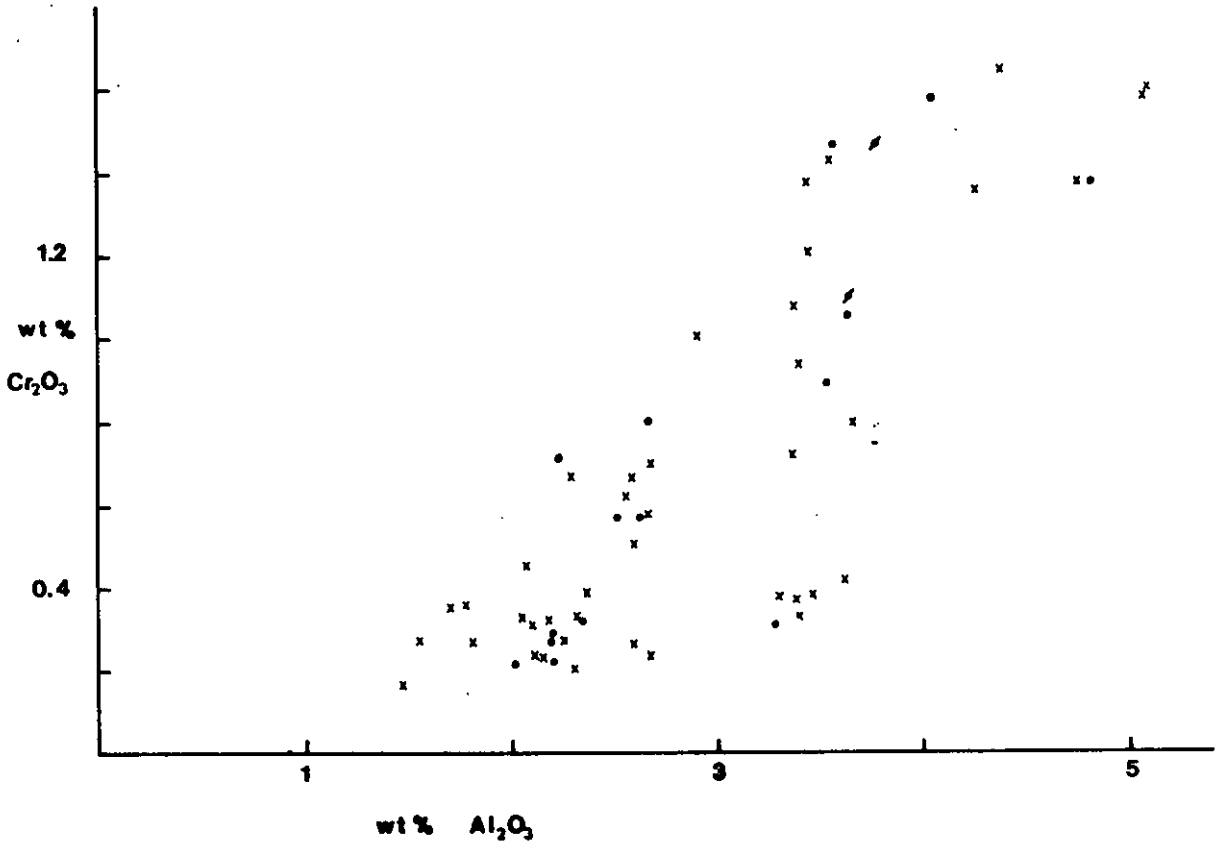

Figure 4.7 Covariation of Cr_2O_3 and Al_2O_3 in clinopyroxene phenocrysts from alkaline (•) and tholeiitic (x) lavas.

Table 4.3

REPRESENTATIVE MICROPROBE ANALYSES OF PLAGIOCLASE PHENOCRYSTS AND GROUNDMASS CRYSTALS.

Sample No.	211	211	204	204	159	235	64	64	211	204
Analysis No.	B-2-C1	B-2-R1	B-2	B-1	A-4	E-D-2	C-1	C-R-2	B-G-2	A-G-4
Key	C	R	C	R	C	C	C	R	G	G
SiO_2	46.15	52.08	45.95	48.42	46.09	46.79	46.35	48.89	51.43	53.34
Al_2O_3	34.49	30.15	34.78	32.88	34.58	34.12	34.32	32.42	30.32	28.83
FeO	-	0.57	0.20	0.27	0.17	0.16	0.16	0.28	0.49	0.93
CaO	17.68	13.18	17.58	15.50	17.57	17.08	17.41	15.44	13.53	12.08
Na_2O	1.58	3.90	1.42	2.82	1.48	1.78	1.68	2.78	4.04	4.71
K_2O	0.08	0.13	0.07	0.11	0.09	0.07	0.08	0.20	0.19	0.11
Total*	100.60	100.84	99.54	100.16	99.20	100.06	101.44	101.65	100.28	99.03
Structure on 32 oxygens										
Si	8.496	9.472	8.460	8.873	8.486	8.600	8.531	8.954	9.384	9.696
Al	7.486	6.464	7.554	7.103	7.506	7.392	7.447	7.000	6.520	6.180
Fe	-	0.088	0.032	0.041	0.026	0.024	0.025	0.043	0.076	0.140
Ca	3.488	2.568	3.468	3.043	3.466	3.364	3.434	3.030	2.644	2.352
Na	0.565	1.376	0.508	1.003	0.529	0.636	0.600	0.989	1.428	1.660
K	0.019	0.028	0.016	0.026	0.021	0.016	0.019	0.047	0.044	0.024
Total	20.053	19.996	20.028	20.090	20.036	20.032	20.055	20.063	20.096	20.052
An	85.7	64.7	86.9	74.7	86.3	83.8	84.7	74.5	64.2	58.3

Key - C = phenocryst core; R = phenocryst rim; G = groundmass; total* = true analysis total, oxides are normalized to 100 wt.%

Table 4.4A

REPRESENTATIVE MICROPROBE ANALYSES OF PYROXENE PHENOCRYSTS

Sample No.	157	144	211	423	425	7	55	55	55	55
Analysis No.	C-2	C-2	A-C-4	C-C-1	H-P-2	E-4	A-A-2	A-A-3	A-R-2	A-R-4
Key	C	C	C	C	C	C	C	C	R	R
SiO_2	51.62	54.07	53.01	52.71	52.24	52.13	53.39	53.44	49.59	51.50
TiO_2	0.33	-	0.27	0.40	0.33	0.45	0.26	0.18	1.30	0.84
Al_2O_3	4.82	2.02	2.63	2.68	3.65	3.85	2.32	2.35	4.52	3.09
Cr_2O_3	1.38	0.21	0.57	0.80	1.05	1.58	0.33	0.32	0.81	0.75
FeO	3.75	4.56	4.45	4.72	3.76	3.76	4.84	4.76	7.05	6.38
MgO	16.46	18.35	18.03	17.92	18.04	17.23	17.58	17.58	15.15	15.59
CaO	21.40	20.78	21.05	20.74	20.92	21.00	20.93	21.15	21.15	21.60
Na_2O	0.24	-	-	-	-	-	0.36	0.22	0.45	0.24
Total*	98.97	99.47	101.00	99.80	100.71	100.30	100.09	99.42	100.41	99.52
Structure on 6 oxygens										
Si	1.880	1.961	1.929	1.920	1.897	1.896	1.945	1.946	1.841	1.901
Ti	0.009	-	0.007	0.010	0.009	0.012	0.007	0.005	0.036	0.023
Al	0.207	0.086	0.113	0.115	0.156	0.165	0.100	0.101	0.198	0.135
Cr	0.040	0.006	0.016	0.023	0.030	0.045	0.010	0.009	0.024	0.022
Fe	0.114	0.138	0.135	0.143	0.114	0.114	0.147	0.145	0.219	0.197
Mg	0.894	0.992	0.978	0.973	0.977	0.934	0.955	0.954	0.837	0.858
Ca	0.835	0.808	0.821	0.809	0.814	0.818	0.817	0.825	0.841	0.854
Na	0.017	-	-	-	-	-	0.025	0.016	0.032	0.017
Total	3.996	3.992	3.999	3.998	3.999	3.986	4.006	4.002	4.028	4.007
Mg/(Mg+Fe)	88.7	87.8	87.9	87.1	89.5	89.1	86.6	86.8	79.3	81.3

Key - C = phenocryst core; R = phenocryst rim; total* = true analysis total, oxides are normalised to 100 wt.%

Table 4.4B

REPRESENTATIVE MICROPROBE ANALYSES OF GROUNDMASS PYROXENES AND AMPHIBOLES.

Sample No.	55	5	211	211	53	53	3A	3A	3A	3A	64D
Analysis No.	B-A-2	B-C-11	B-G-5	B-G-7	A-G-2C	A-G-8C	A-G-1	B-G-5	A-A-5	C-A-1	B-GA-4
Key	G	G	G	G	G	G	G	G	G	G	G
SiO_2	49.76	47.94	50.12	50.28	52.53	49.03	45.81	47.38	37.54	36.66	37.49
TiO_2	1.48	2.53	1.14	1.43	0.48	1.62	3.11	2.22	6.44	7.35	5.16
Al_2O_3	4.53	5.25	3.42	4.89	2.91	3.53	8.99	7.83	14.05	14.66	14.91
Cr_2O_3	0.28	0.19	-	0.19	0.54	0.14	0.27	0.55	-	-	-
FeO	8.37	10.30	12.49	8.23	6.41	13.46	6.28	5.06	14.07	13.90	13.31
MgO	14.36	12.81	13.80	15.91	16.96	11.40	12.95	13.75	10.50	10.31	10.99
MnO	-	0.13	0.19	-	-	0.27	0.21	-	-	-	-
CaO	20.60	20.26	18.47	18.68	19.89	19.97	22.30	22.84	11.73	11.88	12.13
Na_2O	0.62	0.58	0.36	0.38	0.28	0.58	0.50	0.37	2.55	2.74	2.79
K_2O	-	-	-	-	-	-	-	-	1.08	1.16	1.00
Total	99.74	100.82	98.71	99.98	99.16	100.27	100.43	100.23	97.96	98.65	97.79
Structure based on 6 oxygens									:- 23 oxygens		
Si	1.853	1.806	1.887	1.856	0.924	0.870	0.701	1.753	5.652	4.929	5.637
Ti	0.041	0.072	0.032	0.040	0.013	0.046	0.087	0.062	0.729	0.907	0.583
Al	0.199	0.233	0.152	0.213	0.126	0.159	0.393	0.342	2.494	2.836	2.642
Cr	0.008	0.006	-	0.006	0.016	0.004	0.008	0.016	-	-	-
Fe	0.261	0.324	0.393	0.254	0.196	0.429	0.195	0.157	1.772	1.907	1.674
Mg	0.797	0.719	0.775	0.875	0.926	0.648	0.716	0.758	2.356	2.521	2.464
Mn	-	0.004	0.006	-	-	0.009	0.007	-	-	-	-
Ca	0.822	0.818	0.745	0.739	0.781	0.816	0.887	0.906	1.892	2.089	1.955
Na	0.045	0.042	0.026	0.027	0.020	0.043	0.036	0.027	0.745	0.873	0.814
K	-	-	-	-	-	-	-	-	0.207	0.243	0.191
Total	4.025	4.024	4.017	4.009	4.002	4.024	4.030	4.020	15.848	16.304	15.961
Mg/(Mg+Fe)	75.3	68.9	66.3	77.5	82.5	60.2	78.6	82.9	57.1	56.9	59.5

Key - G = groundmass

One sample (55) contains clinopyroxene phenocrysts whose compositions are anomalous. Although not unusual in Mg, Ca, Fe contents (cores of $Ca_{42}Mg_{50}Fe_8$ and Mg/Mg+Fe = 0.87), cores have around 0.38 wt.% Cr_2O_3 but the rims have 0.81 wt.% Cr_2O_3. TiO_2 and Mg/Mg+Fe exhibit normal behaviour; 0.18-1.30 wt.% TiO_2 and Mg/Mg+Fe from 0.87 to 0.79, from core to rim. The groundmass pyroxenes in this sample are typically Ti enriched, to 2.56 wt.% TiO_2, with low Mg/Mg+Fe values (around 0.72) and have a range in Cr_2O_3 of 0.87-0.13 wt.% Cr_2O_3. The Cr-rich groundmass grains have Mg/Mg+Fe = 0.79, lower than the phenocrysts but higher than the Cr-poor groundmass grains. This anomalous Cr distribution can be explained by two models. One possibility is that the physico-chemical conditions that control cpx-melt relations changed. A more reasonable alternative is that the primitive Cr-poor clinopyroxenes are xenocrysts, either included in the magma or through mixing of their host magma with a Cr-rich magma.

Clinopyroxene microphenocrysts and groundmass crystals (Table 4.4B) exhibit chemical variations following on from compositions of the phenocryst rims. All are calcic and the samples analyzed show various trends which are summarized in Figure 4.8. Most follow an iron enrichment trend. Superimposed to various degrees is a calcium depletion trend which probably reflects decreased Ca activity in the melt, through plagioclase feldspar fractionation.

Schweitzer *et al.* (1978) have shown that a Ti against Mg/Mg+Fe plot (using cations per formula unit) can be used to distinguish pyroxenes from alkali basalts and tholeiitic basalts, recovered from various Deep Sea Drilling Project (DSDP) legs. A plot of the Macquarie Island clinopyroxene data shows similarly that pyroxenes from alkaline lavas may be more Ti-rich at the Mg-rich compositions (> Mg/Mg+Fe = 0.80) than corresponding pyroxenes from the tholeiitic lavas (Figure 4.9). Cr is enriched in the Mg-rich pyroxenes in tholeiitic rocks (Figure 4.10). These results support the

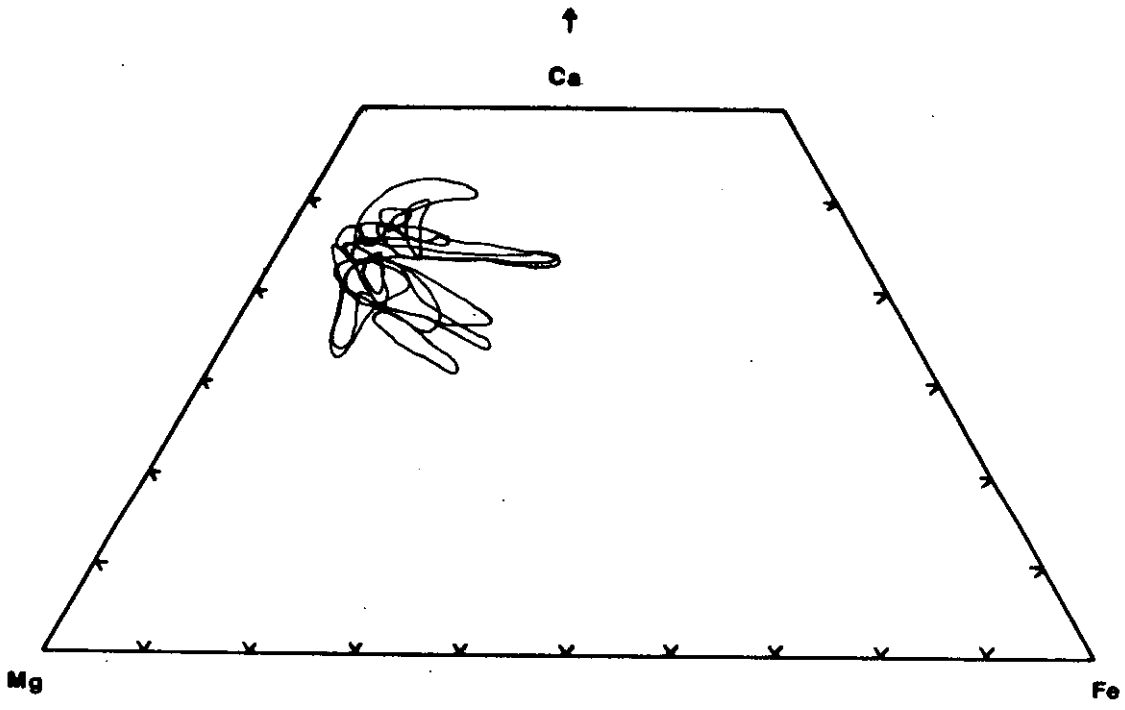

Figure 4.8 Compositional variations of groundmass clinopyroxenes. Each field denotes a different sample.

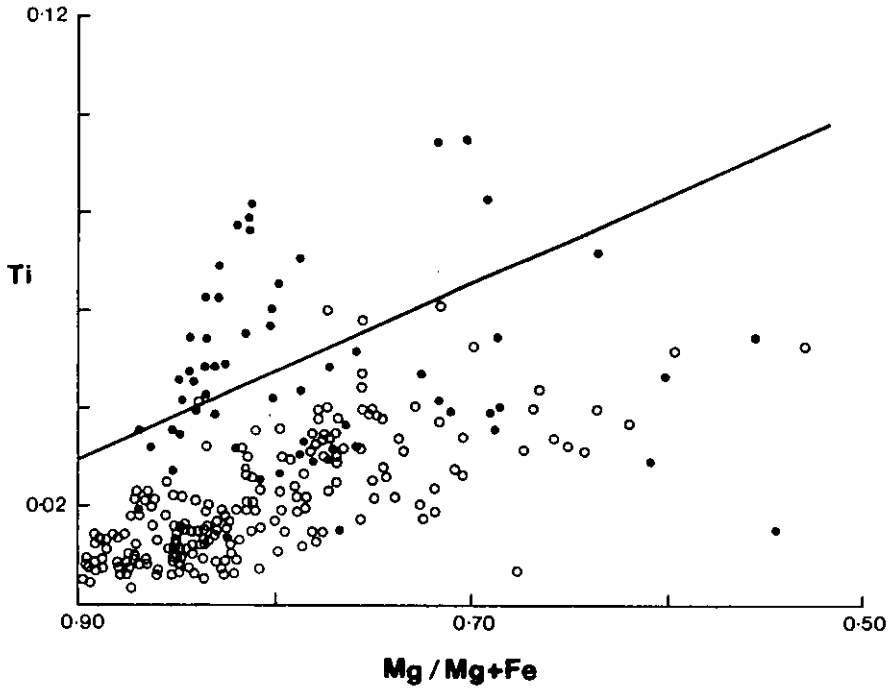

Figure 4.9 Ti vs. Mg/Mg+Fe. The two groups are: alkaline lava pyroxenes (●) and tholeiitic lava pyroxenes (o). Units are cations per formula unit. The pyroxene discriminant line is from Schweitzer *et al.* (1978, fig.2). The rock discrimination is based on the petrography of the lava.

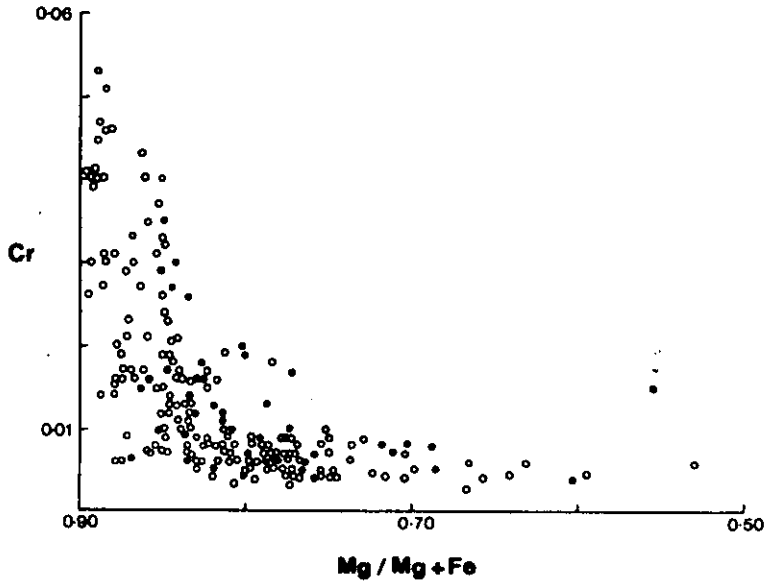

Figure 4.10 Cr vs. Mg/Mg+Fe. Symbols as for Figure 4.9. Units are cations per formula unit.

suggestion by Schweitzer *et al.* (1978) that the non-quadrilateral components of the pyroxenes may be a guide to chemical character of basalts, but only when Mg-rich (i.e. Mg/Mg+Fe > 0.80) compositions are used.

4.2.3 Olivine

Olivine is highly susceptible to alteration, particularly by Cl-rich fluids like sea water (Chapter 5). Consequently it normally occurs as pseudomorphed crystals, recognizable by habit and morphology (Plate 4.9). It formed euhedral crystals everaging 2 mm, but reaching 3.5 mm (38258), in maximum dimension. Although usually present in low percentages (1-3) by volume it composes as much as 10% of some samples (38188, 38122).

Fresh olivine occurs in eight hyaloclastites. The olivine phenocrysts are magnesian, with a range of $Fo_{89.5-85.1}$, most lying between Fo_{89} and Fo_{87}. Representative analyses are given in Table 4.5. Within a single glass the olivine compositions are uniform, with ranges < 2 mol.% Fo. Quench olivines in some samples range down to $Fo_{84.3}$. Fresh olivine phenocrysts and groundmass crystals from a dyke (38189) intruding lavas at Green Gorge have been analyzed. The phenocrysts have an average composition of $Fo_{87.9}$ (nine analyses), similar to the hyaloclastite phenocrysts. Groundmass olivines are $Fo_{73.5}$ in composition.

4.2.4 Spinel

Spinels are the least abundant phenocryst phase, present in 20.5% of the samples examined. They are more abundant in the alkaline lavas (Table 4.2) but rarely (e.g. 38188) form as much as about 1% of the rock. Usually they form less than 0.5% of the rock and are rare as discrete crystals, most occurring as inclusions in olivine and plagioclase phenocrysts (Plate 4.10). These spinels occur as sub- to euhedral crystals, generally about 0.1 mm in maximum section, but rarely up to 0.6 mm. They are reddish-

Table 4.5

REPRESENTATIVE MICROPROBE ANALYSES OF OLIVINE.

Sample No.	40428	252	422	47990	38189	38189	38189	38189
Analysis No.	6	3	3-C	2	E-1	D-4	B-1	B-2
Key	P	P	P	P	P	P	Q	Q
SiO_2	39.37	40.43	40.65	40.47	40.26	40.11	37.56	37.50
Al_2O_3	-	-	-	-	-	-	0.42	0.40
FeO	11.53	12.13	11.60	11.75	11.45	11.77	23.74	23.90
MgO	48.74	47.44	47.74	47.54	47.99	47.82	37.34	37.03
MnO	-	-	-	-	-	-	0.61	0.48
CaO	0.36	-	-	0.22	0.31	0.29	0.34	0.35
Total	100.01	101.89	99.35	100.	100.	100.80	100.70	102.40
Structure on 4 oxygens								
Si	0.976	1.000	1.003	1.000	0.994	0.992	0.986	0.989
Al	-	-	-	-	-	-	0.012	0.012
Fe	0.239	0.251	0.239	0.243	0.236	0.243	0.521	0.527
Mg	1.800	1.749	1.755	1.751	1.766	1.763	1.462	1.456
Mn	-	-	-	-	-	-	0.013	0.011
Ca	0.010	-	-	0.006	0.008	0.007	0.009	0.010
Total	3.024	3.000	2.997	3.000	3.006	3.008	3.007	3.005
Mg/(Mg+Fe)	88.3	87.5	88.0	87.8	88.2	87.9	73.7	73.4

Key - P = phenocryst
Q = quenched crystal.

Plate 4.9 Olivine glomerocryst altered to dark smectites along the margins and lighter mixed-layer sheet silicates and black iron oxides in the bulk of the crystal (sample 38515). Scale: 1 cm = 800 microns.

Plate 4.10 Two dark, euhedral spinel phenocrysts included in a large, altered plagioclase phenocryst. The adjacent olivine phenocryst has been altered to chlorite (sample 202). Scale 1 cm = 0.2 mm.

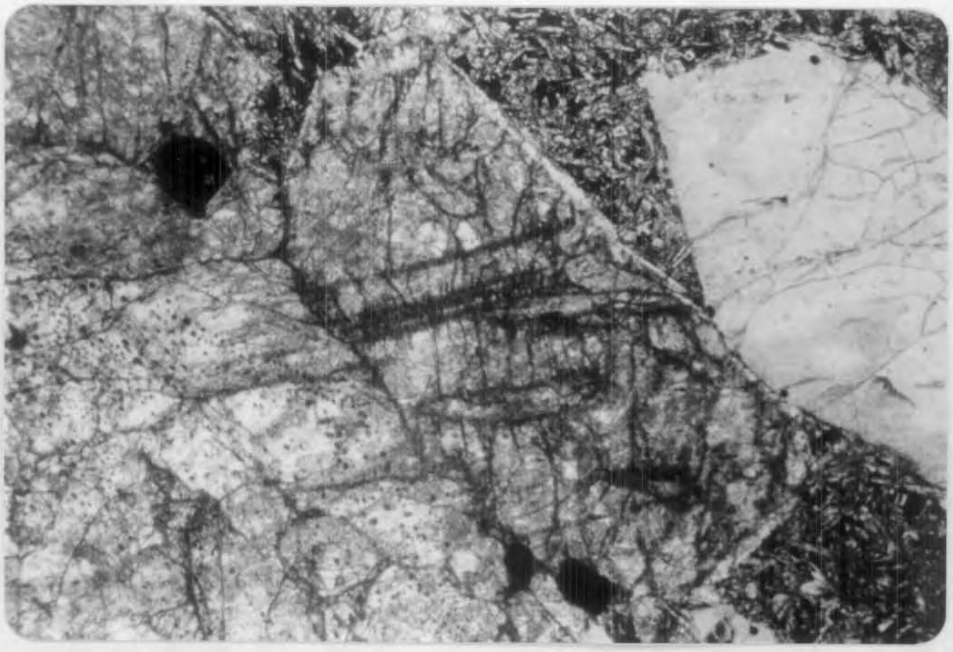

brown in plane polarized light and no colour zoning has been observed in any crystals. The larger spinels contain numerous glass inclusions.

Spinel compositions are represented on a plot of Cr/Cr+Al against Mg/Mg+Fe (Figure 4.11), and representative analyses are given in Table 4.6. Titanium has been removed from the initial analysis as ulvospinel and then Fe^{3+} has been calculated assuming stoichiometry, using the method described by Rodgers (1973). Spinel compositions reported by Cameron *et al.* (1980) from Macquarie Island lavas are also plotted on Figure 4.11 [Because Cameron *et al.* (1980) do not describe their Fe^{3+} recalculation procedure some error is introduced but the low TiO_2 minimises this problem. A difference of +0.02 in the Mg/Mg+Fe ratio results when the TiO_2 and equivalent FeO are subtracted. This error is indicated on Figure 4.11 and applies to all the data from Cameron *et al.* (1980) but does not significantly change the composition field of the mid-Atlantic Ridge spinels.]

4.3 PHENOCRYST CRYSTALLIZATION ORDER

The euhedral form of the spinels and their inclusion in both olivine and plagioclase phenocrysts demonstrates that when spinel occurs, it was the first of these phases to crystallize. Olivine probably precedes plagioclase: although this order of crystallization is not demonstrable petrologically in the Macquarie Island rocks, olivine precedes plagioclase in experimental studies of similar compositions (Green *et al.*, 1979).

Large clinopyroxene phenocrysts occasionally contain rounded inclusions of plagioclase (211 and 217, Plate 4.11). These plagioclases are compositionally identical to the plagioclase phenocrysts and this relationship strongly suggests that plagioclase predates the clinopyroxene. In glomerocrysts or clumped plagioclase and clinopyroxene phenocrysts the clinopyroxene further demonstrates a later growth by subophitically enclosing

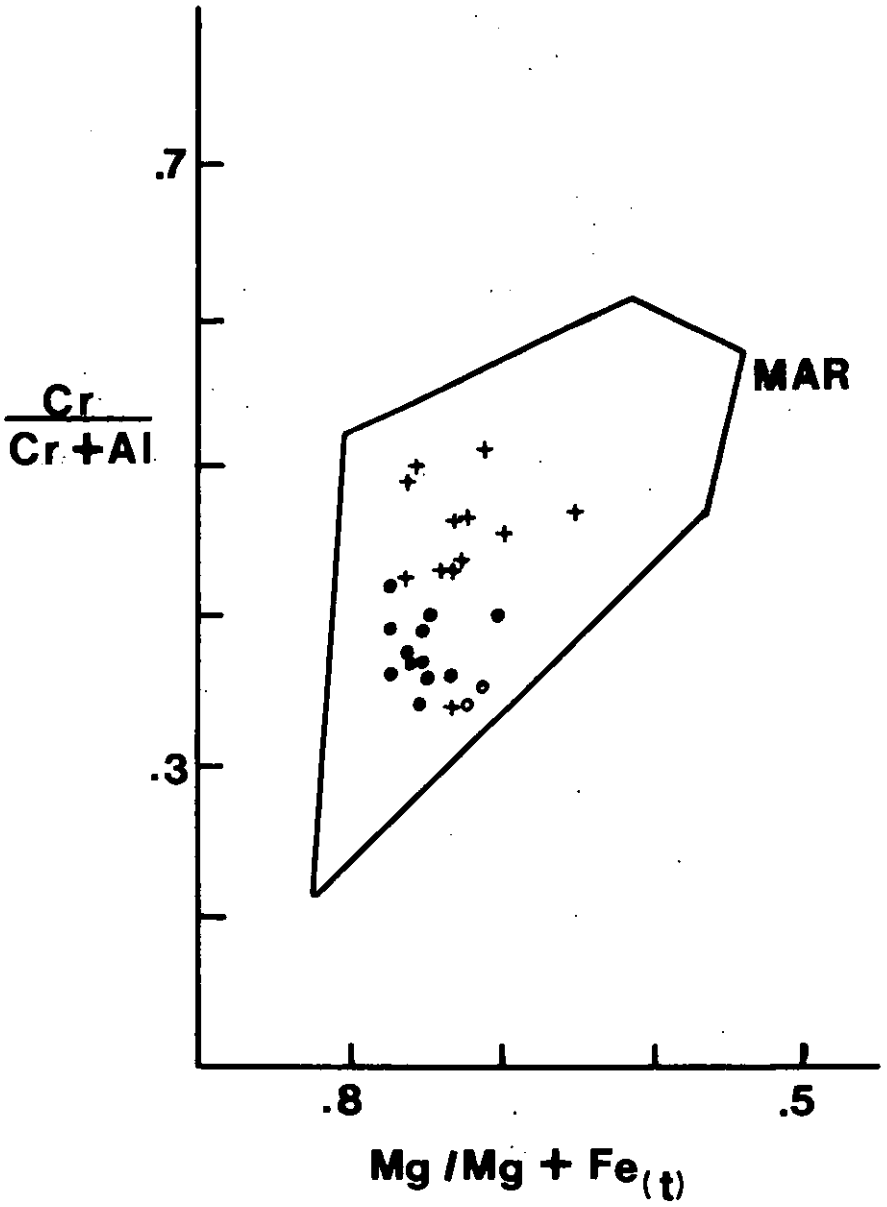

Figure 4.11 Compositions of spinel phenocrysts. The outlined field is for spinels from mid-Atlantic Ridge basalts (Cameron *et al.*, 1981). Key: + this study, ● Cameron *et al.* (1981).

Table 4.6

REPRESENTATIVE MICROPROBE ANALYSES OF SPINELS

Sample No.	47990	47990	38188	38188	40428	47142
Analysis No.	1	2	3*	2		
TiO_2	0.82	0.95	0.63	0.68	0.43	0.70
Al_2O_3	36.41	34.61	34.90	34.37	31.82	32.00
Cr_2O_3	28.02	29.58	30.13	30.12	33.78	32.23
FeO	17.97	17.95	16.76	17.33	16.22	19.18
MgO	16.78	16.91	17.58	17.56	17.73	15.89
Structure based on 32 oxygen**						
Al	9.917	9.510	9.473	9.353	8.690	8.887
Cr	5.118	5.450	5.484	5.497	6.187	6.003
Fe^{3+}	0.965	1.040	1.043	1.150	1.121	1.110
Fe^{2+}	2.222	2.127	1.968	1.959	1.881	2.421
Mg	5.778	5.873	6.032	6.041	6.121	5.579
Cr/Cr+Al	0.34	0.36	0.37	0.37	0.42	0.40
$Mg/Mg+Fe^{2+}$	0.72	0.73	0.75	0.76	0.77	0.70

* Analysis using TPD microprobe, A.N.U., remainder with Jeol/ Edax microprobe, University of Tasmania.

** Normalised to 24 cations (Rodgers, 1973) after removal of ulvospinel component. Progressive calculations are given in Appendix 3.

Plate 4.11 Zoned clinopyroxene phenocryst with typical rounded form (sample 211). Rounded plagioclase grains are included in this pyroxene (within the marked circle). Scale: 1 cm = 0.2 mm. Crossed nicolls.

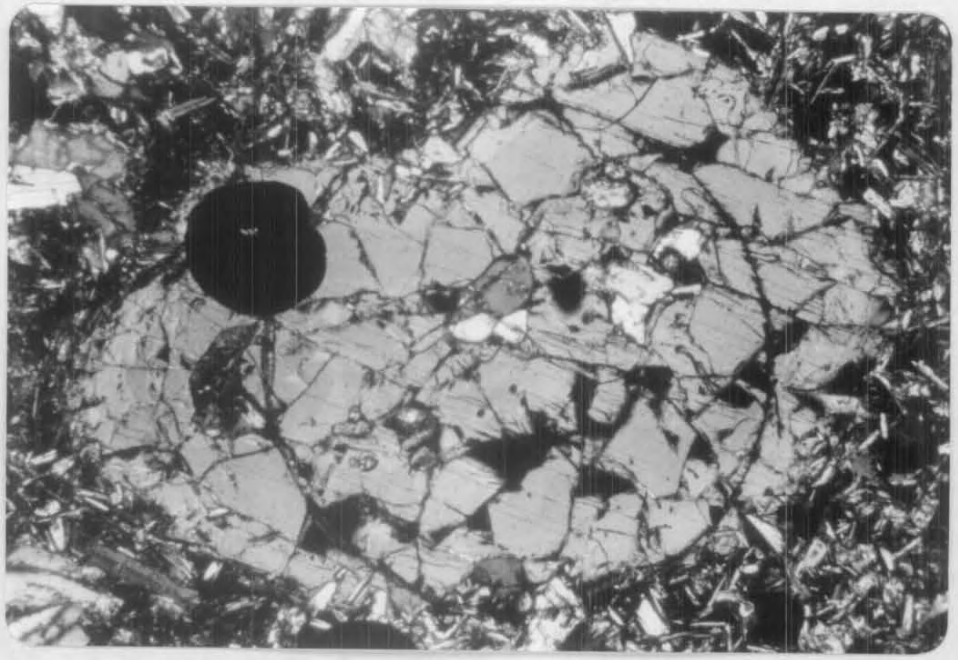

the plagioclase. Thus petrographic and other evidence gives a crystallization sequence for the phenocryst phases in order of appearance:

spinel ± olivine → plagioclase ± clinopyroxene

There is no evidence of orthopyroxene as a phenocryst phase within the lavas at any stage. Olivine and spinel show no evidence of reaction with the lavas but both plagioclase and clinopyroxene have reacted, with the exception of the plagioclase inclusions in the clinopyroxenes. This last feature is a result of protection of the plagioclase by the mantling clinopyroxene and it shows that the plagioclase was in equilibrium with the liquid at the time of clinopyroxene crystallization.

4.4 ORIGIN OF THE PHENOCRYSTS

The term "phenocryst" has been used up until this point but the analytical results demonstrate that at least in some cases this term is incorrect. More specifically the reversed distribution of chromium between phenocryst and groundmass pyroxene in sample 55 (Section 4.2.2) identifies these particular crystals as *xenocrysts*, i.e. they did not crystallize from their eventual host liquids. Indeed this is probably true of many of the other phenocrysts, particularly the Mg-rich olivines present in the glasses (Section 4.2.3), but it is difficult to generalize. The phenocryst compositions are compatible with crystallization from the lavas with respect to experimental studies of the liquidus and near-liquidus phases. The xenocrystic nature of some of the crystals could result from a magma mixing process. In view of this the term "phenocryst" is retained for these crystals without the assumption that a genetic relation relates crystal and rock. Further discussion as to the origin and role of these phenocrysts is included in the discussion of the petrogenesis of these lavas (Chapter 6).

4.5 PETROGRAPHY AND MINERALOGY OF YOUNG OCEAN-FLOOR BASALTS

It is now appropriate to consider the petrography of young ocean-floor basalts. As noted by Coleman (1977), there is a surprising lack of petrographic descriptions available. Nicholls (1964) presented one of the first reviews of dredge samples from the deep ocean floor and described them as tholeiitic in their general affinities, ranging from glasses to holocrystalline porphyritic basalts containing as phenocrysts: plagioclase, olivine and augite. Ophitic textures were reported in some samples. These descriptions covered samples recovered in later dredging projects, for example at 30°N Mid-Atlantic Ridge (M.A.R.) (Muir & Tilley, 1966), 22°N M.A.R. (Melzon *et al.*, 1968) and 24°N and 30°N M.A.R. (Miyashiro *et al.*, 1969, 1970), and with associated geochemical studies the concept of a uniform mid-ocean ridge basalt (MORB) was established (Cann, 1971; Schilling, 1971).

However basalts with alkaline affinities had been described in detail by Muir & Tilley (1964) in dredge haul samples from 45°50'N M.A.R. They noted that within their sample collection "the basalts with alkali affinities may be distinguished from the rest [tholeiitic basalts] by the slightly more iron-rich nature of the olivine occurring in two generations, and the deeper colour of the titaniferous pyroxene...". Additional alkaline samples from the M.A.R. near 45°N were described by Aumento (1968) who compared the Discovery collection (Muir & Tilley, 1964) with his samples from the Confederation Peak area. Aumento (1968) suggested that "volcanoes begin their existence on the floor of the Median Rift Valley (the central feature of the M.A.R.) with the extrusion of tholeiitic lavas with low alkali and normative olivine content. As the volcanoes develop, they extrude progressively more alkali-rich lavas on the top of the tholeiitic cores. A large volcano ends its eruptive cycle with a capping of alkali lavas with considerable normative nepheline."

Thus evidence was present for the alkaline nature of some ocean-floor basalts and Cann (1971) recognised that the term "oceanic tholeiite" had become misleading. In his conclusions he noted, with respect to ocean-floor basalts, that "the basalts range from definitely tholeiitic types to definitely alkaline types with a wide zone of transitional basalts between the two extremes."

Considerable information has since been accumulated on modern ocean-floor basalts and Bryan *et al.* (1976), in a summary of information from the DSDP sites in the North and South Atlantic Ocean, the Nazca Plate, and the eastern Indian Ocean recognized two groups of ocean-floor basalts on chemical and to a less extent petrographic grounds. Group I basalts correspond to the uniform classical abyssal tholeiite with large-ion lithophile (LIL) depletion, whereas the Group II basalts are heterogeneous and are characterized in particular by a titaniferous groundmass clinopyroxene and rarely by phenocryst clinopyroxene, spinel being rare or absent. Plagioclase phenocrysts are characteristic of both groups and are not diagnostic. Both groups can carry olivine in the range Fo_{90-85}. Most of the Macquarie Island lavas are Group I basalts but a significant proportion fall into the Group II category on these petrographic criteria, and some are transitional as was the case for FAMOUS and leg 37 DSDP lavas (Bryan *et al.*, 1976).

4.6 COMPARISON WITH OTHER OPHIOLITE COMPLEXES

The Troodos ophiolite complex is the best documented ophiolite at present. Two volcanic episodes are recognised and are separated by an unconformity which represents a time break when metamorphism, mineralisation, and submarine erosion of the Axis Formation occurred (Smewing, 1975). The overlying Upper Pillow Lava sequence contains mainly basaltic lavas with rare ultramafic types rich in olivine and pyroxene.

Within the basaltic lavas phenocrysts of olivine, clinopyroxene, orthopyroxene and plagioclase feldspar have been reported, in that order of abundance, in contrast to the Macquarie Island volcanic sequence where plagioclase feldpsar is predominant amongst the phenocryst phases and orthopyroxene has not been observed. The pillow lavas and dyke swarm rocks, which form equal parts by volume of the underlying Axis Formation, were considered by Smewing (1975) to be petrographically identical to the Upper Pillow Lavas and thus significant differences exist between the Troodos ophiolite volcanic sequence and the corresponding sequences of the Macquarie Island ophiolite complex.

Cameron *et al.* (1980) also noted this difference and in a summary of the petrography of must documented ophilites recognized the volcanic members of the Macquarie Island ophiolite and the Newfoundland west coast ophiolites as being comparable to young ocean-floor basalts whereas other ophiolites, including Troodos, Othris, Vourinos and Betts Cove form a group which is distinguished in particular by the presence of orthopyroxene, chromium spinels (Cr/Cr+Al > 0.7) and pigeonites with $Mg/Mg+Fe^{2+}$ as high as 0.86 unreported so far from the ocean floors.

4.7 SUMMARY

The following general points summarize the petrography and phase mineralogy of the lavas and dykes:

1. A continuous spectrum is present, between basalts with subophitic textures with tholeiitic affinities, and basalts with intersertal textures with alkaline affinities.
2. Most lavas are porphyritic: plagioclase is the dominant phenocryst phase followed, in order of decreasing abundance, by olivine, clinopyroxene, and spinel. Aphyric lavas are more common amongst the alkaline varieties. Orthopyroxene and pigeonite are not present.

3. The phenocryst compositions are primitive, i.e. olivines and clinopyroxenes are Mg-rich and the plagioclase is calcium-rich. In some cases the chemistry demonstrates that they may be xenocrysts, indicative of magma mixing. The crystallization sequence inferred from petrographic studies is:

   spinel → olivine → plagioclase → clinopyroxene.

4. Similar petrography has been reported in young ocean-floor basalts but not from other ophiolites.

Chapter 5

METAMORPHISM OF THE LAVAS AND DYKES

5.1 INTRODUCTION

This study is the first detailed investigation of the metamorphism of the basalts and dolerites of the Macquarie Island Complex. The approach has been principally to record the metamorphic assemblages that occur in the available collections on both local and regional scales to establish whether or not a systematic variation in metamorphism exists within the samples, and then to consider if such a variation is a result of one coherent metamorphic process acting within the oceanic crust. Other questions to be considered are (i) at what stage in the evolution of the oceanic crust did the metamorphism(s) occur, and (ii) what sort of time scale(s) is (are) involved.

Apart from these problems the study is also aimed at providing information (i) to aid recognition of "on-land" oceanic crust through the comparison of metamorphic styles (patterns), (ii) on the nature and evolution of the hydrothermal fluid involved in the metamorphic processes, particularly with respect to sulphide mineralization, and (iii) on major and trace element migration during the metamorphic process(es).

5.2 SAMPLE COLLECTIONS AND MINERAL IDENTIFICATION TECHNIQUES

The sample collections used were those described in Chapter 4 together with vein and amygdule material that was collected during the 1975-76, 1976-77 and 1979 field trips. This latter material formed the basis of the samples used for XRD studies because in general the amygdules are only 1-2 mm in diameter and only rarely monomineralic, usually containing at least three, and up to five, intergrown phases.

Weathering produces a reddish-brown colouration in the rocks, fresh material in general having a dark blue-grey appearance. The presence of zeolites in the field is easily determined but beyond that identification is very difficult with only thomsonite and matrolite being positively identifiable, a contrast to the Troodos Massif where Smewing (1975) was able to recognize all seven species of zeolites present in hand specimen. Other secondary assemblages are virtually impossible to identify in the field due to the fine grained nature of the material. Consequently microscopic and electron microprobe studies formed the major part of the work. The approach used was to distinguish the various phases using their optical properties and follow this by electron microprobe and XRD examination (Appendices 4-7) to identify the phases present, thus developing the necessary experience and expertise required for correct optical recognition of the various phases. Detailed microprobe studies of diagnostic assemblages are described later.

5.3 METAMORPHISM: DEFINITIONS AND TERMINOLOGY

It is firstly necessary to define the terminology applied to the changes encountered in the samples. Miyashiro (1973) discussed the concept of metamorphism and notes that recently through the work of Coombs (1954) and others the studies of metamorphism and diagenesis have begun to converge. Miyashiro (1973) defined *diagenesis* to include those changes taking place at essentially the same temperature as that of the original deposition, and *metamorphism* to include those changes taking place at essentially higher temperatures, as Coombs (1961) pointed out. Miyashiro (1973) subsequently presented an argument that ocean-floor metamorphism must occur mainly beneath the crust of mid-ocean ridges because of the high geothermal gradients there, relative to elsewhere on the ocean floor. Because, principally, the large-scale recrystallization occurred without penetrative deformation, this

metamorphism is considered to be one aspect of burial metamorphism. In his more detailed discussion of ocean-floor metamorphism, Miyashiro (1973) noted that most metabasalts recovered from the ocean floor belong to the zeolite and greenschist facies, with some in the greenschist facies transitional to the amphibolite facies.

These definitions and discussions are difficult to apply to ocean-floor rocks in that samples altered under conditions lower than those required to form zeolite facies assemblages may be more extensively altered from the pristine state than those containing metamorphic assemblages of relatively high grade, e.g. greenschist facies. Indeed this important aspect of extent of alteration of samples is one which has been, to a large extent, ignored by most workers in this area. Steiner (1977) however, considered it in some depth based on his studies of the Wairakei geothermal area. He defined two features of the alteration of a rock sample: rank and intensity, and gives the following definitions: "The term 'rank of alteration' implies a definite assemblage of hydrothermal minerals associated with more or less unaltered primary minerals, irrespective of whether this assemblage is in equilibrium or not within a measured range of temperature and pressure" and "'intensity of alteration' defines whether the alteration is incipient, partial, or complete." Steiner (1977) also noted that the intensity of alteration usually corresponds with the degree to which the original texture of the groundmass is obliterated by hydrothermal alteration and finally that it is not always certain whether incomplete alteration is due to dis-equilibrium, to lack of time, or lack of necessary reactants. The concept of *intensity* is very useful and this formal definition is felt necessary to avoid ambiguity or misconceptions.

Coleman (1977) reviewed the metamorphism of ocean-floor rocks and ophiolites and dealt with the secondary processes acting on ocean-floor rocks under the classification of "oceanic hydrothermal metamorphism".

As did Miyashiro (1973), Coleman (1977) discussed zeolite facies metamorphism as representing the lowest grade of metamorphism encountered. He incidently noted that, in his opinion, "spilite" metamorphism results from hot circulating H_2O within the newly formed parts of the oceanic crust and that "spilites" probably do not have a primary igneous origin (c.f. Amstutz, 1974).

Both Coleman (1977) and Miyashiro (1973) failed to consider sub-zeolite facies alteration effects in the oceanic pillow lava layer. This reflects the fact that the Macquarie Island complex is one of the few, if not the only one, of the ophiolites to have preserved within it the zone of rocks which have suffered sub-zeolite facies alteration, i.e. Ocean-floor weathering. Also it is only in recent years with the successful DSDP and other basement drilling projects that attention has focussed on this area (Andrews, 1977; Pritchard *et al.*, 1979; Robinson *et al.*, 1977). The most significant point of this discussion then is that ocean-floor metamorphism must be considered to include this style of alteration, thus extending the concept of metamorphism to lower temperature and pressure conditions.

5.4 METAMORPHIC ASSEMBLAGES WITHIN THE PILLOW LAVA AND DYKE SWARM UNITS OF THE MACQUARIE ISLAND COMPLEX

Results from this study have confirmed the previous preliminary studies (Chapter 2). The levels of metamorphism and alteration recognized within the pillow lava section are (1) ocean-floor weathering (halmrolysis), (2) zeolite facies metamorphism, and (3) lower greenschist facies metamorphism.

Dykes intruding the pillow lava section contain assemblages similar to the host lavas but within the dyke swarms, as noted by Varne & Rubenach (1972), secondary assemblages are typical of upper greenschist to lower amphibolite facies metamorphism.

The following sections describe the mineralogy and petrography of each group of assemblages, including electron microprobe analyses of the various phases.

5.4.1 Ocean-floor weathering (halmrolysis)

Distribution (localities)

Rocks from the North Head block of pillow lavas have previously been described as either unmetamorphosed (Varne & Rubenach, 1972), or as having suffered low temperature oxidation (Levi *et al.*, 1978) and it is from this area that samples most clearly illustrate the effects of low-temperature sea water interaction. Samples showing similar styles of alteration occur in the Pyramid Peak area, within a block of pillow lavas that have generally been metamorphosed to zeolite facies grade. Other samples occur sporadically, again within blocks of lavas showing zeolite facies grade metamorphism, and this sporadic occurrence reflects firstly the uneven character of these low grades of metamorphism and secondly the lack of exposure in the inland sections of the island, as discussed earlier.

Mineralogy

Minerals present include calcite ± smectites ± celadonite ± phillipsite ± saponite ± hematite ± Fe (OH)'s, with glasses being replaced by palagonite to varying extents.

The phases are listed in approximate order of abundance. Calcite and smectites are ubiquitous. In holocrystalline samples, olivine and mesostatis are affected by this style of alteration. The alteration is initially along grain boundaries and cracks in the olivine and from there, the bulk of the crystals. Commonly fresh augen of olivine remain, in the less altered samples. Yellow-orange smectites and/or saponitic material form along the grain boundaries and cracks, with either calcite, commonly coarse granular sparry material, replacing the central portions of the crystals or fibrous subradiating pale green smectite (Plate 5.1,

sample 38389). This green smectite is very similar to chlorite except that it displays birefringence up to low second order colours, and not the characteristic anomalous "Berlin blue" birefringence of the chlorite family.

In other samples from North Head, e.g. 38391 and 35, the green smectite is fairly rare, the dominant secondary phases being the yellow-orange smectite and calcite. The smectite is commonly present as granular or massive material but where it occurs as thin rims to calcite it shows a fibrous vermicular structure. It is notably paler in this habit, probably due simply to thinner wedges being observed in the sections.

Interstitial glass is totally replaced by smectite-carbonate and these assemblages also fill amygdules in the rocks. Original feldspars are little-affected: glass inclusions are altered and smectites are developed along fractures in the crystals.

Hyaloclastite breccias and glassy selvedges on pillows, are common in the North Head block and these glasses are variably altered. The alteration starts along cooling contraction cracks in the glass and expands away from these, resulting in augen of fresh glass set in a matrix of alteration products. Smectites form either as pale yellow, fine, fibrous rims along the veins with centre fills of phillipsite, or as massive yellow rims. Around these cracks the glass is altered to brownish palagonite. Calcite is only present as thin veinlets cutting the breccias and selvedges, locally cutting through both altered and fresh glass. This suggests that the calcite precipitation is later than the smectite-palagonite alteration of the glass. Further evidence for late calcite precipitation is present in 38335 where the calcite is often present as finely fibrous radiating bands within areas of altered mesostasis, apparently isomorphously replacing smectites. These calcite zones are turbid with myriads of inclusions, commonly opaque, trapped between the fibres.

Plate 5.1 Altered olivine phenocryst replaced by dark yellow-orange smectites along the rims and pale green smectite and calcite in the core. Sheaves of tabular, purplish titanaugite crystals, typical of the more alkaline lavas, are present in the right-hand top corner of the photo. Scale: 1 cm = 0.1 mm. Sample 38389.

Plate 5.2 Amygdules with dark smectite rim and centre fill of zeolites. The brown fine fibrous form is a intergrowth of natrolite-thomsonite -mesolite and the bladed clear variety is thomsonite. The gradation between the two is shown in the left-hand area of the photo. Scale: 1 cm = 0.1 mm. Sample 151.

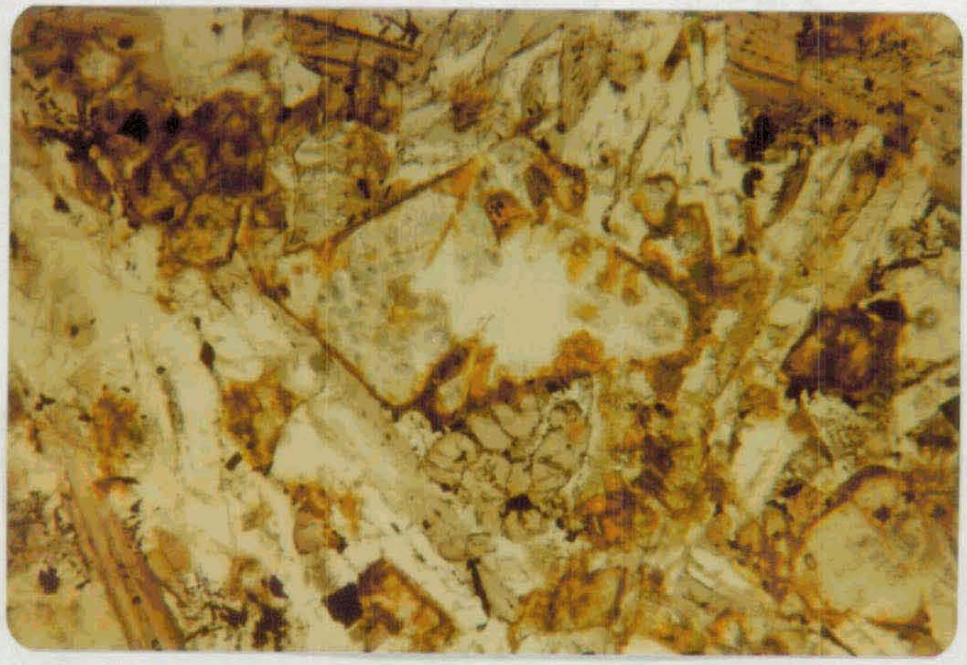

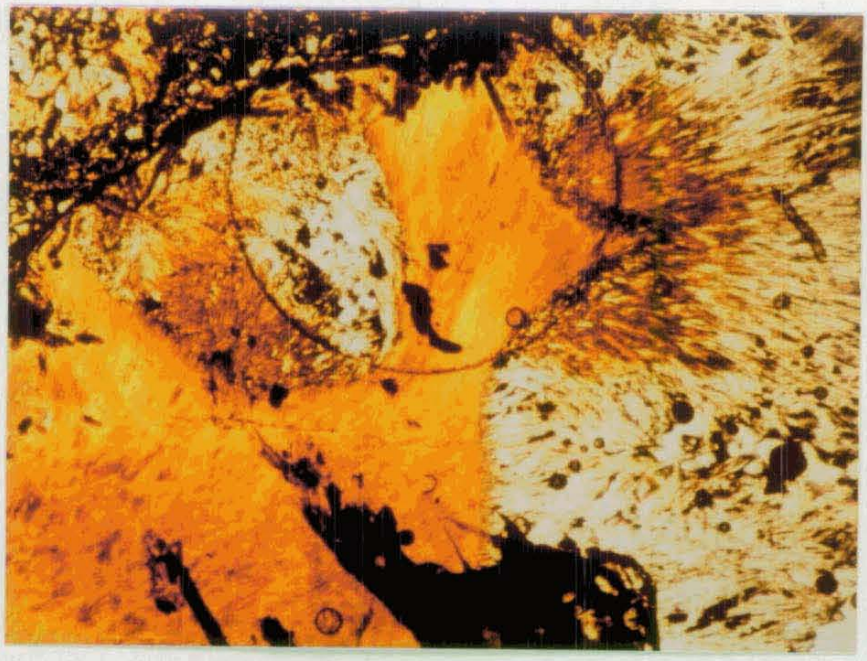

The alteration is pervasive in all samples but variable in that in some samples fresh augen of olivine remain, e.g. 38389 and 38365, whereas in others, all the olivine has been altered, e.g. 35. All interstitial glass has been altered in the samples examined. Within the hyaline material the maximum alteration observed is ~50% of the sample (352) although this is only a rough estimate as incipient palagonitization of glass is often not optically recognizable. As olivine and interstitial glass are the only material affected, the abundance of these determines the extent of alteration in terms of whole rock compositions, with the more alkaline olivine-phyric samples being most affected. The effects of this alteration on whole rock chemistry are considered later (Section 6.1).

Chemistry of the secondary phases

Phillipsite and smectites in samples 35 and 252 have been analysed by electron microprobe and results are presented in Table 5.1. The possibility that specimen damage occurs during analysis is suggested by the low and variable totals of these analyses, particularly the smectites. The phillipsite compositions are stoichiometrically correct and lie between compositions reported from DSDP leg 37 samples, by Robinson *et al.* (1977) and Barager *et al.* (1977) and from DSDP leg 49 by Pritchard *et al.* (1979). The variations in composition occur both between and within samples and, as many others have noted, appears to reflect local variations in conditions which at present have not been determined.

The smectite analyses (Table 5.1) are variable but firstly show only a minor illite composition ($K_2O < 0.88$). Structural formula calculations based on 22 oxygens suggest that the smectites are tri-octahedral and that both oxidized and reduced varieties are present. In sample 252 there is no optical difference between the oxidized and reduced varieties. The oxidized smectites in 35 are brownish, similar to those described by Pritchard *et al.* (1979).

Table 5.1

REPRESENTATIVE MICROPROBE ANALYSES OF SMECTITES

Sample No.	252	35	35	117	252	252
Analysis No.	B-SM	B-SM-2	SAP-1	N-4	SM-1-r	SM-2-r
SiO_2	43.70	42.68	34.33	35.83	40.43	40.09
TiO_2	-	-	-	-	1.20	1.23
Al_2O_3	15.06	3.68	8.18	18.57	13.62	13.79
Fe_2O_3*	6.55	0.81	19.88	12.12	10.77	12.04
MgO	11.81	22.62	20.31	3.42	16.55	15.65
CaO	2.97	0.52	0.78	19.17	1.83	1.99
Na_2O	0.65	-	0.59	-	-	-
K_2O	0.88	0.36	0.57	-	0.82	0.72
Total	81.62	70.67	84.67	89.10	85.24	85.55
	Structure based on 22 oxygen					
Si	6.704	7.377	5.488	5.481	6.090	6.044
Ti	-	-	-	-	0.136	0.139
Al	2.724	0.750	1.542	3.349	2.419	2.451
Fe^{3+}	0.756	0.105	2.392	1.395	1.221	1.366
Mg	2.700	5.827	4.839	0.780	3.715	3.516
Ca	0.488	0.096	0.134	3.142	0.295	0.321
Na	0.194	-	0.183	-	-	-
K	0.172	0.079	0.116	-	0.158	0.138
Total	13.739	14.235	14.694	14.147	14.033	13.977

* total iron expressed as Fe_2O_3.

	Phillipsite		
Sample No.	252	252	252
Analysis No.	1	2	3
SiO_2	54.12	55.62	57.37
Al_2O_3	21.05	21.77	22.43
CaO	2.14	1.99	2.50
Na_2O	5.73	5.36	5.38
K_2O	5.91	6.55	5.81
Total	88.96	91.30	93.49
Si	24.81	24.84	24.88
Al	11.37	11.46	11.47
Ca	1.05	0.95	1.16
Na	5.09	4.65	4.52
K	3.46	3.73	3.21

5.4.2 Zeolite facies alteration

Distribution

Zeolite-bearing assemblages predominate in the central and eastern parts of the middle section of Macquarie Island and occur irregularly in the southern section (Figure 5.1). These assemblages are best developed around Pyramid Peak and Green Gorge although assemblages representing the highest levels of zeolite facies metamorphism occur in the Caroline Creek area at the southern end of Macquarie Island and on the mid-west coast just north of Aurora Point within blocks of pillow lavas containing dominantly lower greenschist facies metamorphic assemblages.

Mineralogy and metamorphic petrography

The basic assemblage within this group is Na,Ca,K zeolites ± smectites ± $CaCO_3$ ± chlorite ± sericite ± K-feldspar with the zeolites, in order of abundance: thomsonite, mesolite, phillipsite, wairakite, natrolite, analcite, laumontite, heulandite, and gyrolite. Hydrated calcium silicates (?hillebrandite) also occur.

Styles of alteration within this grade of metamorphism are very similar to ocean-floor weathering except that primary plagioclase is strongly affected. As the lavas are dominantly plagioclase phyric (Chapter 4) and plagioclase is a major groundmass phase, the potential for alteration is far greater than with ocean-floor weathering. However, this potential is seldom realised with zeolite development being essentially restricted to amygdules and veins, and areas adjacent to these. Commonly (e.g. 157), plagioclase phenocrysts within a sample are unaltered except where cut by or in the immediate vicinity of a vein or amygdule. Even where cut by veins the alteration is rarely complete, with relicts of primary plagioclase set in an alteration matrix of zeolites within the original crystal boundaries.

The pervasive alteration of olivine and interstitial glass observed within the ocean-floor weathered samples also is observed within these

Figure 5-1 Distribution of secondary assemblages in Macquarie Island lavas.
- o ocean floor weathering
- • zeolite facies
- + lower greenschist facies

(symbols are combined where appropriate)

samples, again demonstrating that fluid completely permeated the samples at some stage during the alteration.

Zeolite mineralogy

Few of the zeolite minerals are distinctive and consequently the group present identification problems. Three zeolites on Macquarie Island are identifiable macroscopically: natrolite, as translucent fine elongate tabular prisms forming loose matted aggregates; thomsonite, as fine fibrous radiating masses; and laumontite, as massive white tabular crystals in subradiating aggregates.

XRD identification techniques have been successfully applied to samples containing large (>5 mm) veins and amygdules (≥2.3 mm) (Appendix 5), but generally because of small amygdule size and complex intergrowths of up to four zeolite species within any single amygdule, this method was not generally useful.

The following electron microprobe analysis technique was devised for use when zeolites could not be identified by XRD methods. The problem of volatilization of the samples by the electron beam is less pronounced using energy dispersive analytical techniques than by conventional wavelength dispersive methods due to the lower (~3 nA) beam currents used. Secondly to minimize volatilization still further, reduced area scan (RAS) techniques were employed, scanning the electron beam over areas up to 100 x 100 microns in size, depending upon the crystal size.

Analyses were then checked using the fundamental property of the zeolite group that the number of Si + Al atoms in the structural formula is equal to half the number of oxygen atoms. For reasons discussed later, a standard value of 72 oxygens was used in structure calculations, following the methods of Steele *et al.* (1976) and ideally Si + Al = 36. The charge balance was also used as a check, because in the ideal structural formula, 2CA + Na + K = Al. The zeolite analyses are presented in terms of these checks in Figures 5.2 to 5.5. It is notable that the

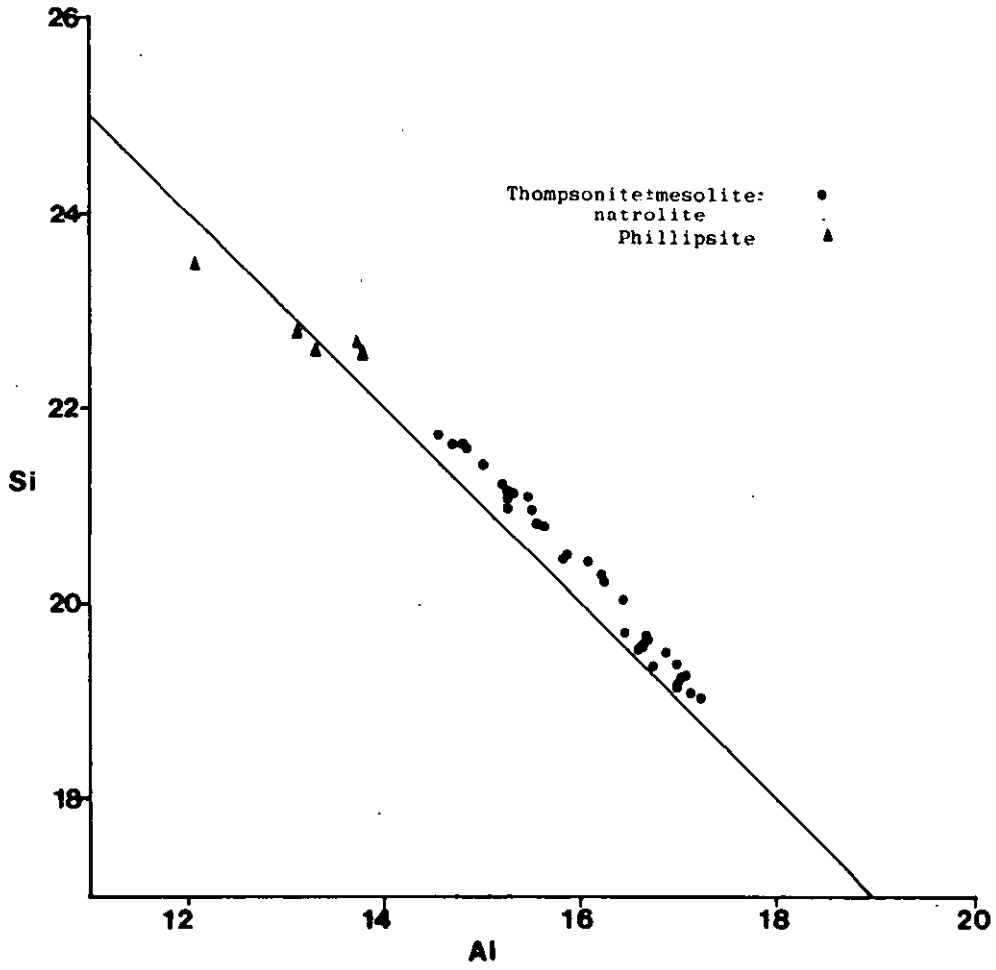

Figure 5.2 Mass balance for zeolites analysed using the TPD microprobe. The line represents the ideal relationship Si+Al=36, based on 72 oxygen.

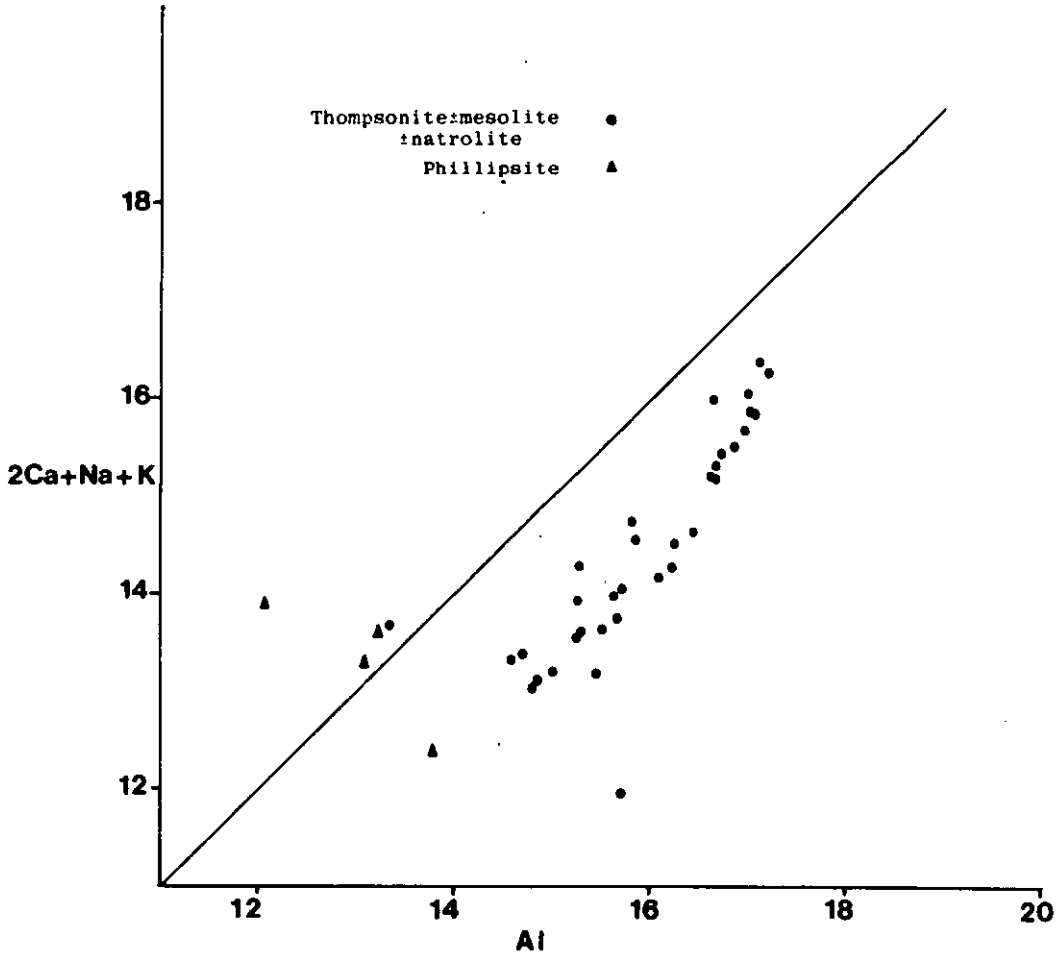

Figure 5.3 Charge balance of zeolites analysed using the TPD microprobe. The line represents the ideal relationship 2Ca+Na+K=Al.

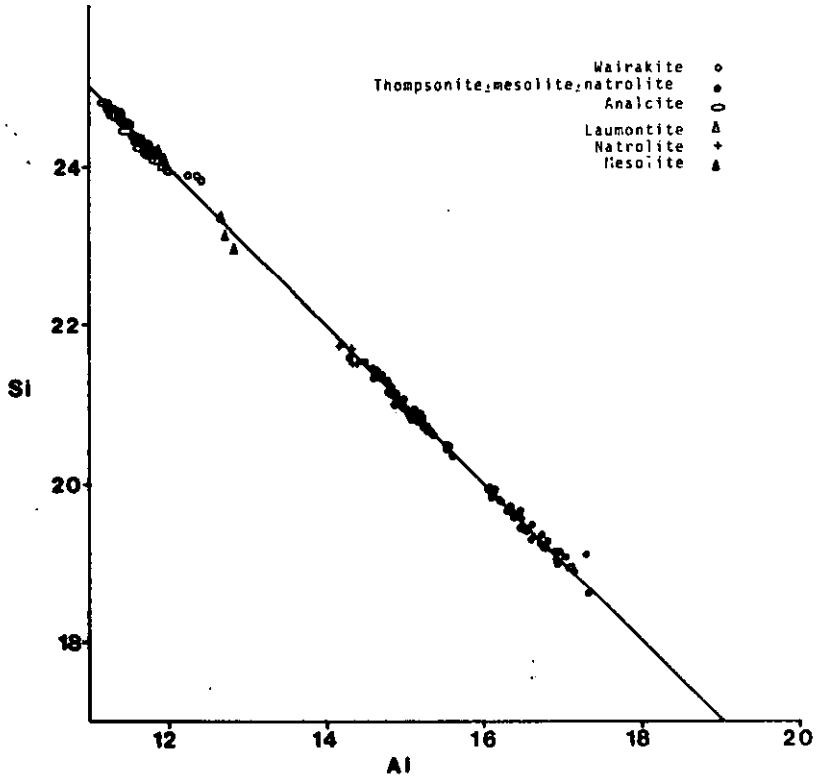

Figure 5.4 Mass balance for zeolites analysed with the EDAX system.

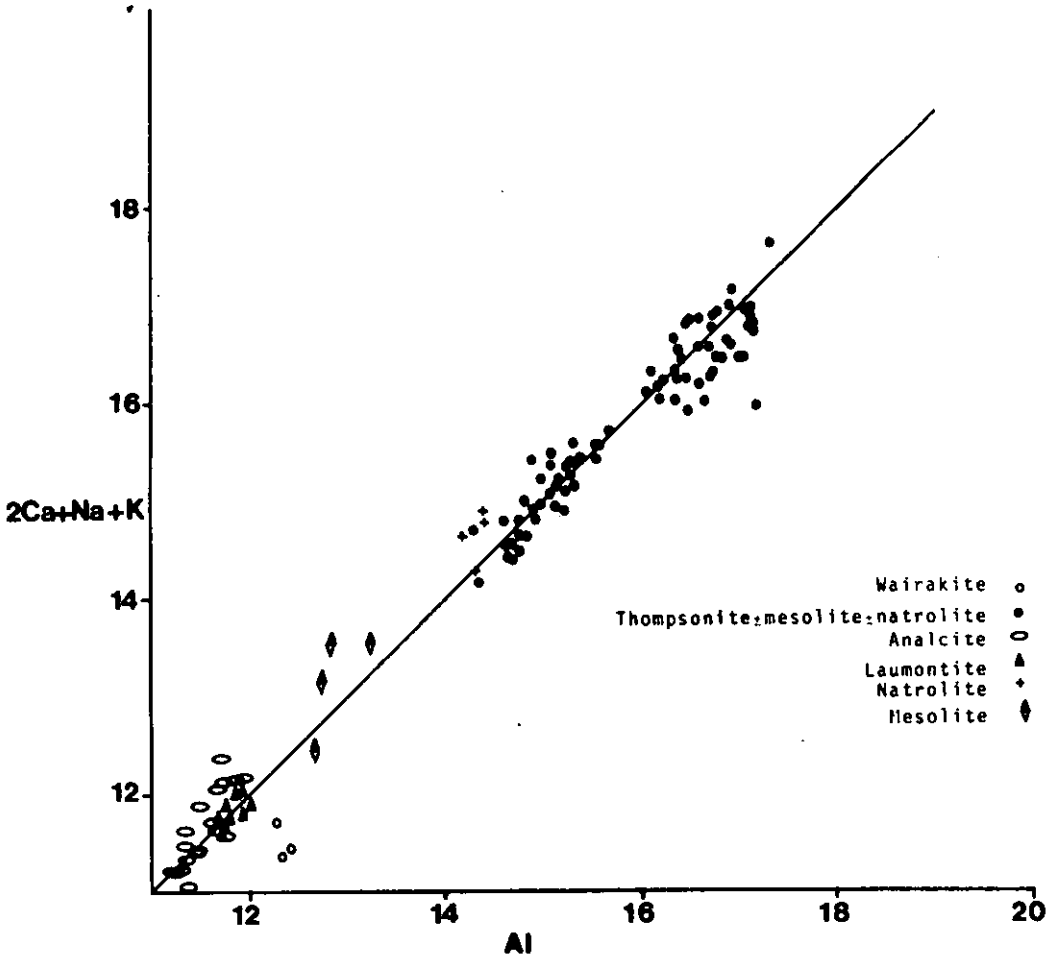

Figure 5.5 Charge balance for zeolites analysed with the EDAX system.

data set collected using the TPD electron microprobe at the Australian National University (where it was not possible to use a RAS analysis method) deviate from the ideal ratio significantly, being high in the Si + Al sum, and low in alkalis with respect to Al in terms of the charge balance, except for the phillipsite analyses. The analyses collected using the EDAX system at the University of Tasmania, where RAS analysis methods were used, are very close to ideal Si + Al and are also acceptable in terms of charge balance (Figures 5.4 and 5.5). These results are within the acceptable error margins defined by Passaglia (1970).

Having tested the analyses for accuracy the problem is then to identify the species. Because the analyses are only partial (H_2O, CO_2 not being determined) it is difficult to identify different Na,Ca species and so a ternary plot was developed using the structurally derived values for Na, Ca and Si. To maximize the data spread and separation, the following values were used: Na, 2Ca and (Si-16), and tested on analyses made by conventional techniques collected from the literature. As shown in Figure 5.6 this plot descriminates well between the different species. The potassium-rich varieties are easily identifiable chemically.

Data from Macquarie Island plotted on this zeolite discrimination diagram are shown in Figure 5.7 with the fields from the literature review. This information was then combined with the XRD results as a basis for optical studies and ten species were found to be present. These are listed in Table 5.2 with ideal chemical formula, using the classification described by Flanigen (1977). Macro- and microscopic properties are also given in Table 5.2.

Zeolites: occurrence and chemistry

Thomsonite is the most abundant zeolite species. In a pure form it occurs as coarse interlocked bladed crystals which are clear and show birefringence up to low second order. It is found principally in

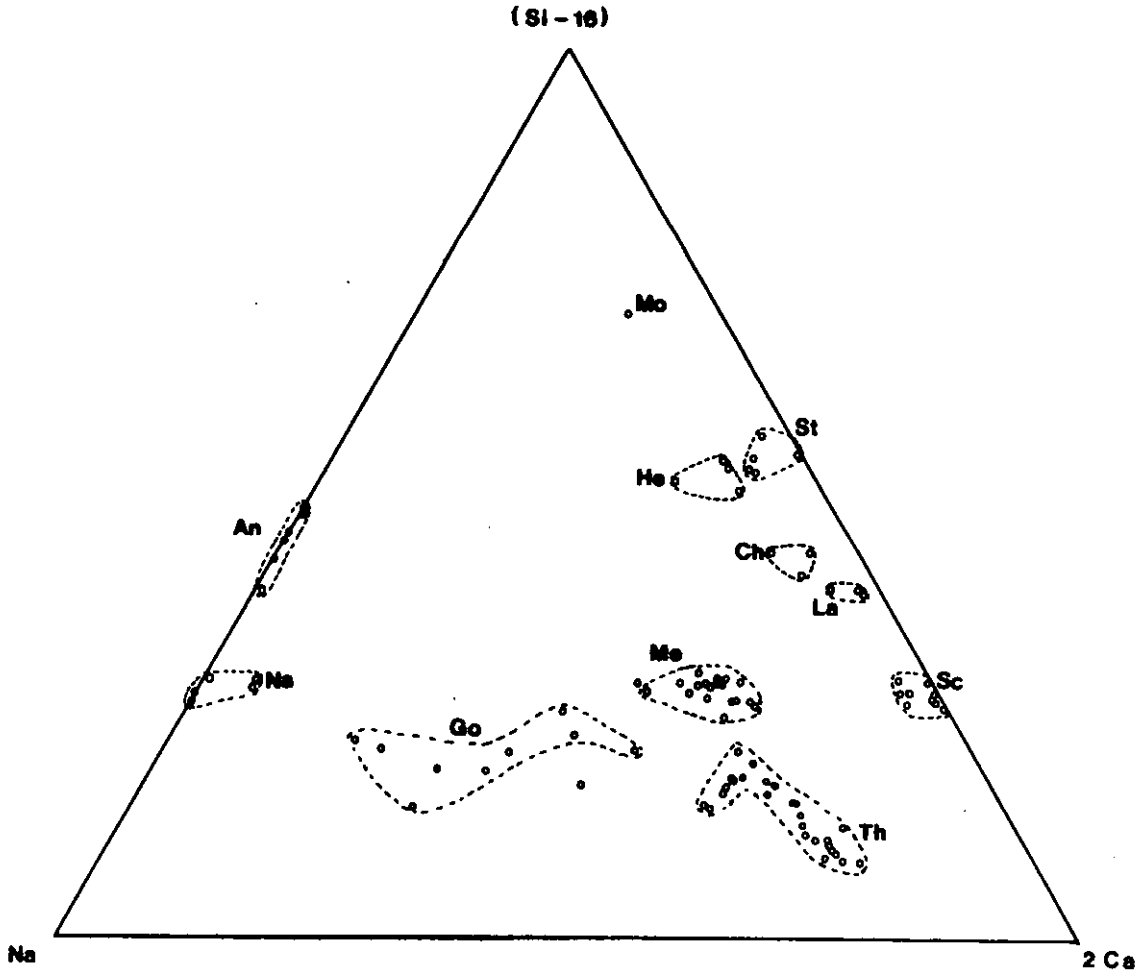

Figure 5.6 Compositional fields for zeolites on a Na:2Ca:(Si-16) plot. Cation values from structural formulae based on 72 oxygen are used.

An	analcite	La	laumontite	Sc	scolecite
Ch	chabazite	Me	mesolite	St	stilbite
Go	gonnardite	Mo	mordenite	Th	thomsonite
He	heulandite	Na	natrolite		

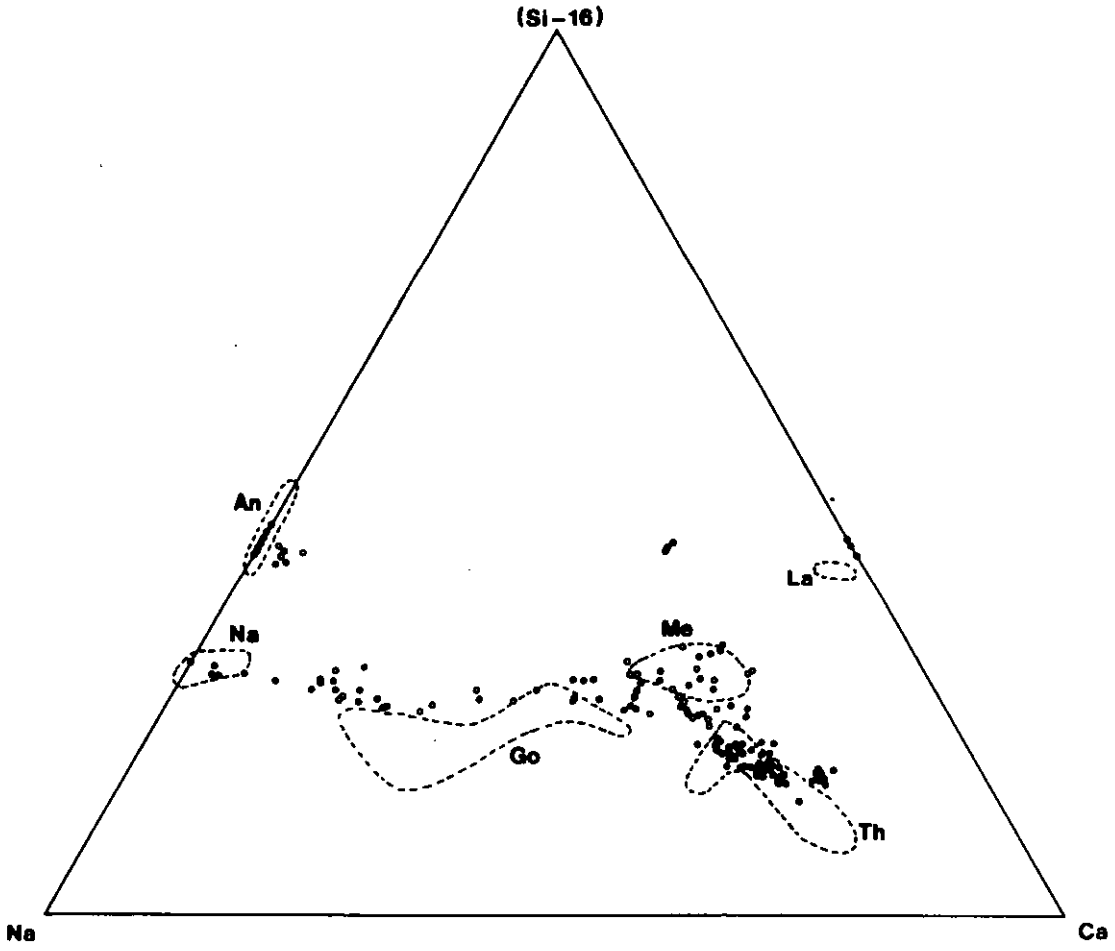

Figure 5.7 Zeolite analyses from Macquarie Island lavas plotted on a Na-2Ca-(Si-16) cation plot. Compositional fields are from Figure 5.6. Abbreviations as for Figure 5.6

Table 5.2

ZEOLITE STRUCTURES AND OPTICAL PROPERTIES IN MACQUARIE ISLAND ROCKS

Structural Group*	Name		Form	Colour
GROUP 1 S4R	1. Analcite	$Na_{16}[(AlO_2)_{16}(SiO_2)_{32}].16H_2O$	massive	clear
	2. Wairakite	$Ca_8[(AlO_2)_{16}(SiO_2)_{32}].16H_2O$	massive	clear
	3. Phillipsite	$(K,Na)_{10}[(AlO_2)_{10}(SiO_2)_{22}].20H_2O$	tabular radiating	clear-white
	4. Laumontite	$Ca_4[(AlO_2)_8(SiO_2)_{16}].16H_2O$	coarse tabular	clear-white
GROUP 2 (T_5O_{10})	1. Natrolite	$Na_{16}[(AlO_2)_{16}(SiO_2)_{24}].16H_2O$	acicular	clear
	2. Mesolite	$Na_{16}Ca_{16}[(AlO_2)_{48}(SiO_2)_{72}].64H_2O$	radiating fine fibrous intergrowths.	white-brown
	3. Thomsonite	$Na_4Ca_8[(AlO_2)_{20}(SiO_2)_{20}].24H_2O$	tabular	white
GROUP 7 ($T_{10}O_{20}$)	1. Heulandite	$Ca_4[Al_8Si_{28}O_{72}].24H_2O$	bladed	white
	Associated hydrated calcium silicates			
	1. Gyrolite ("glimmer" zeolite)	$Ca_2Si_3O_7(OH)_2.H_2O$	platey	white
	2. ?Hillebrandite	$Ca_2SiO_3(OH)_2$	curved sheaves	white

* Groups from Flanigen (1977).

amygdules, generally associated with other zeolites and is apparently the last phase to form as it is developed on the outer edges of other zeolite species and often the crystals are interlocked with cavities between the central crystals. Chemically it shows a fairly limited compositional range with the major variation being in Ca (Table 5.3, Figure 5.7). Excluding wairakite, and laumontite and heulandite, it is the most Ca-rich of the zeolites present, with relatively low Si and high Al.

The next most abundant material is a fine fibrous form which is generally a turbid brownish colour due to minute inclusions. It displays low birefringence of the first order and the fibres show parallel or subparallel (0-5°) extinction. XRD results from this material are not conclusive in that they indicate the presence of natrolite, mesolite, and thomsonite. Chemically this material shows a wide compositional range from a thomsonite end member towards a natrolite end member (Figure 5.7). A colour variation towards a clear form also exists in some specimens and this clearer material approaches the thomsonite compositional field. Thus this material is recognized as a fine intergrowth of these three zeolite species: natrolite, mesolite and thomsonite in varying proportions, as indicated by the compositional range.

Analcite is also very common, in amygdules, veins and replacing primary plagioclase. In form it is massive and clear with low relief and undulose low first-order birefringence. No major cleavages or partings are present and twinning, if present, is a poorly developed simple variety and in this alone can it be distinguished optically from its calcium-analogue, wairakite. Chemically it has a restricted composition (Figure 5.7, Table 5.3) and it is notably a Si-rich phase (~54 wt.% SiO_2), as well as being a pure Na species. When present with other zeolites analcite occurs near the rims of the amygdules, bordering

Table 5.3a

REPRESENTATIVE MICROPROBE ANALYSES OF GROUP I ZEOLITES

Zeolite	Analcite		Wairakite		Phillipsite		Laumontite	
Sample No.	1	7	1	1	38190	38190	226	227
Analysis No.	A-A-2	B-M-2	A-W-1	A-W-2	B-P-2	B-P-1	B-L-1	D-Z-4
SiO_2	54.61	53.83	48.71	48.39	45.52	44.97	51.13	50.06
Al_2O_3	22.16	22.10	21.54	21.28	21.28	20.69	20.69	21.11
CaO	-	-	7.23	7.18	1.44	1.33	11.19	11.40
Na_2O	13.43	13.06	3.60	3.38	8.44	7.54	-	-
K_2O	0.24	0.25	0.75	0.84	5.14	5.23	0.57	0.58
Total	90.45	89.25	81.83	81.07	81.85	79.74	83.58	83.14
	Structure based on 72 oxygens							
Si	24.33	24.29	23.82	23.89	23.13	23.36	24.35	24.04
Al	11.64	11.76	12.42	12.38	12.74	12.67	11.61	11.94
Ca	-	-	3.79	3.80	0.78	0.74	5.71	5.86
Na	11.54	11.42	3.41	3.24	8.31	7.59	-	-
K	0.14	0.14	0.47	0.53	3.33	3.47	0.34	0.35
Total	47.70	47.61	43.91	43.84	48.29	47.83	42.01	42.18
	Charge balance*							
Si+Al	35.97	36.05	36.24	36.27	35.87	36.03	35.96	35.97
Na+K+2Ca	11.73	11.56	11.46	11.37	13.22	12.54	11.76	12.07

* ideally (Si+Al) = 36 and (Na+K+2Ca) = Al.

Table 5.3b

REPRESENTATIVE MICROPROBE ANALYSES OF GROUP 5 ZEOLITES

	Natrolite			Thomsonite (coarse)				Thomsonite (fine)			
Sample No.	117	38299	157	1	7	38191	117	1	60	38190	38190
Analysis No.	B-N-1	B-N	Nat.	C-C-2	C-2	A-C-1	A-F-1	A-T-1	C-1	F-B-1	A-F-3
SiO_2	45.63	41.61	45.74	39.60	39.49	40.15	38.01	42.91	41.93	42.36	41.99
Al_2O_3	25.92	24.13	25.81	27.91	27.83	27.93	30.04	25.91	27.08	25.23	25.92
CaO	0.50	1.04	-	11.04	10.93	10.97	03.05	8.59	10.33	6.65	7.44
Na_2O	15.64	13.44	15.81	4.73	4.84	4.73	4.15	6.23	5.03	8.16	7.49
K_2O	0.25	-	-	-	-	0.28	-	-	-	-	-
Total	87.95	80.20	87.36	83.28	83.09	84.07	85.25	83.64	84.35	82.39	82.85
	Structure based on 72 oxygens										
Si	21.48	21.40	21.60	19.67	19.66	19.77	18.60	21.03	20.45	21.13	20.84
Al	14.38	14.63	14.37	16.34	16.34	16.21	17.33	14.97	15.56	14.83	15.17
Ca	0.25	0.57	-	5.88	5.83	5.79	6.85	4.51	5.40	3.55	3.96
Na	14.27	13.40	14.50	4.56	4.68	4.52	3.94	5.92	4.75	7.89	7.21
K	0.15	-	-	-	-	0.17	-	-	-	-	-
Total	50.53	50.00	50.46	46.45	46.51	46.46	46.72	46.43	46.16	47.40	47.18

Table 5.3c

REPRESENTATIVE MICROPROBE ANALYSES OF GYROLITE AND ?HILLEBRANDITE

	Gyrolite				?Hillebrandite		
Sample No.	11	11	11	Reference*	38188	38188	38188
Analysis No.	1	2	4		F-E-1	F-E-2	F-Ep-7
SiO_2	51.26	52.09	51.26	50.70	53.76	56.30	55.32
Al_2O_3	1.61	1.63	1.38	1.48	4.65	4.38	3.36
MgO	0.91	1.51	1.11	0.18	-	0.76	-
CaO	30.28	29.71	29.48	33.24	30.94	30.32	30.78
Na_2O	-	0.46	-	-	-	-	-
K_2O	-	-	-	-	3.61	3.19	4.48
Total	84.05	85.39	82.80	85.82	92.96	94.95	93.94
	Structure based on 32 oxygens						
Si	11.79	11.77	11.87	11.60	11.38	11.55	11.61
Al	0.44	0.43	0.38	0.40	1.16	1.06	0.83
Mg	0.31	0.51	0.38	0.06	-	0.23	-
Ca	7.46	7.20	7.31	8.15	7.01	6.66	6.92
Na	-	0.20	-	-	-	-	-
K	-	-	-	-	0.98	0.84	1.20
Total	20.00	20.11	19.94	20.20	20.53	20.34	20.57

* Palache *et al.* (1951)

the smectites, and in these cases is the first zeolite to crystallize from the altering fluid. This is a widespread phenomenon through the samples.

Wairakite is far less abundant, having been observed in only six samples. Optically it is identical to analcite except for typical multiple twinning. Chemically it has a narrow field which is intermediate between compositions given by Seki *et al.* (1969) and analcite.

Natrolite is generally found as fine elongate prisms in matted aggregates. It is particularly abundant in the Pyramid Peak area in vein networks up to 7 cm in width, with individual veins of up to 2 cm. In this area the growth of natrolite and associated zeolites, principally the intergrown natrolite-mesolite-thomsonite material, along fractures in the rocks has caused minor brecciation in the vicinity of the vein systems. These zones may represent major channelways for the altering fluid. The compositions of the analyzed natrolites are also given in Figure 5.7 and Table 5.3, falling within the field of analyses obtained from the literature.

Phillipsite is the only zeolite species common to both ocean-floor weathering and zeolite facies grades of metamorphism (Boles, 1977). In 38190 it occurs in amygdules as massive clear material with a very high 2V, low birefringence and simple twinning. The similarities to albite, K-feldspar, analcite and wairakite are obvious. Chemically it is immediately distinguishable by its K_2O content (Table 5.3). Phillipsites reported from DSDP sites generally are less calcic than those from Macquarie Island but comparable analyses are reported (Table 5.4) and this is shown in Figure 5.8, using Ca, Na and K cation components from structural formula calculations based on 72 oxygens (to avoid analysis total errors).

Laumontite has been found only in veins, up to 2 cm wide, in the undeformed samples. Laumontite is not associated with the other described

Table 5.4

PHILLIPSITE ANALYSES FROM LITERATURE

Reference No.	1	1	1	1	1	1	1	1	1	2	2	3	3	3	3
SiO_2	51.35	53.92	53.30	53.33	52.80	55.30	55.18	56.06	55.96	44.39	45.95	56.36	46.44	57.70	56.54
Al_2O_3	19.98	17.40	17.00	18.28	17.86	17.78	17.72	19.28	18.82	22.19	22.57	19.23	26.28	18.65	19.12
FeO	0.41	-	0.19	-	-	-	-	-	-	-	-	0.06	0.20	0.13	0.14
MgO		-	-	-	-	-	-	-	-	0.03	-	-	-	-	-
MnO		-	-	-	-						0.07	-	-	-	-
CaO	0.60	-	0.13	-	0.32	0.13	0.36	0.10	0.16	5.21	5.03	0.26	0.52	0.16	0.10
Na_2O	2.88	5.90	4.09	3.86	3.99	2.42	2.82	3.72	3.33	4.44	4.05	5.26	4.00	6.36	3.80
K_2O	8.38	7.04	8.91	7.97	8.52	7.45	7.58	7.90	7.80	4.71	4.51	7.19	5.54	5.40	5.92
P_2O_5	-	-	-	-	-	0.25	0.27	-	-	-	-	-	-	-	-
Total	83.60	84.27	83.62	83.44	83.49	83.31	83.94	87.06	86.06	81.04	82.12	88.36	82.98	88.40	85.62
	Structure based on 72 oxygens														
Si	25.13	26.08	26.18	25.78	25.89	26.58	26.44	26.04	26.24	22.67	22.96	25.89	22.67	26.25	26.34
Al	11.52	9.92	9.84	10.50	10.32	10.08	10.02	10.56	10.40	13.36	13.30	10.41	15.12	10.00	10.50
Fe	0.17	-	0.08	-	-	-	-	-	-	-	-	0.02	0.08	0.05	0.05
Mg	-	-	-	-	-	-	-	-	-	0.02	-	-	-	-	-
Mn											0.03	-	-	-	-
Ca	0.32	-	0.08	-	0.17	0.06	0.19	0.05	0.08	2.85	2.69	0.13	0.27	0.08	0.05
Na	2.73	5.54	3.90	3.65	3.79	2.25	2.63	3.35	3.03	4.40	3.92	4.69	3.79	5.61	3.43
K	5.23	4.34	5.58	4.95	5.33	4.56	4.64	4.68	4.66	3.07	2.88	4.21	3.45	3.13	3.52
P						0.09	0.11								
Total	45.10	45.88	45.66	44.88	45.50	43.62	44.03	44.68	44.41	46.37	45.78	45.35	45.38	45.12	43.89

1. Pritchard *et al.* (1979)
2. Robinson *et al.* (1977), Table 6.
3. Barager *et al.* (1977), Table 2.

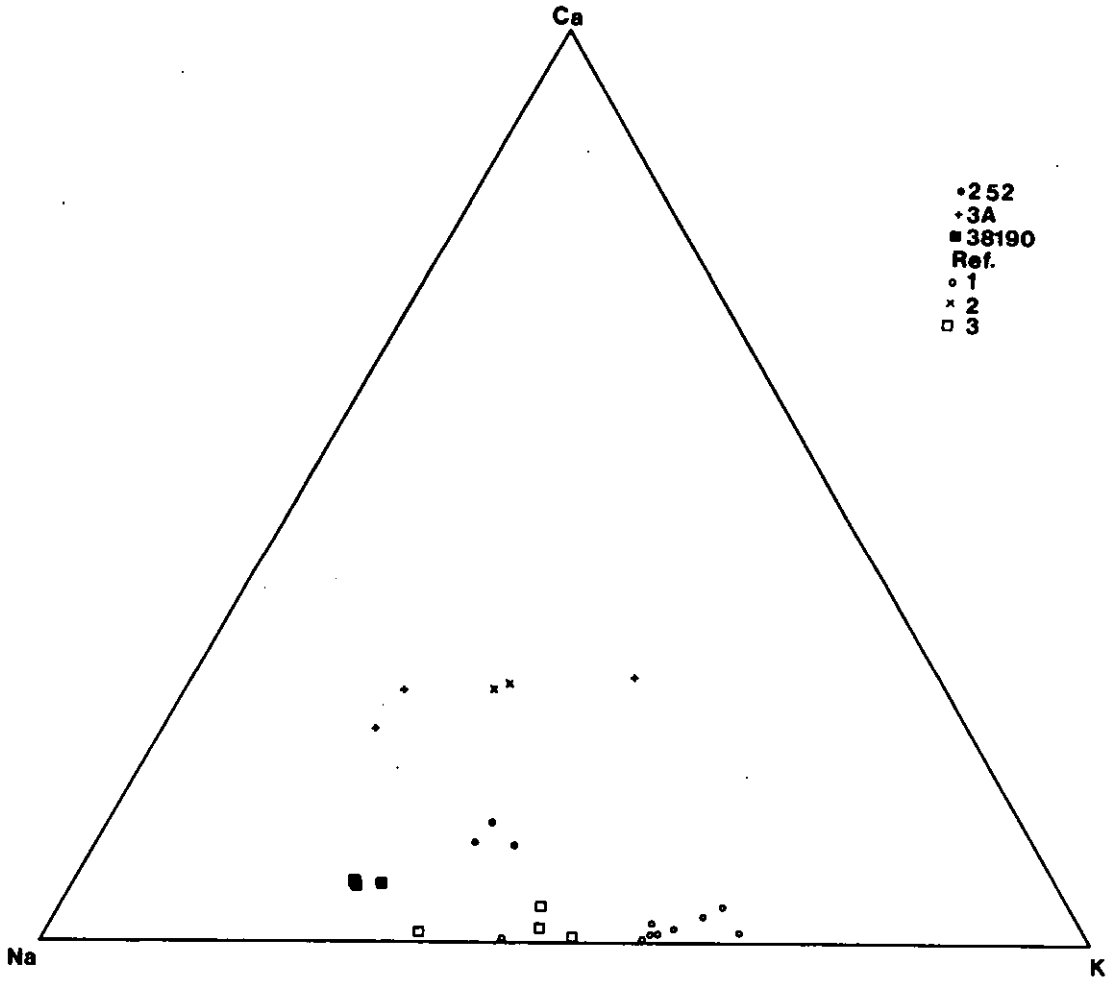

Figure 5.8 Phillipsite analyses from Macquarie Island lavas and modern ocean-floor basalts. References are as for Table 5.4.

zeolites and is found in rocks containing assemblages transitional to lower greenschist facies grades of metamorphism and represents the highest grade of zeolite facies metamorphism. The best example is sample 440 from the south coast of Macquarie Island or where massive veins of laumontite and calcite cut pillow lavas. In places these veins open up to form vugs with linings of bladed laumontite and calcite. In other areas it is found in sheared basalt zones almost totally replacing the original mineralogy (Plate 5.3, sample 226). Compositionally it is identical to other reported analyses (Table 5.3, Figure 5.7).

The final two phases recognized, heulandite and gyrolite, have unique occurrences. Heulandite, confirmed by XRD results, occurs with natrolite as white bladed crystals up to 7 mm x 1.5 mm in veins from the Pyramid Peak area. Gyrolite, an exotic phase, also referred to as truscottite or "glimmer" zeolite, is found in a large vug in pillow lavas just north (~300 m) of Green Gorge on the east coast. The vug consists of a lining of white radiating thomsonite-mesolite intergrowths almost completely filled by white pearly subradiating aggregates of gyrolite with a small central cavity containing yellowish dogstooth calcite. Compositionally (Table 5.3c) it is notable in that it is a high Si,Ca phase and it is also interesting that the three analyses presented by Palache *et al.* (1951) are identical even though they were obtained over the period 1851-1889.

Another hydrated calcium silicate has also been found in the Green Gorge area. Sample 38188, a pillow lava, contains small vesicles filled with white curved fibrous sheaves, colourless in thin section, with low birefringence, undulose subparallel extinction and moderate relief. Chemically (Table 5.3) it is similar to gyrolite but distinctly higher in Al and K.

Plate 5.3 Coarse laumontite grains filling a vein rimmed by small euhedral albite crystals. Scale: 1 cm = 0.1 mm. Sample 226. Crossed nicolls.

Plate 5.4 Euhedral calcite rhombs rimmed by brown smectites in a zeolite filled amygdule. The intergrown, brown thomsonite-mesolite-natrolite and clear, bladed thomsonite are the zeolites present. Scale: 1 cm = 0.7 mm. Sample 157.

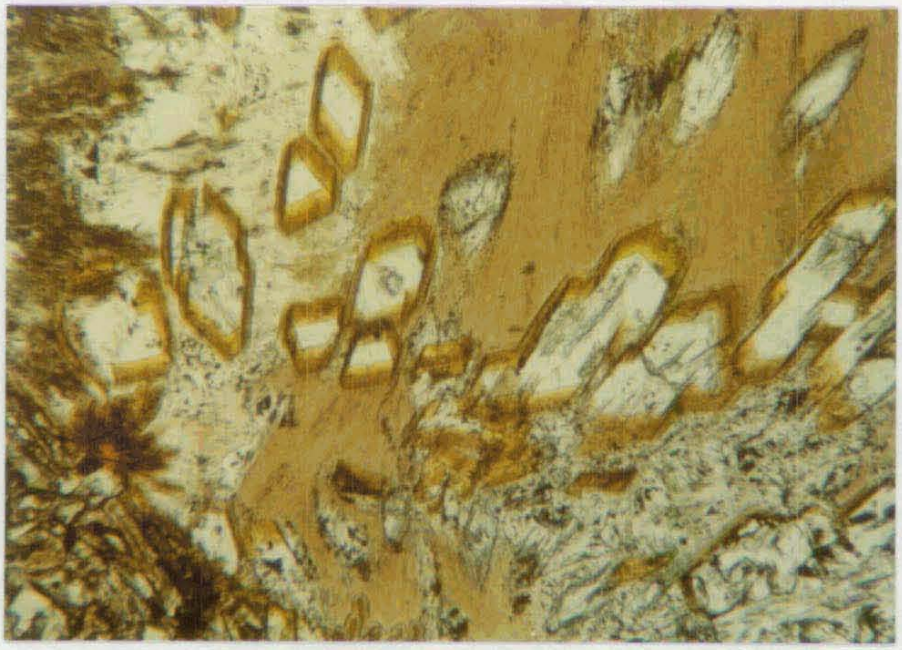

Smectites

Smectites occur in the groundmass and as rims in vesicles, similar in paragenesis to smectites in DSDP leg 49 rocks (Pritchard *et al.*, 1979). Again two forms are present, one a massive yellow-orange brown species which commonly forms botryoidal rims to the amygdule growing into the centre, the second being an overgrowth of pale green fibrous material (Plate 5.17). The deep colour of the massive material masks its optical properties. The pale green fibrous material is optically identical to the material described on the OFW samples.

Chlorite

Chlorite is rare in zeolite facies rocks, occurring only in those samples that are transitional to greenschist facies metamorphism. It occurs as pale green fibrous sheaves with "typical" anomalous birefringence, rimming and filling amygdules and in the groundmass, where it replaces olivines and interstitial glass.

Calcite

This phase occurs throughout the assemblages, most commonly filling vesicles with smectite rims. In some samples, e.g. 156c, calcite occurs as coarse granular spar material and also in a fibrous radiating form full of microscopic inclusions, often opaque, giving these calcite rosettes a very turbid appearance. A thin layer of sparry calcite is often present on the edges of the rosettes with incipient dogstooth development. In other samples, e.g. 157, spar calcite is present as coarse separate crystals, generally rhombohedral in section but occasionally showing hexagonal sections (Plate 5.4). Smectite rims are present on these coarse crystals, generally the fibrous green variety but occasionally a thin massive yellow-brown rim pre-dates the fibrous lining. Zeolites occupy the rest of the amygdule.

Minor phases

Sericite occurs within altered plagioclase, both groundmass and phenocrysts. K-feldspar is also present in these areas as well as occurring rarely in veins. Albite occurs in veins, commonly with calcite but is only present in the rocks transitional to greenschist facies metamorphism.

5.4.3 Lower greenschist facies alteration

Distribution

Rocks of this metamorphic grade are the most abundant on Macquarie Island (Figure 5.1). They occur as a narrow strip on the isthmus between North Head and the main part of the island in the north and then extend in a zone down the west coast from the Eagle Point-Langdon Point area to the major fault at Sandell Bay. The southern block of pillow lavas is almost entirely composed of lower greenschist facies rocks. These areas include the previously reported occurrences and no conflicting results have been obtained.

Mineralogy and metamorphic petrography

It is firstly necessary to define the principal features of lower greenschist facies metamorphism in these samples. Smewing (1975) lists five features which mark the incoming of the greenschist facies:

"1. The smectite mineral takes on a much clearer appearance due to the loss of goethite and is eventually replaced by chlorite which occurs in light green flakes up to 0.25 mm long.

2. Titanomagnetite is rimmed by sphene.

3. Plagioclase feldspar (labradorite - An_{60}) is rimmed by a less calcic plagioclase, typically in the andesine range (An_{30-50}) and is subsequently sericitized.

4. Secondary quartz is formed and may interact with the plagioclase feldspar to form albite, back-veining the quartz.

5. Disappearance of zeolites."

Smewing (1975) also noted the presence of quartz, epidote, pyrite, calcite and clinozoisite towards the top of the greenschist facies, with actinolite becoming an essential mineral at depth. Coleman (1977) recognized these mineralogical changes, apart from Smewing's (1975) point three, which he did not mention. Although sericitization of the feldspar is undoubtedly a feature of this style of alteration, rims of An_{30-50} are a primary crystallization feature of tholeiites in general, as they are in the Macquarie Island samples (Chapter 4), and not necessarily a metamorphic feature.

In the Macquarie Island samples the phases typical of lower greenschist facies metamorphism are:

chl + sph + ab ± ep ± k-feld ± mag ± ser ± preh

As indicated, the first three phases are ubiquitous, with varying abundance of the other phases present. The extent of alteration of samples within this grade is extremely variable. In some samples cpx and spinel are the only relict phases with all other phases replaced whereas in others, e.g. 56, from the Mawson Point area, only interstitial glass, olivines, and rims of the plagioclase feldspars and titanomagnetites are affected, the rocks appearing unaltered at first glance (Plate 5.5).

Chlorites

Chlorites are ubiquitous in this grade of metamorphism and are found in the groundmass, rimming and filling amygdules, and in veins. In form they are generally typical, occurring as pale green fibrous subradiating sheaths with low birefringence, commonly the distinctive "anomalous" Berlin blue colour. The fibres vary in size up to 0.2 mm long. Some are difficult to distinguish from green smectites and as an identification check some chlorites were hand-picked and studied using XRD techniques: all are Mg-chlorites (Appendix 5). Electron microprobe analyses were collected from a number of samples, including some of the XRD sample set, and results are summarized in Table 5.5.

Plate 5.5 Fibrous actinolite, sphene and chlorite developed in interstitial glass (middle left and right areas of photo) in a medium grained tholeiitic lava. Pale yellow granular augite encloses
low relief plagioclase, with minor subhedral titan-magnetite. Scale: 1 cm = 250 μm. Sample 56.

Plate 5.6 Strongly pleochroic brown-olive green Ti-rich chlorite developed near opaque, primary titanmagnetite. Mg-chlorite is present as a matrix to the low relief, pale feldspar and high relief, pale brown augite. The lava has been strongly altered under lower greenschist facies conditions. Scale: 1 cm = 0.1 mm.
Sample 227.

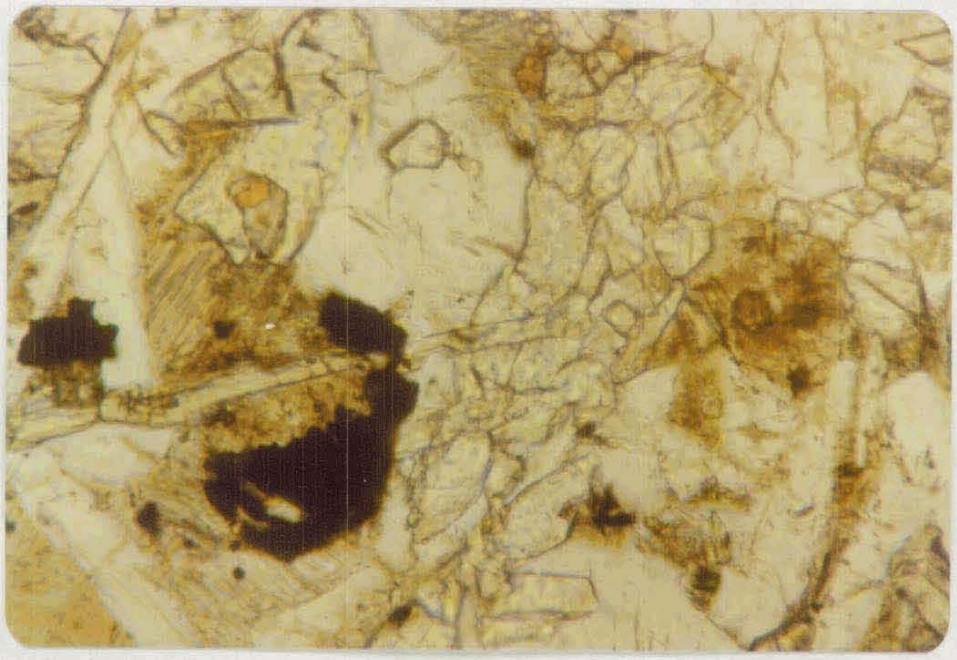

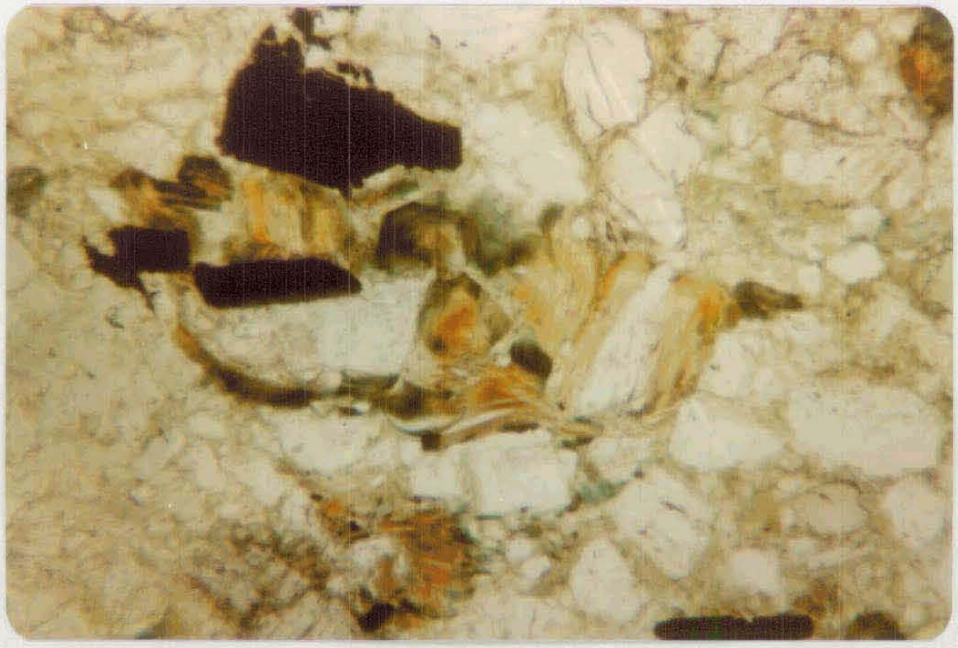

Table 5.5a

REPRESENTATIVE MICROPROBE ANALYSES OF MIXED-LAYER SILICATES

Sample No.	64	428B	200	423	50	221	214	55A	55A	147A	147A
Analysis No.	A-1	C-2	C-1	A-2	E-2	A-3	C-2	4	3	C-1	C-2
SiO_2	41.96	31.72	41.33	32.02	31.13	31.54	31.44	33.57	32.93	29.39	29.36
Al_2O_3	7.45	15.66	10.43	14.83	15.02	16.83	15.49	14.99	14.44	16.49	16.84
Fe	3.85	10.91	15.88	14.34	16.53	18.49	19.26	20.82	23.55	24.85	25.20
MnO	-	0.36	-	0.31	-	0.16	0.19	0.15	-	0.19	0.17
MgO	23.15	23.41	17.34	23.31	22.70	20.71	22.78	18.99	19.04	17.27	17.81
CaO	1.00	0.25	1.57	0.32	0.34	0.36	0.22	0.34	0.31	0.22	0.23
Na_2O	0.50	-	-	-	-	-	-	-	-	0.29	0.26
K_2O	0.20	-	0.57	-	-	-	-	-	-	-	-
Total	78.11	82.32	87.11	85.52	85.73	88.73	89.39	88.87	90.27	88.70	89.87
	Structure based on 28 oxygens										
Si	8.61	6.54	8.13	6.59	6.37	6.32	6.26	6.72	6.60	6.09	6.01
Al	1.80	3.81	2.42	3.53	3.62	3.98	3.63	3.54	3.41	4.03	4.06
Fe	0.66	1.88	2.61	2.39	2.83	3.10	3.20	3.49	3.94	4.31	4.31
Mn	-	0.06	-	0.05	-	0.03	0.03	0.03	-	0.03	0.03
Mg	7.08	7.20	5.09	7.02	6.92	6.19	6.75	5.67	5.68	5.33	5.43
Ca	0.22	0.06	0.33	0.07	0.07	0.08	0.05	0.07	0.07	0.05	0.05
Na	0.20	-	-	-	-	-	-	-	-	0.12	0.10
K	0.05	-	0.14	-	-	-	-	-	-	-	-
Total	18.62	19.55	18.73	19.65	19.82	19.69	19.93	19.51	19.70	19.96	20.01

Table 5.5b

MICROPROBE ANALYSIS OF Ti-RICH MIXED-LAYER SILICATE

Sample No. 227 Analysis No.	A-2	D-C	B-2	4	A-C-2
SiO_2	28.60	27.30	28.99	30.27	28.04
TiO_2	0.65	1.17	1.53	1.82	2.47
Al_2O_3	11.92	9.20	13.38	13.40	13.98
FeO	17.14	31.57	24.87	16.83	14.32
MnO	-	-	0.32	-	0.52
MgO	19.48	15.26	16.68	22.12	23.51
CaO	0.65	-	0.78	0.63	0.59
Total	78.47	84.47	86.56	85.07	85.51
	Structure based on 28 oxygen				
Si	6.49	6.28	6.21	6.29	6.17
Ti	0.11	0.20	0.25	0.28	0.38
Al	3.19	2.49	3.38	3.28	3.37
Fe	3.26	6.07	4.46	2.93	2.45
Mn	-	-	0.06	-	0.09
Mg	6.59	5.23	5.33	6.85	7.17
Ca	0.16	-	0.18	0.14	0.13
Total	19.80	20.27	19.85	19.78	19.76

The FeO vs MgO plot has been used by various workers (e.g. Pritchard *et al.*, 1979) to present this type of data as this plot involves no assumptions on Fe^{2+}/Fe^{3+} ratios. The Macquarie Island data are presented on this plot in Figure 5.9, where a striking covariance of FeO and MgO is apparent within the data, for material both from the greenschist grade and from lower grades of metamorphism. The chlorite analyses from greenschist facies rocks range from high iron (~24 wt.% FeO) and moderate magnesium (~17 wt.% MgO), to low iron (~10 wt.% FeO) and high magnesium (~24 wt.% MgO) compositions. Analyses from individual samples (Figure 5.10) have limited compositional ranges with the exception of chlorites in sample 227 which span the entire FeO-MgO ranges. The chlorites from sample 227, however are unique amongst the Macquarie Island varieties in that they contain considerable and variable concentrations of TiO_2 (0.65-2.69 wt.%, Table 5.5b). The TiO_2 is covariant with FeO and MgO. These chlorites are also unique in that they are strongly pleochroic from a deep yellow-brown to olive green, depending on section and also show a colour zoning (Plate 5.6). The occurrence and chemistry of these are not understood.

The variation in FeO/MgO of the chlorites is related to their level of metamorphism. Samples with high Mg chlorites, e.g. 428B and 423, show (within the greenschist facies) the lowest grade of metamorphism with only minor development of albite and sphene rims around titanmagnetite. With increasing FeO/MgO of the chlorites, epidote appears and becomes abundant, followed in the highest grades of metamorphism by the development of actinolitic amphibole as beards on clinopyroxenes or as a minor component of amygdule assemblages, e.g. 212, 55A. These samples have the highest FeO/MgO in the chlorites, with the exception of 147A. Sample 147A contains chlorites with the highest FeO/MgO but does not contain any secondary amphibole. However it is extensively altered with albite, K-feldspar and sericite replacing plagioclase feldspar and

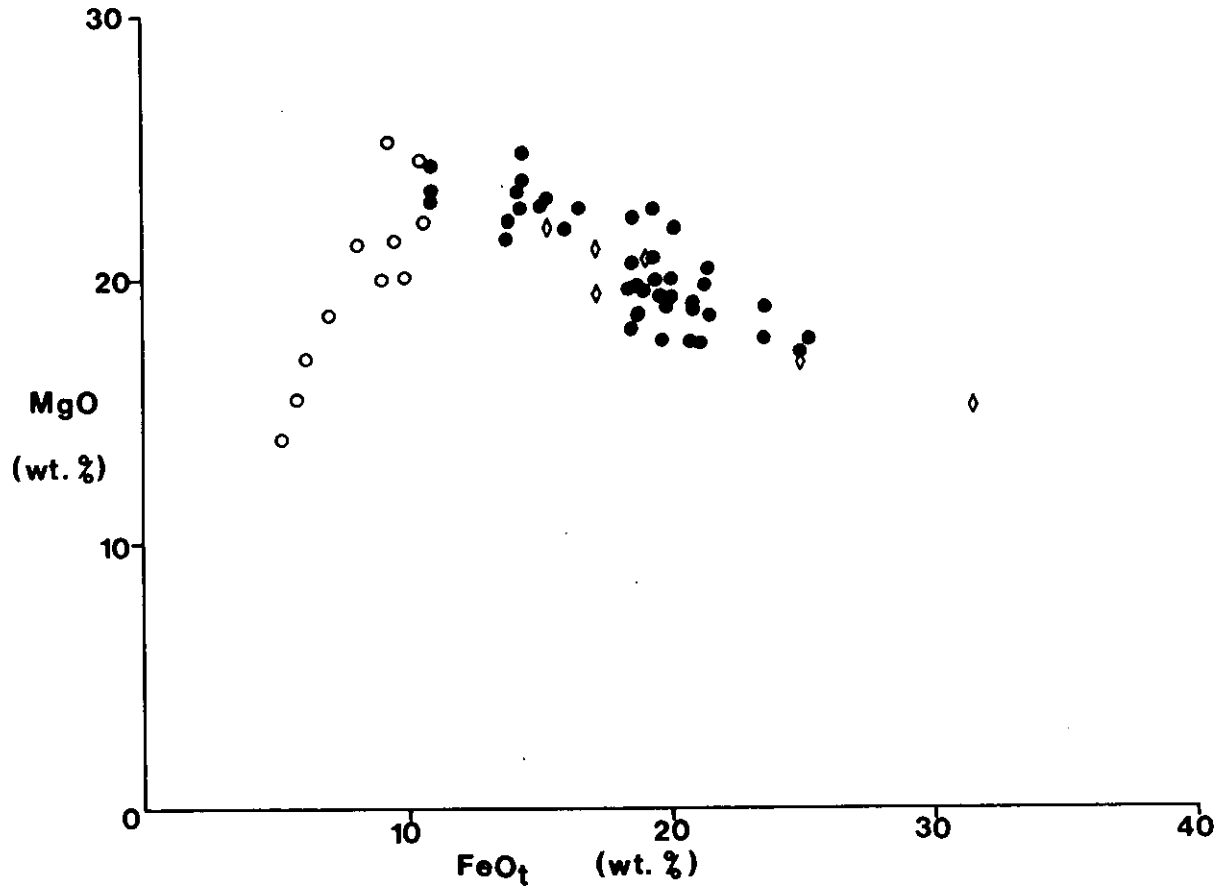

Figure 5.9 FeO vs. MgO plot for "chlorites" from Macquarie Island lavas from different metamorphic grades. Key: o - zeolite facies, ● - greenschist facies, ◊ Ti-rich chlorite.

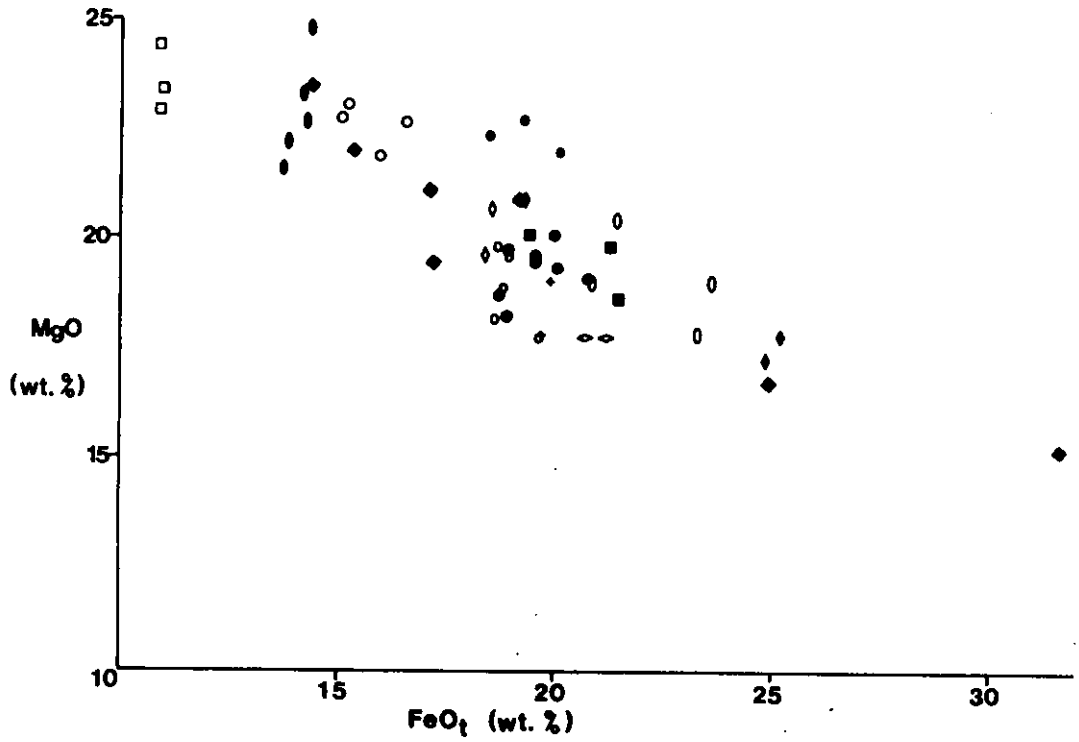

Figure 5.10 FeO vs. MgO plot for chlorites from individual lavas that have undergone lower greenschist facies metamorphism. Different symbols represent different samples.

chlorite, epidote, albite and K-feldspar abundant in veins and amygdules, indicating that it is high within this grade of metamorphism and thus reasonably consistent with the previous observations.

Secondary feldspars

Albite and K-feldspar occur as replacements of primary plagioclase feldspar, both as phenocrysts and in the groundmass, and in veins and amygdules. They are generally intergrown as small subhedral to anhedral crystals in random orientations except in veins where they may form cockscomb intergrowths away from the edges of the veins. The extent of replacement of the primary plagioclase is variable and where complete the rocks have a typical "spilite" appearance with a relict clinopyroxene and spinel set in a low relief matrix of K-feldspar, albite and chlorite, with minor proportions of higher relief secondary phases including epidote and sphene. They are chemically uniform (Table 5.6). Minor chemical variations may be a result of small inclusions being present in the analyzed area although care was taken to avoid the visible inclusions.

Prehnite

This phase is present in a number of samples and is not restricted in location, i.e. it occurs replacing feldspars, and in veins and amygdules. It is found both as massive anhedral grains and as interlocked blades. Bow-tie structures are fairly rare. Generally it is only a minor component but it occasionally is very abundant and samples from location 134 at Caroline Cove on the southwest corner of Macquarie Island are composed of up to 70 wt.% prehnite in a dense vein system along a minor shear zone. This occurrence is similar in form to that of laumontite in sample 226.

Compositionally (Table 5.7) analyzed prehnites are fairly uniform and are stoichiometric. The only substitution is of Fe^{3+} for Al^{3+} (Table 5.7), as noted by Deer *et al.* (1966), and the analyzed samples range up to 4.46 wt.% FeO (total iron) from a low of 0.45 wt.%.

Table 5.6

REPRESENTATIVE MICROPROBE ANALYSES OF ALBITE AND K-FELDSPAR

	Albite				K-feldspar			
Sample No.	147A	214	221	423	50	64	147A	214
Analysis No.	A-B-1	C-1	A-A-1	A-1	K-A	A-O-2	A-K-2	C-4
SiO_2	67.89	66.42	67.43	67.17	63.75	64.01	64.71	64.12
Al_2O_3	21.12	20.68	12.59	20.67	18.73	18.21	18.71	18.92
FeO	-	0.13	-	-	-	-	-	-
CaO	1.09	1.53	1.69	1.08	1.23	0.37	-	-
Na_2O	11.59	10.73	10.90	11.40	-	0.13	-	0.27
K_2O	0.14	0.15	0.40	0.37	14.80	16.48	16.71	16.69
Total	101.83	99.66	101.95	100.71	99.08	99.21	100.14	100.01
	Structure based on 32 oxygens							
Si	11.70	11.70	11.62	11.72	11.90	11.96	11.96	11.89
Al	4.29	4.29	4.39	4.25	4.12	4.01	4.08	4.14
Fe	-	0.02	-	-	-	-	-	-
Ca	0.20	0.29	0.31	0.20	0.25	0.08	-	-
Na	3.87	3.67	3.65	3.86	-	0.05	-	0.10
K	0.03	0.03	0.09	0.08	3.53	3.93	3.94	3.95
Total	20.10	20.00	20.05	20.12	19.80	20.03	19.97	20.07
An	5.6	8.0	9.9	6.8	6.60	2.00	-	-
Or	0.75	0.75	2.2	1.9	93.4	96.8	100.	97.5

Table 5.7

REPRESENTATIVE MICROPROBE ANALYSES OF PREHNITE

Sample No.	134	134	212	212	227	425	425	425
Analysis No.	A-1	B-1	C-2	C-1	B-P-1	A-1	A-3	E-2
SiO_2	43.92	44.60	42.42	43.00	42.59	43.53	44.20	42.48
Al_2O_3	23.13	24.05	20.97	22.84	23.47	24.21	24.05	21.99
Fe_2O_3*	1.91	0.66	4.96	1.38	2.00	0.50	0.99	3.90
CaO	26.47	26.68	26.15	26.26	26.58	26.74	26.92	25.31
Total	95.43	96.00	94.50	93.48	94.65	94.97	96.16	93.69
	Structure based on 22 oxygens							
Si	6.07	6.09	6.00	6.06	5.95	6.02	6.04	6.02
Al	3.77	3.87	3.45	3.80	3.87	3.95	3.88	3.67
Fe^{3+}	0.20	0.07	0.53	0.15	0.21	0.05	0.10	0.42
Ca	3.92	3.90	3.96	3.97	3.98	3.96	3.94	3.84
Total	13.96	13.94	13.99	13.97	14.01	13.98	13.97	13.95

Analyses from sample 134 show a range of 0.59-1.72 wt.% FeO with no obvious control on the iron content. In sample 425, prehnite in veins is more iron-rich (~3.5 wt.% FeO) than massive material replacing a plagioclase phenocryst (~0.5-1.0 wt.% FeO): this may reflect a local compositional control with iron more available to the material forming in the veins, than in the plagioclase site. Mid-vein prehnite is low in iron (0.51 wt.% FeO) suggesting that iron has been depleted in the hydrothermal fluid through incorporation in the earlier-formed prehnite.

Epidote

Epidotes in the Macquarie Island samples are pistacitic and thus are a bright yellow and strongly pleochroic. They occur in granular masses and as interlocked bladed crystals and also, frequently, as unusual subradiating coarsely fibrous masses (Plate 5.7). These masses are small (to 0.4 mm) with fibres up to 0.15 mm, and compose only up to ~5% of the secondary phases so although quite common, epidote is only a minor phase. Analyzed epidotes are fairly uniform with ~12.14 wt.% Fe_2O_3 (total iron calculated as Fe_2O_3) within a particular sample and in different samples (Table 5.8).

Sphene

Although not volumetrically a major phase (~1-2% by volume) sphene is ubiquitous in rocks of this grade. It is present as fine granular aggregates, rarely to 0.1 mm across, and as rims on primary Fe-Ti oxides. Optically it is characterized by its granular form and high relief. The extreme birefringence is generally difficult to discern because of the small size and granularity of the sphene. In some of the most altered samples it shows incipient development of characteristic wedge-shaped sections.

A feature revealed by electron microprobe studies is that within these aggregates of the sphene there may also be some epidote. This is not optically recognizable, but is suggested by the presence of iron and

Plate 5.7 Amygdule filled by radiating chlorite (blue-black) and sub-radiating epidote (bright) in an altered tholeiitic lava. Relict clinopyroxene is distinguishable in the groundmass by its moderate birefringence. Scale: 1 cm = 0.1 mm. Sample 214C. Crossed nicolls.

Plate 5.8 Uralitized doleritic dyke from dyke swarm with primary twinning preserved in uralitized clinopyroxene (centre of photo). Primary plagioclase is unaltered during the uralitization event. Scale: 1 cm = 0.3 mm. Sample 38214. Crossed nicolls.

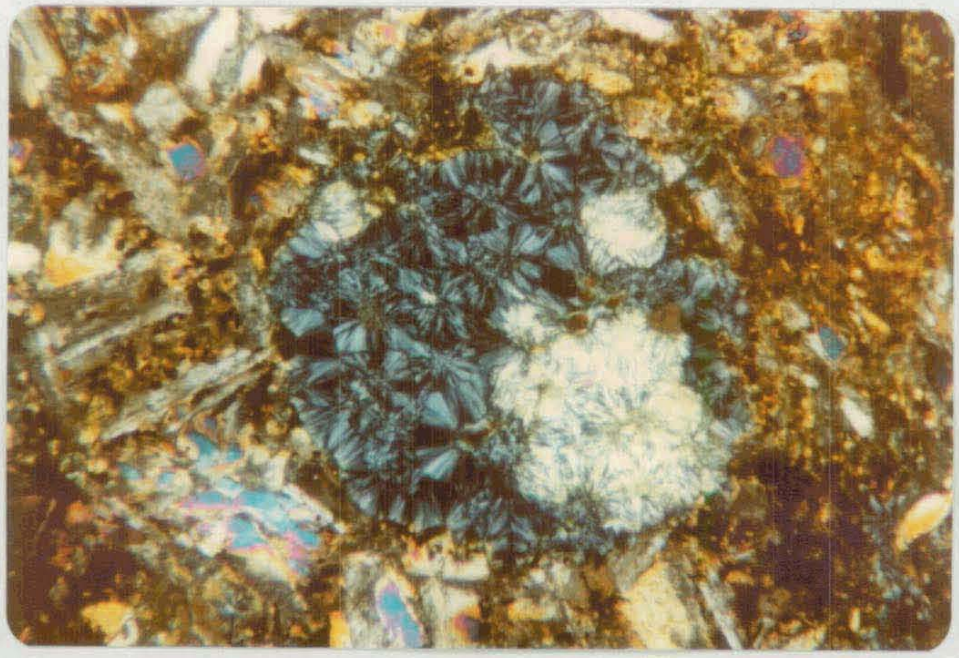

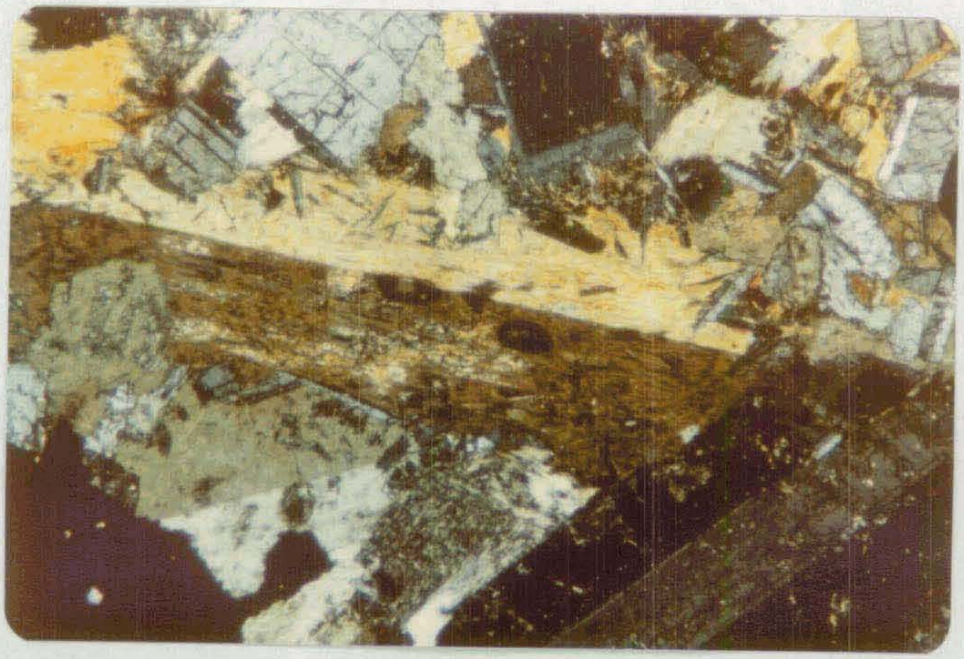

Table 5.8

REPRESENTATIVE MICROPROBE ANALYSES OF EPIDOTES

Sample No.	50	50	214	214	220	220	419	419
Analysis No.	A-1	A-2	C-P-1	C-P-3	A-1	A-2	C-E-1	C-E-2
SiO_2	37.61	37.92	37.34	37.11	37.65	37.33	37.33	38.23
Al_2O_3	25.09	25.06	23.50	23.94	23.75	23.22	23.66	24.02
Fe_2O_3	10.64	10.75	14.15	13.25	13.77	14.11	12.77	12.88
MgO	-	-	1.33	0.84	-	-	-	-
CaO	23.32	23.44	21.74	22.37	22.36	22.35	22.65	22.54
Total	96.66	97.21	98.07	97.51	97.53	97.00	96.41	97.68
	Structure based on 25 oxygens							
Si	6.01	6.03	5.93	5.92	6.00	6.00	6.01	6.06
Al	4.72	4.69	4.40	4.50	4.46	4.40	4.49	4.49
Fe^{3+}	1.28	1.28	1.69	1.59	1.65	1.71	1.55	1.54
Mg	-	-	0.32	0.20	-	-	-	-
Ca	3.99	3.99	3.70	3.82	3.82	3.85	3.91	3.83
Total	16.00	15.99	16.03	16.04	15.93	15.95	15.97	15.92

aluminium in analyses of sphene aggregates (Table 5.8, sample 50). Using the aluminium content as an indication of the epidote component present, epidote was removed from the analysis and then the modified analysis recalculated to the original total. Results are given in Table 5.9, where it can be seen that the residual composition is that of sphene. The epidote composition used was from the same sample. This indicates that epidote may be more widespread than initially apparent in the samples and also that epidote occurrence in this form may not be recognized in studies not using electron microprobe techniques.

5.4.4 Upper greenschist to amphibolite facies metamorphism

These grades of metamorphism are encountered in dykes in the sheeted dyke swarm complexes (Figure 3.1), as noted by Varne & Rubenach (1972). Alteration within the lavas does not reach these high grades. The metamorphic grade varies up to lower amphibolite facies but in general the grade encountered is upper greenschist facies and this is dominated by alteration of the pyroxenes to fibrous actinolitic amphibole or "uralite". At this grade the plagioclase feldspar is not affected but in many samples alteration of this phase has occurred during another distinct metamorphic event. Other phases associated with the upper greenschist "uralitization" are sphene, quartz, tremolite and talc. Chlorite is replaced by amphibole. Secondary phases associated with alteration of plagioclase are prehnite, epidote, albite and minor sericite. In the highest grades attained massive amphibole is developed, an Fe-rich variety, together with veinlets of hornblende and very rarely, allanite.

Mineralogy and metamorphic petrography

Samples both from within the one area and from different areas of dyke swarm show a wide variation in the degree of alteration of the rock, although the secondary mineralogy indicates similar basic metamorphic conditions, i.e. pressure and temperature.

Table 5.9

REPRESENTATIVE MICROPROBE ANALYSES OF SPHENE AND RECALCULATED SPHENE AND EPIDOTE ANALYSES

Sample No.	428B	50	50	50	50
Analysis No.	A-S	D-S-2	D-S-1	Ep-1	D-S-1**
SiO_2	31.92	32.39	32.37	37.61	31.06
TiO_2	28.42	29.71	29.64	-	38.64
Al_2O_3	6.22	5.10	4.93	25.09	-
Fe_2O_3*	1.93	2.36	2.43	10.64	(0.42)
CaO	27.89	27.72	27.66	23.32	28.69
Total	96.38	97.28	97.03	96.66	97.03
	Structure based on 20 oxygen			Structure based on 25 oxygen	
Si	4.27	4.29	4.30	6.01	4.11
Ti	2.86	2.96	2.96	-	3.85
Al	0.98	0.80	0.77	4.72	-
Fe^{3+}	0.19	0.24	0.24	1.28	-
Ca	3.99	3.94	3.94	3.99	4.07
Total	12.29	12.23	12.22	16.00	12.03

* Iron recalculated as Fe_2O_3.

** (i) D-S-1 analysis recalculated after subtraction of 19.65 wt.% Ep-1 and recalculation to previous analysis total.
(ii) residual Fe_2O_3 ignored in structure calculation.

The least-altered samples have actinolite and tremolite developed within chloritized mesostasis and as actinolite beards on clinopyroxenes (Plate 5.9, samples 38443 and 38206), together with saponite replacing olivines and sphene replacing titanmagnetite. Plagioclase feldspar is unaltered except for minor chlorite/saponite development along fractures. With increasing degree of alteration, replacement of the clinopyroxene becomes more extensive until it is all pseudomorphed by pleochroic green fibrous amphibole. The amphibole fibres parallel the long axis of the original crystal with primary twinning being preserved optically (Plate 5.8, samples 38214 and 38446). Amphibole also replaces mesostasis, occurring as fibrous crystals with a randomly oriented interlocking pattern (Plate 5.10, sample 38446). There is no difference chemically between amphiboles from the different environments, as can be seen in Table 5.10. At intermediate stages clinopyroxene augen reside in beds of fibrous amphibole (Plate 5.15, sample 38217). The relict pyroxenes are indistinguishable from pyroxenes in fresher dykes and the phenocrysts in the lavas (Table 5.11). In some samples large clinopyroxene phenocrysts have relict cores with all of the groundmass pyroxenes totally altered. Analyses of amphibole rims on the pyroxenes (Table 5.10) are intermediate in composition between the relict clinopyroxene and the fibrous amphibole.

Sphene is very abundant both as rims on titanmagnetite and as subhedral to anhedral grains dispersed through the groundmass (Plate 5.11, sample 38493).

Tremolite, talc and magnetite occur together in some samples as replacements of earlier formed chlorite and calcite, either after olivine or filling amygdules. These areas are common in sample 38493, which as described previously contains totally "uralitized" groundmass clinopyroxenes and partially "uralitized" clinopyroxene phenocrysts. The tremolite occurs as acicular needles to 0.6 mm, lining the edges, growing inwards towards centrally located bands of small euhedral magnetite grains

Table 5.10

REPRESENTATIVE MICROPROBE ANALYSES OF SECONDARY AMPHIBOLES AND TALC IN THE DYKE SWARM SAMPLES

	Massive Ferroactinolite		Fibrous Actinolite		Acicular Tremolite		Talc	
Sample No.	38493	38493	38493	38446	38446	38446	38446	38446
Analysis No.	D-A-1	B-A-3	C-A-1	B-A-2	A-A-1	A-A-2	T-2	T-3
SiO_2	48.58	48.02	53.78	50.10	57.72	56.75	62.29	61.63
TiO_2	0.82	0.88	0.38	0.33	-	-	-	-
Al_2O_3	4.38	4.82	2.36	6.69	-	0.72	-	-
FeO	25.03	22.78	10.68	12.90	4.23	7.26	2.01	1.74
MnO	0.50	0.28	-	-	-	-	-	-
MgO	10.00	10.63	17.74	16.63	22.78	21.29	30.16	29.81
CaO	9.65	9.85	12.37	10.68	12.22	12.15	-	-
Na_2O	1.73	1.63	-	1.33	-	-	-	-
K_2O	0.29	0.45	-	-	-	-	-	-
Total	100.98	99.36	97.33	98.37	96.92	98.17	94.47	93.18
	Structure based on 23 oxygens.							
Si	7.227	7.197	7.684	7.184	7.997	7.882	8.003	8.015
Ti	0.091	0.100	0.041	0.036	-	-	-	-
Al	0.769	0.851	0.398	1.131	-	0.118	-	-
Fe	3.115	2.855	1.276	1.547	0.490	0.843	0.215	0.189
Mn	0.063	0.036	-	-	-	-	-	-
Mg	2.217	2.374	2.779	3.491	4.706	4.408	5.777	5.780
Ca	1.539	1.582	1.894	1.640	1.814	1.807	-	-
Na	0.498	0.474	-	0.371	-	-	-	-
K	0.055	0.085	-	-	-	-	-	-
Total	15.574	15.554	15.072	15.400	15.007	15.058	13.995	13.983

Table 5.11

RELICT CLINOPYROXENE AND RIM AMPHIBOLE MICROPROBE ANALYSES

	Relict Clinopyroxene		Rim amphibole		
Sample No.	38446	38446	38446	38446	38446
Analysis No.	D-C-2	C-C-1	C-R-1	C-R-2	B-A-3
SiO_2	52.20	53.22	53.61	52.43	48.80
TiO_2	0.28	0.28	0.30	0.47	0.53
Al_2O_3	3.68	2.78	3.06	4.12	6.58
Cr_2O_3	1.53	0.76	0.95	0.70	0.34
FeO	3.25	3.78	4.08	10.07	13.34
MnO	-	-	-	-	-
MgO	18.19	18.60	18.51	17.78	14.96
CaO	20.88	20.57	20.93	12.86	11.39
Na_2O	-	-	-	0.67	1.21
K_2O	-	-	-	-	-
Total	99.67	99.93	101.46	99.10	97.16
Structure:	4 oxygens		23 oxygens		
Si	1.894	1.928	7.353	7.397	7.136
Ti	0.008	0.008	0.031	0.051	0.059
Al	0.158	0.119	0.495	0.685	1.134
Cr	0.044	0.022	0.103	0.078	0.039
Fe	0.099	0.115	0.468	1.188	1.632
Mn	-	-	-	-	-
Mg	0.984	1.005	3.784	3.738	3.261
Ca	0.812	0.798	3.077	1.994	1.785
Na	-	-	-	0.184	0.344
K	-	-	0	-	-
Total	3.999	3.995	15.311	15.264	15.390
Mg/(Mg+Fe)	90.9	89.7	89.0	75.9	66.7

Plate 5.10 Randomly oriented actinolitic amphibole replacing a glassy zone of a doleritic dyke. Scale: 1 cm = 0.1 mm. Sample 38446. Crossed nicolls.

Plate 5.9 Relict clinopyroxene with marginal replacement by actinolitic amphibole in a partly uralitized dyke from the dyke swarm complex. Scale: 1 cm = 0.3 mm. Sample 38217.

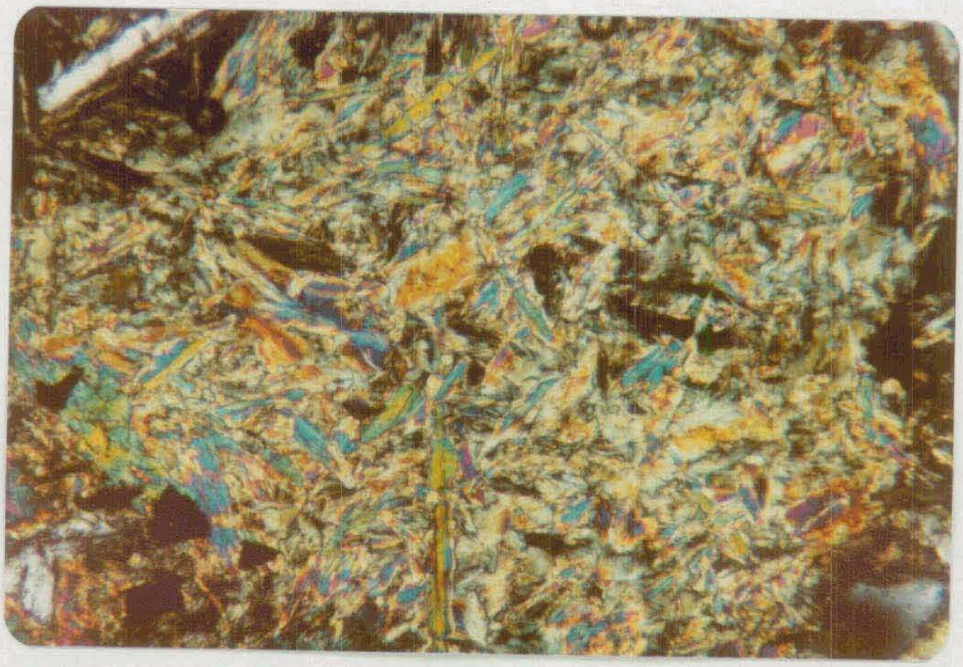

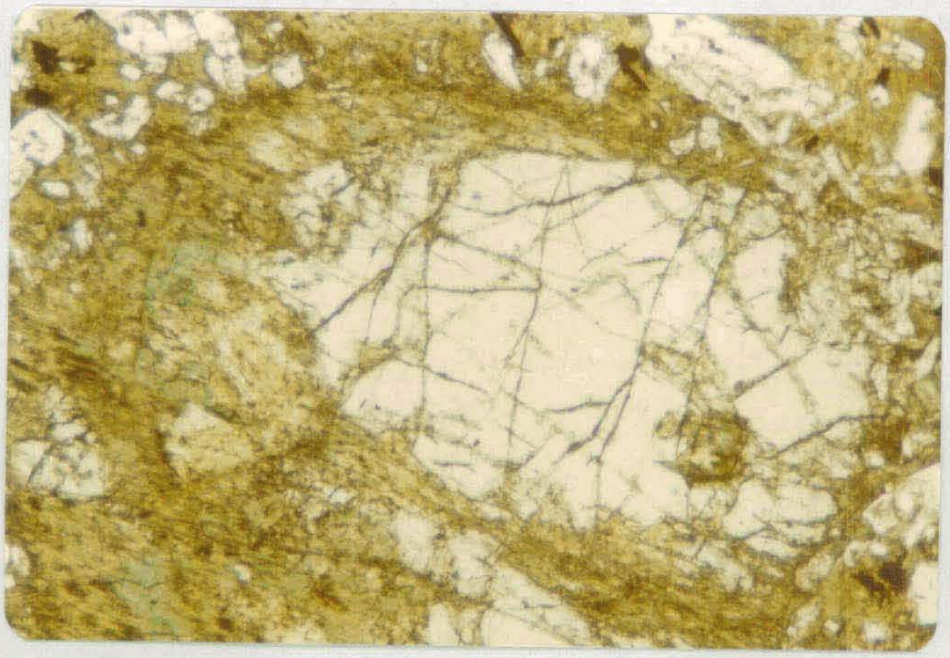

Plate 5.11 Secondary sphene mantling primary titanmagnetite in a groundmass of green uralitized pyroxene and unaltered clear plagioclase. Scale: 1 cm = 0.1 mm. Sample 38493.

Plate 5.12 Acicular needles of tremolite (moderate birefringence) in a matrix of fine grained talc (high birefringence) and small euhedral magnetite crystals (opaque). These are filling an amygdule in a doleritic dyke. Scale: 1 cm = 0.1 mm. Sample 38446. Crossed nicolls.

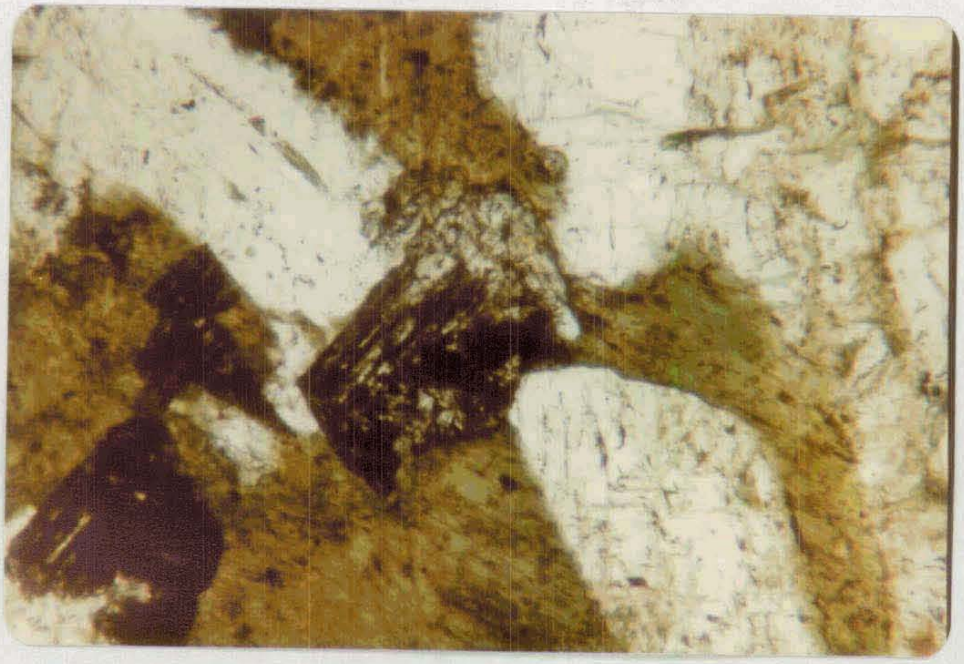

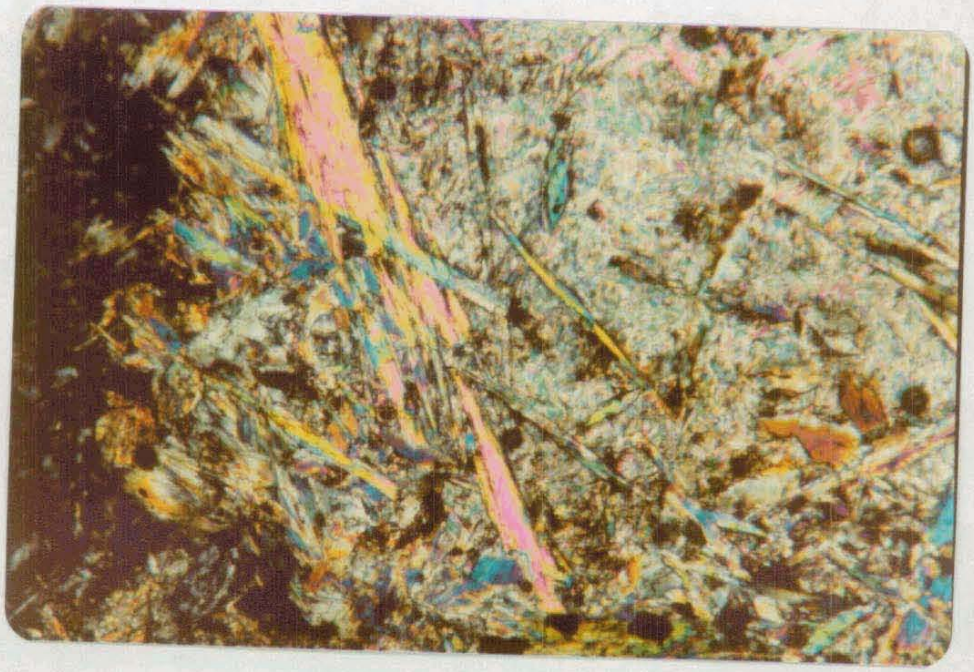

which in some cases cluster around relict chlorite or rarely calcite. Talc occurs as large cleaved grains surrounding the tremolite and magnetite (Plate 5.12, sample 38493). Analyses of tremolite and talc are given in Table 5.10 and it is notable that both are low in Al and Fe and very Mg- and Si-rich. Iron is taken up by the magnetite but Al must be released from these areas and Si added, Mg being from the original chlorite. The size of these areas (to 2 mm) and their abundance (10% in 38353) would suggest that these areas were originally amygdules rather than olivine sites since olivine has not been found as large phenocrysts in association with clinopyroxene in fresh samples (Chapter 4) and also as no relict spinels are present within these areas, which would be likely if olivine had been the replaced phase.

With increasing grade of metamorphism, to lower amphibolite facies, a massive pleochroic brown-green amphibole develops within areas of actinolite (Plate 5.13, sample 38493). This amphibole is chemically distinct as it is more Fe-rich than the other amphiboles (Table 5.10). Compositionally it is transitional between the ferroactinolite and hornblende series. If the arbitrary division of Si → Al replacement of 0.5 atoms per formula unit is used (Deer *et al.*, 1966) then the analyses include both species. Plagioclase feldspars in these samples appear quite fresh but compositionally they are distinct in that they are sodic varieties, An_{30-36} (Table 5.12) and do not conform to the range of igneous plagioclase compositions. Thus with the development of the massive "ferroactinolite", plagioclase feldspar is altered to a sodic variety ($\sim An_{30}$). This is consistent with the attainment of low amphibolite facies conditions of metamorphism within the samples (Miyashiro, 1973).

Many of the samples contain veins of other phases, principally albite, epidote, chlorite, calcite and prehnite. Zeolites are also present in two samples (38445 and 38451) from the dyke swarm zone at

Plate 5.13 Massive Fe-rich amphibole growing in strongly altered dyke. Scale: 1 cm = 0.1 mm. Sample 38493. Crossed nicolls.

Plate 5.14 Palimpsest structure in sulphide-bearing quartz vein. Translucent brown sphalerite is present in the top left of the photo. Scale: 1 cm = 0.1 mm. Sample 242.

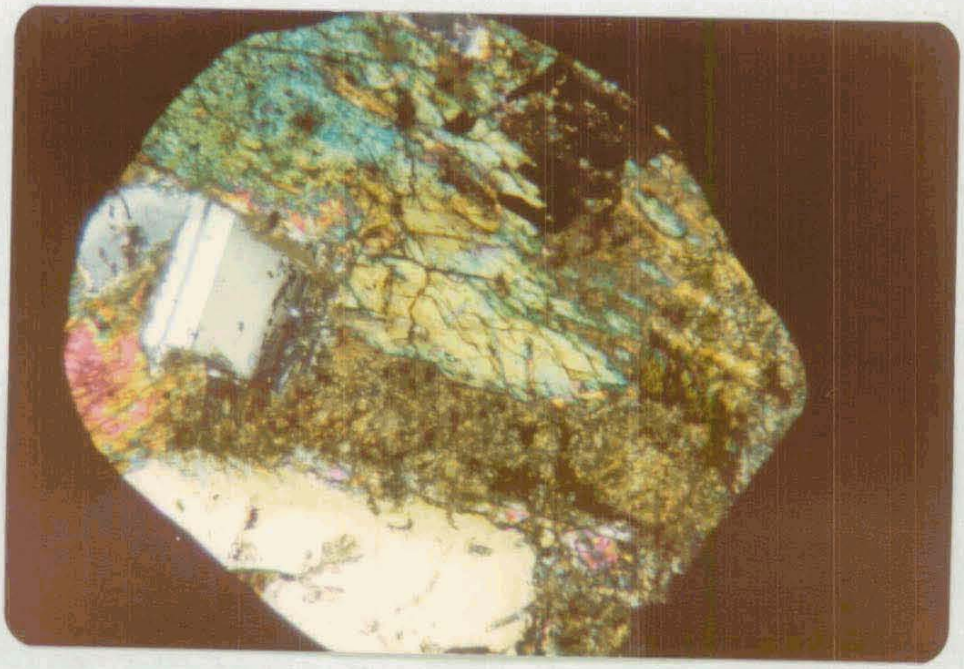

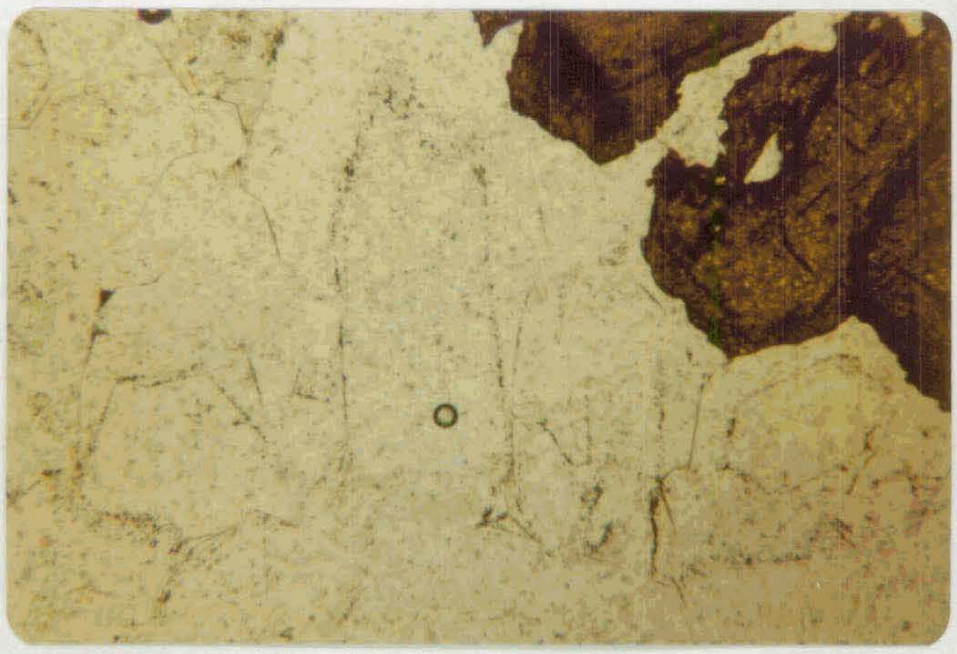

Table 5.12

SECONDARY AND PRIMARY PLAGIOCLASE FELDSPAR COMPOSITIONS FROM ALTERED DYKE SWARM SAMPLES

	Relict primary plagioclase			Secondary plagioclase	
Sample No.	38446	38446	38446	38493	38493
Analysis No.	D-P-1	B-P-1	B-P-2	D-P-2	D-P-3
SiO_2	53.78	51.43	52.99	60.52	59.26
Al_2O_3	28.74	30.46	29.27	24.53	25.34
FeO	0.54	0.35	0.49	-	-
CaO	11.75	13.98	12.65	6.52	7.70
Na_2O	5.19	3.80	4.58	8.10	7.44
K_2O	-	-	0	0.34	0.28
Total	101.22	99.79	100.04	98.96	99.53
	Structure based on 32 oxygens				
Si	9.753	93.70	9.625	10.792	10.598
Al	6.143	6.541	6.267	5.155	5.342
Fe	0.082	0.053	0.074	-	-
Ca	2.284	2.729	2.462	1.246	1.475
Na	1.825	1.343	1.614	2.801	2.580
K	-	-	-	0.077	0.063
Total	20.087	20.036	20.042	20.071	20.058
An	55.6	67.0	60.4	30.2	35.8

Gadgets Gully, high on the northeastern coast. These samples are unlike those lacking veins, because the plagioclase in the veined rocks show marked alteration either in the immediate vicinity of the veins or throughout the sample. The plagioclase becomes turbid because of the growth of sericite, chlorite, epidote ± prehnite ± albite within the crystals. One of the zeolite-bearing samples from Gadgets Gully clearly illustrates the local alteration of feldspar around veins.

Thomsonite is the main zeolite species present. These phases are anomalous in terms of the grade of metamorphism of the groundmass, representing lower temperature conditions. The mineralogy is comparable to that found in the metamorphosed lavas and in view of this it is reasonable to conclude that the metamorphism produced during the vein-forming episode was part of and identical to, the system involved in alteration of the lava sequence. It must post-date the "uralitization" event otherwise the low temperature phases would show some signs of reaction, particularly the zeolite species.

5.5 SULPHIDE MINERALIZATION AND ASSOCIATED ALTERATION

5.5.1 Introduction

A detailed study of the sulphide mineralization present in the lavas and dyke swarms exposed on Macquarie Island is beyond the scope of this thesis. However, these deposits are an integral part of the metamorphism and so are briefly described in the following section with recommendations for further studies.

Sulphides and associated phases are found in three modes of occurrence on Macquarie Island:

(1) as rare discrete grains of sulphides within metamorphosed lavas and dykes;

(2) in small vein systems with carbonate, sulphate, quartz epidote, chlorite, pyrite, chalcopyrite, sphalerite and galena; and

(3) in a large stockwork system with the phases listed in (2), apart from sulphate.

Mawson (1943) described the occurrence of sulphide-bearing veins in both the lavas (i.e. his Younger Basic Group) and dyke swarm zones (i.e. his Older Basic Group). According to Blake (quoted by Mawson, 1943) "veins of quartz and calcite occur between the successive igneous sheets (... of the Older Basic Group); veinlets of the same minerals fill the fissures formed by some of the larger joints. Pyrite is the common sulphide mineral associated with these veins, but chalcopyrite, galena, and sphalerite also occur." Within the pillow lavas (Younger Basic Group), Mawson (1943) quoted Blake as stating, "quartz, associated with sphalerite, galena and pyrite, occurs in the form of true fissure veins." Mawson (1943) also noted the occasional presence of selenite in some of the quartz-calcite-pyrite veins and the occurrence of veins of an alabaster type of gypsum containing occasional small crystals of marcasite in joints and fissures in dolerites at Nuggets Point, just south of the isthmus on the east coast (Figure 3.1). More recent studies have not discussed the occurrence of sulphide mineralization.

5.5.2 Discrete sulphides amongst lavas and dykes

Sulphide grains occur rarely within veins and amygdules in samples of both zeolite and lower greenschist grades of metamorphism. The main sulphide is pyrite which occurs as anhedral grains. Chalcopyrite occurs as a rim to hematite in one zeolitized lava (sample 7, from near Mount Ifould) and coarse bladed covellite is rimmed by massive chalcocite in a lava of lower greenschist facies grade (sample, 428, from north side of Sandell Bay). In all cases these occurrences represent a very minor proportion of the sample (<1% vol.).

5.5.3 Vein mineralization

The vein sulphide mineralization on Macquarie Island is characterized by the presence of quartz as the dominant non-sulphide and this distinguishes the sulphide-associated alteration from the general styles of alteration of the lavas and dykes where quartz is either absent or very rare. No new major occurrences were found during the present study. The main areas are (1) the southern end of the isthmus at North Head, (2) Douglas Point, high up on the west coast, (3) on the west coast, northwest of Mount Fletcher, (4) Lusitania Bay, low on the east coast, (5) Gadgets Gully, and (6) the Nuggets, the last two being high on the east coast. As can be seen in Figure 5.11, occurrences 1 to 3 are within lavas of lower greenschist facies metamorphism and occurrences 4 to 6 are within dyke swarms of higher metamorphic grade.

The best example of this style of mineralization in pillow lavas is the occurrence on the isthmus at the northern end of Macquarie Island (sample 1). It occurs along a minor fault zone which varies from 1 mm to 1.5 m in width. The volcanics are slightly brecciated along this zone and the sulphide-bearing veins now form the matrix around the fragments. The veins are dense and reach only 5 mm in width with occasional more massive patches of up to 2 cm across. Quartz and calcite are the dominant minerals within the veins, giving a whitish appearance. Pyrite is disseminated through the lava fragments and pyrite (80%), sphalerite (15%), and chalcopyrite (<5%) occur in veins. Minor amounts (<1% of sulphides) of galena are visible on microscopic examination. The sulphides form 30% of the vein material with quartz (~45%) calcite (~20%), minor epidote (2-3%) and chlorite (2-3%).

The pillow lavas within this zone are aphyric with quenched sub-variolitic textures and they have been totally altered with the plagioclase feldspar albitized and the pyroxenes replaced by chlorite,

Figure 5·11 Sulphide occurrences. Numbers referred to in text. Other symbols as for Fig. 5·1.

together with fine grained sphene and other very fine granular phases, possibly epidote and calcite. No primary opaque phases are identifiable, most having been pseudomorphsed by sphene. Pyrite is disseminated evenly through the lower fragments as discrete euhedral crystals, generally cuboid, in a range of sizes up to 0.1 mm. On average this pyrite forms ~5% of the groundmass.

The quartz varies in form from coarse euhedral crystals to 2 mm x 0.6 mm, to smaller intergrown crystals in "comb" structures. A later generation of quartz occurs as anhedral grains generally up to 0.1 mm in section but rarely to 0.3 mm. This occurs as overgrowths on the larger crystals and the original crystal boundaries are defined by planes of inclusions and granular material. In some cases the first generation material has been marginally corroded and replaced but crystalline outlines are preserved by the lines of inclusions (Plate 5.14, sample 242(1)) giving rise to palimpsest textures. Calcite is later than the first generation quartz and grows between the coarse crystals. It occurs normally as massive grains but it also is present as rhombs and these show successive growth stages through inclusion bands, in the same manner as the quartz. Epidote occurs either as small euhedra to 0.1 mm, or as anhedral grains to 0.3 mm, within the second generation quartz. It is iron-rich, exhibiting strong yellow pleochroism. Chlorite does not occur within the central parts of the veins but along the edges, although this is not common. As mentioned earlier both epidote and chlorite are only minor components (~2-3%).

Pyrite in the veins is larger than the host lava and many of the crystals are clumped, forming clots up to 3.5 mm. Individual grains range to 2 mm. The sphalerite is present as coarse anhedral grains up to 3 mm. In transmitted light the grains have pale brown cores progressing to yellowish-brown bands, defined by concentrations of minute chalcopyrite grains, with subsequent rims of further pale brown sphalerite.

Up to four growth stages are defined by the concentrations of chalcopyrite and in all but the last stage, crystal forms are sub- or euhedral. The chalcopyrite inclusions are also dispersed throughout the grains. Chalcopyrite also occurs as discrete grains, up to 1 mm. The sphalerite occasionally includes or partially encloses pyrite. Rarely this is reversed. The sphalerite appears to have formed after most of the pyrite, contemporaneously with or just prior to completion of final pyrite growth.

The Nuggets Point mineralization is unique in that gypsum is associated with the sulphides. The gypsum occurs as thick veins with the sulphides. Two varieties of gypsum veins are recognizable in the field. Massive veins, up to 12 cm across, randomly transect one 5 m section of the dyke swarm exposure. The gypsum in these veins is opaque white with a coarse fibrous crystal structure. Crystals are commonly curved. Small euhedral, clear gypsum crystals project into minor (<1 cm long) cavities in and on the edge of the thick veins. The second variety of veins is small, up to 1 cm thick, containing translucent gypsum that is present throughout the dyke swarm exposures. Optically similar gypsum is also present in the sulphide-bearing quartz veins, postdating the quartz by filling cavities in these veins. Sulphides are present only in the small variety of gypsum veins, apart from in the quartz-rich veins. These latter veins are identical to those described from the pillow lavas earlier except that actinolite is present as a minor phase, growing as fine needles and fibrous sheaves within the quartz grains, particularly near the edges of the veins.

The origin of the gypsum is suggested later to be a result of heating of sea water penetrating oceanic crust (Section 5.9). The larger sulphide-free veins are probably due to remobilization. The curved nature of the crystals in these veins is considered to be a deformation feature in view of the brecciated nature of outcrops in this area.

5.5.4 Stockwork mineralization

Only one sample of this more extensive form of sulphide mineralization has been found; at Caroline Cove at the southern end of Macquarie Island (occurrence 7, Figure 5.11). This previously indescribed mineralization occurs in a wedge-shaped, fault-bounded block with a 150 m northwest facing beach frontage and two 250 m long sides. The limits of the altered zone are very sharp, the fault shear zones being narrow, reaching a maximum width of 2 m on the northern boundary.

Sulphides occur as both disseminated through the pillow lavas, hyaloclastite breccias and paraconglomerates, and in quartz veins, up to 1 m thick that contain up to 10-15% sulphides. No massive sulphide lenses are exposed. All outcrops are heavily weathered, commonly with ferruginous gossan-like surface layers. All are altered, depending on the chlorite content but primary textures are preserved. Pillow lavas showing typical quenched textures, e.g. samples 174 and 193, with albite replacing plagioclase, chlorite replacing glass, clinopyroxenes, and olivine, and sphene scattered through the groundmass with the last locally concentrated where primary Fe-Ti oxides have been altered. Sample 181 is a totally altered hyaloclastite breccia and outlines of glass fragments are clearly preserved. Thus texturally these rocks are recognizable as members of the volcanic sequence of the Macquarie Island complex.

Pyrite is the dominant sulphide, followed by (in order of abundance) sphalerite, chalcopyrite and galena. The pyrite is present as stringers in veins up to a maximum of 1 cm, but generally only 3-5 mm in width. The disseminated pyrite varies widely from fine material, identical to that observed in the other occurrence of mineralization, to more coarsely crystalline material in the matrix of one paraconglomerate sample (171A), with well formed pyrite crystals with the characteristic striated facies up to 0.6 mm across. As in this sample, the pyrite may form up to 40% of the sample over areas up to 1 m. Sphalerite occurs as large irregular grains containing up to 5% of chalcopyrite as minute inclusions.

These are commonly concentrated around the grain margins and in irregular zones within the crystals. Chalcopyrite also occurs as rare discrete irregular grains within sphalerite-rich areas. Galena has only been observed as inclusions in sphalerite grains.

Non-sulphide phases associated with this mineralization in the veins are quartz, calcite- chlorite, epidote, albite, and rarely actinolite The quartz varies from coarse crystalline material to fine granular forms with palimpsest textures occasionally present. Many of the coarser grains are slightly strained, with undulose extinction and minor recrystallization around the grain boundaries. The fine granular material often cuts through more coarsely crystalline material and sulphides in the ores are slightly brecciated. This deformation is strongest near the faulted boundary on the northern flank of the deposit and suggests that the mineralization was earlier.

Chlorite occurs in both coarse sheaves and fibrous forms within the host rock and as vermicular flakes in the veins. Calcite occurs as irregular grains in veins and dispersed through the host rock. Fe-rich epidote, shown by its strong yellow pleochroism, occurs generally as well formed tabular crystals to 0.1 mm or in clots of granular and bladed, striated grains. Sphene is scattered through the host rock. Actinolite is rare and occurs as fine fibres growing within quartz in the veins.

5.5.5 Sulphide mineralization - a summary

1. Sulphide occurrences observed on Macquarie Island are encountered within rocks of lower greenschist facies metamorphism or higher.
2. Those mineralized areas are restricted to the lower parts of the volcanic layer and the dyke swarm layer.
3. The sulphide mineralogy is:

   pyrite (~85-90%) + sphalerite (5-10%) + chalcopyrite (1-2%) + galena (~0.1%).

4. The associated vein phases are:

   quartz (80%) + calcite (15%) + chlorite (2-3%) + epidote (2-3%)
   + rare actinolite.

5. Host rocks are totally altered to assemblages of:

   albite + chlorite + sphene + epidote + rare actinolite.

6. The mineralization dominantly occurs in veins. Disseminated pyrite is present in the host rocks. Primary textures in the host rocks are preserved.

5.6 OXYGEN AND CARBON ISOTOPE STUDY OF THE METAMORPHISM

This section contains results and conclusions from the first stage of a joint study on the stable isotope geochemistry of the Macquarie Island ophiolite complex. The study is being carried out with Dr J. D. Cocker and Dr K. Muehlenbachs. Analyses were performed at the Department of Geology, University of Alberta, Edmonton, Canada. The results are summarized here and for a more detailed account the reader is referred to Cocker *et al.* (in prep.) in Appendix 8.

Results for δO^{18} and δC^{13} from all components of the ophiolite complex are presented in Figures 5.12 and 5.13. The basaltic glass samples have a δO^{18} range of 5.7 to 6.0‰ , a typical range for fresh ocean-floor basalts (Taylor, 1968; Pineau *et al.*, 1976). The ocean-floor weathered basalts and the more highly altered extrusives both have enriched δO^{18} values with ranges of 7.9 to 9.5‰ and 6.9 to 9.6‰ respectively. The intrusive rocks are depleted relative to the fresh basalt norm with a range of 3.2 to 5.9‰. Dykes within the extrusive sequence have enriched values matching their host rocks.

The δC^{13} values for the ocean-floor weathered samples are similar to results from DSDP leg 29 and the basaltic oceanic crust (Anderson & Lawrence, 1976; Muehlenbachs, 1979) with ranges of 0.7 to -2.2‰ and 1.0 to -0.8‰ respectively. Values from the more highly altered

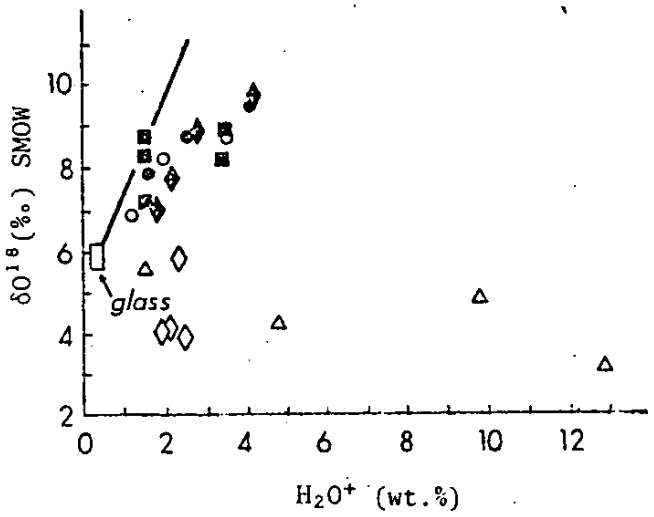

Figure 5.12 Oxygen isotopic composition for whole rocks of the Macquarie Island ophiolite vs. H_2O^+ content. The δO^{18} values are divided into two groups with respect to the fresh glass compositions - enriched rocks including subzeolite facies weathered basalts (●), zeolite facies metabasalts (■), greenschist facies metabasalts (◆), and subgreenschist facies diabase dykes (○); and depleted rocks including greenschist to amphibolite facies diabase dykes (◇), gabbros and serpentinised harzburgites (△). The solid line is the locus of DSDP seafloor basalts.

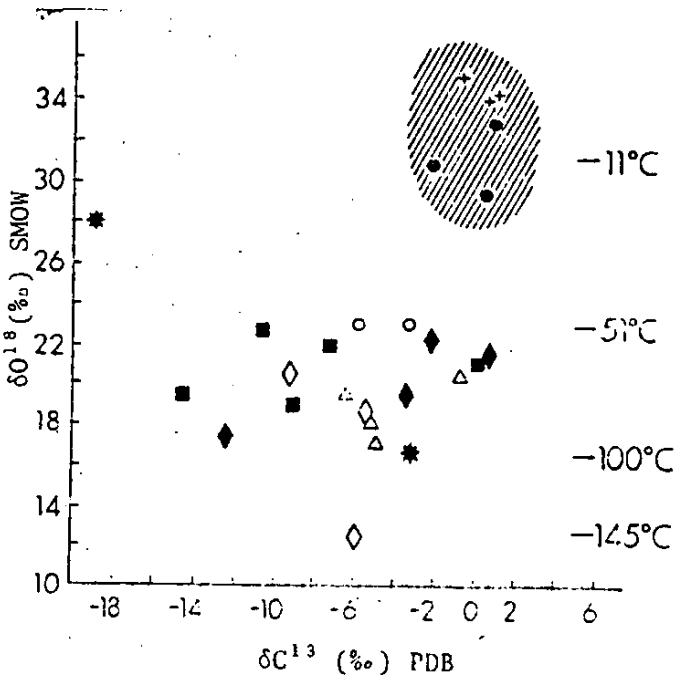

Figure 5.13 Oxygen and carbon isotopic composition for calcite in the Macquarie Island ophiolite. Symbols as for Figure 5.12, except the two vein calcite samples (*) and three samples from DSDP leg 29 holes 278, 279 and 279A(+). The calcite compositions are clearly divided into three groups - typical seafloor basalt carbonate (shaded field), metamorphosed rocks, and the vein calcite with a low δC^{13} value. The temperature scale is based on calcite water fractionation (20) and the assumption that the calcite was deposited in equilibrium with seawater ($\delta O^{18} \approx 0‰$).

extrusive rocks and for the intrusive rocks do not show the same differentiation observed with the δO^{18} results. The overall range for these samples is 0.9 to -14.6‰ with the intrusive rocks being slightly more restricted with a range of 0.9 to -9.2‰, although this may be a sampling bias. One calcite sample from a natrolite-gyrolite-calcite vein in zeolitized basalts has a value of -18.9‰ and a δO^{18} value of 28.1‰. This depleted δC^{13} value suggests a closed system (Muehlenbachs, 1979) and an anomalously low temperature of 24°C, calculated from the δO^{18} result assuming a δO^{18} = 0‰ for the fluid, indicates that this latter assumption is incorrect and supports the closed vein model for this calcite formation.

Information from ocean-floor and ophiolite studies allows several conclusions to be drawn from these Macquarie Island results. Firstly, the results confirm a low temperature, sea-water based alteration process for the samples that have been recognized on mineralogical grounds as ocean-floor weathered basalts. The enriched values for the more altered basalts however are not consistent with alteration by sea water at the higher temperatures indicated by the mineralogy, as the values for δO^{18} at temperatures around 200-250°C should remain similar to the pristine composition. Thus these results indicate reaction with a δO^{18} enriched fluid. It is suggested that this fluid is upwelling fluid that has been enriched through reaction with the intrusive rocks under low water/rock ratio conditions. Using the intrusive rocks, which have been depleted by 1.6‰ (average δO^{18} = 4.2‰) as an example, reacting sea water would be enriched to δO^{18} values of 2.6 to 3.9‰ for water/rock ratios (weight %) of 0.3 to 0.2 over the 300-500°C temperature range. The δC^{13} results for these samples support the low water/rock ratios for this part of the alteration.

In summary, the isotopic results indicate a sea water based hydrothermal alteration process with the sea water penetrating down into the

intrusive layer where, under conditions of low water/rock ratios, it is enriched in O^{18}. The alteration in the lower parts of the extrusive section is a result of interaction with this evolved fluid. It is probable that this overprints alteration produced by the descending fluid (Cocker *et al.*, in prep.).

5.7 CONDITIONS AND PROCESSES OF METAMORPHISM

In the previous sections the petrography of the various metamorphic assemblages has been described. The ranges of secondary phases between these assemblages are summarized in Figure 5.14. The following section discusses the processes and chemistry involved in the formation of these assemblages and the structural implications of their spatial distribution on Macquarie Island.

5.7.1 Specific conditions of metamorphism

Each subdivision of the metamorphism is considered separately in the following sections, and summed up in Section 5.8.

Ocean-floor weathering or halmrolysis

The alteration is a hydration event: the lack of deformation, and the fracture controlled alteration of glassy material demonstrate a static alteration with dynamic fluid movement along fractures, cracks and in amygdules. Within holocrystalline samples, interstitial glass and at least part of any olivine present have been altered, indicating a thorough permeation of the samples by the fluid.

The predominance of clay minerals and lack of alteration of the feldspar suggests low temperatures during the alteration. The lack of Na,Ca zeolites indicates temperatures less than ~100°C (Table 5.15) but these species may have been suppressed by high X_{CO_2} in the fluid in which case the lack of chlorite and epidote would suggest an upper temperature limit of 200°C (Tomassen & Kristmannsdottir, 1972).

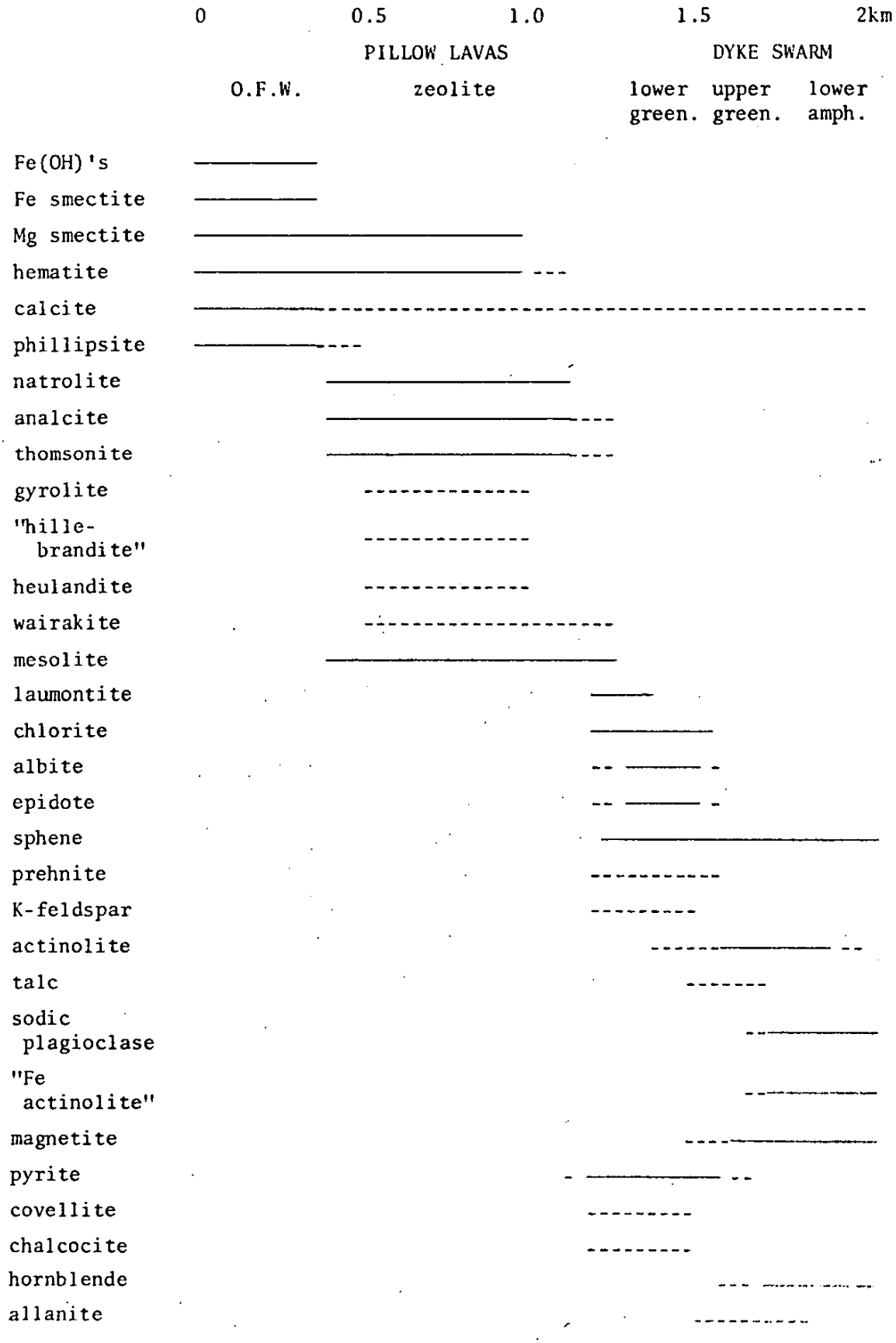

Figure 5.14 SECONDARY PHASE DISTRIBUTION IN MACQUARIE ISLAND UNITS. The dashed line indicates sporadic occurrence and the solid line the common occurrence of the particular phase.

Table 5.13

Fe^{2+}/Fe^{3+} RATIOS, H_2O^+ AND CO_2 DATA FOR O.F.W. LAVAS AND DYKES

	Lavas			Dykes		
Sample No.	35	38265	38391	231	38337	38471
H_2O^+*	2.44	4.03	1.54	1.93	1.10	3.44
CO_2*	3.25	0.59	0.99	0.16	0.29	0.48
Fe^{2+}/Fe^{3+}	0.60	-	1.40	1.71	1.64	-
Fe^{2+}/total Fe	0.38	-	0.58	0.63	0.62	-

* values in wt.%

The oxygen isotope geochemistry of comparably altered samples from DSDP leg 37 (Muehlenbachs, 1977) indicates temperatures of 4°C for the alteration and similar results have been obtained from Macquarie Island samples (3-17°C, Section 5.6), supporting a low temperature process.

Structural recalculations of the clay compositions are presented in Table 5.1. The smectites from the hyaloclastite (sample 252) are tri-octahedral saponites with a high Al component in the octahedral site. This Al component is higher than generally found in smectites and may represent interlayering of chlorite or kaolinite. The latter is precluded by its requirement of non-alkaline conditions for formation, in contrast to smectites (Deer *et al.*, 1966). Pritchard *et al.* (1979) have suggested that similar saponites are reduced, with conditions becoming more oxidizing to produce the celadonites. The observation of a change to more oxidizing conditions during smectite formation is in agreement with conclusions reached by Robinson *et al.* (1977) and others on DSDP leg 37 samples. The massive yellow material replacing olivines in the Macquarie Island data is extremely iron-rich and the structural calculations indicate, using this approach, an oxidized nature with significant Fe in the tetrahedral site (Table 5.1, sample 35). These would then have to form late in the alteration episode after alteration of the interstitial glass.

Calcite forms late in the alteration, filling vesicles and replacing smectites, as described previously (Section 5.4.1). The late formation reflects the relative concentration of Ca in the fluid through removal of other phases, with depletion of CO_2 in the fluid. This CO_2 is introduced to the rock by the fluid and high CO_2 contents are a feature of samples that have undergone this type of alteration (Table 5.13). The overall oxidising effect of this process is demonstrated by the low whole rock $Fe^{2+}/Fe^{2+}+Fe^{3+}$, relative to fresh basalts and glasses (Table 5.13).

Zeolite facies metamorphism - temperature and pressure conditions

Total pressure variations through the sequence containing zeolite assemblages are not high. The first zeolite-bearing samples occur at a stratigraphic depth of 300-500 m which, including a maximum water depth of 3000 m, would give a total pressure of 400-500 bars rising to about 900 bars at the bottom of the zeolite sequence where an overburden of 1.8 km is indicated. These are only rough estimates because P_{total} may not be the same as P_{fluid}, depending on permeability, presence or activity of fluid circulatory convection systems within the sequence, and other factors. This order of *total* pressure variation has little effect on zeolite stability as most low-grade metamorphic reactions involve relatively small changes in volumes of solids (Zen, 1974) although local variations in P_f/P_t have been demonstrated to cause displacement of the equilibrium boundary between hydrous and less hydrous phases (Boles & Coombs, 1977). Ivanov & Gurevich (1975) found that a variation in P_f from 500 bars to 1000 bars expanded the laumontite stability field appreciably but had little effect on the temperature stability field, confirming the minor pressure effect with temperature. Generally P_f is less than P_t in shallow burial settings (Fyfe, 1974; Boles, 1977), suggesting low P_f conditions during the alteration of these Macquarie Island samples.

Temperature is widely recognized to be very important in controlling zeolite stability from both experimental studies (e.g. Liou, 1971a, 1971b) and the temperature zonations found in many active hydrothermal fields (e.g. Iceland - Kristmannsdottir & Tomasson, 1978). Minimum temperatures of formation of zeolites in these areas are low. The isotope studies on the clay-carbonate assemblages of the OFW samples indicate temperatures to 17°C with the less reliable data from the zeolite-bearing samples giving results from 52-79°C. Samples of clay-carbonate assemblages from near the transition to zeolite samples were not available for analysis and

samples are stratigraphically above this transition and give temperatures which are presumably lower than the transition temperature which was probably around 30-40°C.

Highest temperatures in the zeolite facies are more clearly constrained by the disappearance of laumontite and the smectite-chlorite transition. Experimental work by Liou (1971a) suggested an upper temperature of around 200-250°C for the laumontite stability field, at P_{fluid} = 1 kb; in close agreement with maximum temperature stabilities in active geothermal fields of 220°C (Liou, 1970). Further support for a temperature of 200-250°C is provided by Tomasson & Kristmannsdottir (1972) who reported a temperature of about 230°C for the smectite-chlorite transition in the Iceland area and more recently Kristmannsdottir & Tomasson (1978) defined the upper temperature limit of the laumontite zone in this area as about 230°C. In summary, both experimental and direct measurement studies are consistent with a temperature of about 230°C for the upper stability limit of laumontite and the smectite-chlorite transition which is found at the base of the zeolite sequence in the Macquarie Island volcanic sequence.

Laumontite is only sporadically developed at the base of the zeolite sequence and temperatures range up to this maximum at the base. No distinct zeolite zones have been spatially delineated amongst the Maxquarie Island volcanics, possibly reflecting the structural complexity, making temperature variations within the sequence difficult to ascertain. Many of the zeolite species have been found to exist over relatively wide temperature ranges, that also differ between localities (Figure 5.15), and these are of little use.

The sporadic occurrence of wairakite in areas of zeolite facies alteration may indicate the existence of localized "hot spots" within the zeolitized sequence. Analyses of wairakite from Macquarie Island are sodic (~ 3.60 wt.% Na_2O), in the mid-range of wairakites reported

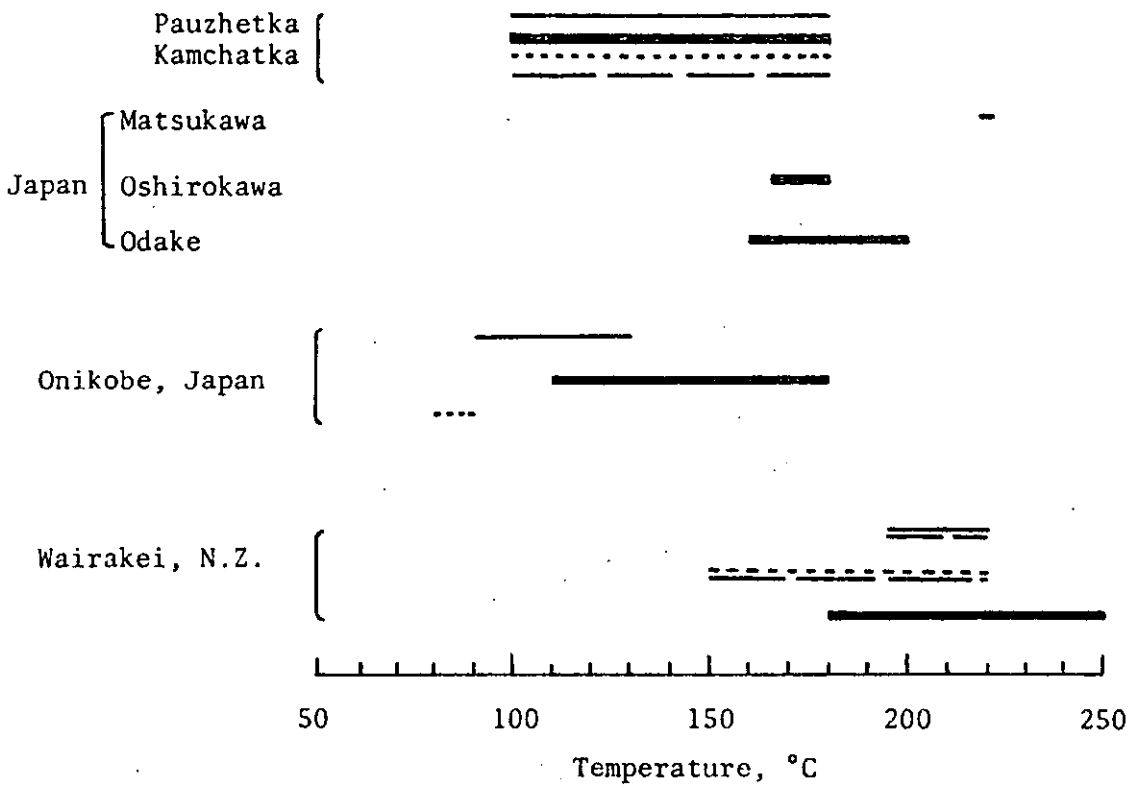

Figure 5.15 Temperature ranges of zeolites in active hydrothermal areas.

▬▬▬	Wairakite	100-250°C
———	Laumontite	90-220°C
-------	Mordenite	80-220°C
—— —	Heulandite	100-220°C

from meta-volcanics in British Columbia by Surdam (1967) (average CaO 7.9-12.2 wt.%; Na_2O 0.7-5.7 wt.%). Liou (1970) suggested that the Na component tends to decrease the crystallization temperature, allowing Na-wairakites and laumontite to coexist. In active geothermal areas wairakite is reported from as low as 110°C, although generally it occurs from about 180°C up to 250°C (Figure 5.15). Where developed extensively it occurs with laumontite or phases characteristic of lower greenschist facies grades of metamorphism, e.g. chlorite, epidote, prehnite, quartz, and sodic plagioclase, or in higher temperature zones underlying laumontite-bearing assemblages (Seki, 1972; Surdam, 1967; Steiner, 1977). Thus its presence on Macquarie Island amongst lower temperature zeolites is somewhat anomalous unless the Na_2O component allows a lower formation temperature, as Liou (1970) suggested. The sporadic occurrence of wairakite could then reflect local variations in the activity of Na in solution but the widespread development of other Na-rich zeolites, e.g. thomsonite, analcite and natrolite, argues against this. Consequently the most reasonable theory is that of locally higher temperatures, with laumontite formation being suppressed by high Na activity in the fluid. Following from this, these wairakite occurrences may define conduits or channelways for the hydrothermal fluids.

Chemistry of the alteration process

Having estimated the pressure and temperature conditions it is now appropriate to consider the alteration process in terms of chemical processes. The mineralogy, mineral chemistry and phase relations have been described in Section 5.4. In summary a general paragenetic sequence of smectites–Na,Ca zeolites–carbonate is present in the samples and amongst the zeolites there is a progression to silica-deficient calcium-rich varieties during crystallization in many samples.

The smectites that rim the amygdules and that line veins show a marked variation in chemistry with a strong linear correlation between Mg and Fe which meets the FeO/MgO trend shown by chlorites from greenschist facies samples (Figure 5.9). This trend represents an increasing interlayered chlorite component in the smectites leading to an Mg-chlorite composition which is the lowest temperature variety found in the lower greenschist facies samples (Section 5.4.2). Calcium-rich varieties also line some amygdules and occasionally contain TiO to 1.35 wt.%, but only in the material in the immediate vicinity of the vesicle wall. This indicates a rapid fixation of Ti in the clays from Ti-enriched fluids moving through the groundmass, thus preventing any large scale mobility of this element. It further suggests that the amygdule assemblages may arise from mixing of fluid that has percolated through the groundmass and fluid moving through amygdules and along fractures. The botryoidal growth of the smectites in many samples (157, Plate 5.15) requires reasonably still (static) fluid conditions, as does the fine fibrous form of the natrolite, and this would suggest a gentle mixing of the two fluids. In the hundreds of amygdule sections observed in the optical studies of the samples a direct connection between amygdules is only seen where veins cut the samples and this is an uncommon event relative to the number of amygdules. Hence fluid supply to the amygdules, in general, must be through the groundmass. The initial formation of smectites increases the relative activities of Na, Ca, K and Si in solutions as the smectites are less siliceous than the phase broken down by the fluid, and contain only minor amounts of these other elements. The activity of K must be fairly low or illitic components would be more abundant in the phyllosilicates.

Plate 5.15 Botryoidal smectite in a zeolite-filled amygdule. Two stages of smectites are recognizable, a massive yellow-brown variety rimmed by a pale green fibrous variety. The brown fibrous zeolite is a thomsonite-mesolite-natrolite intergrowth and the clear coarser material is thomsonite. Scale: 1 cm = 0.1 mm. Sample 157.

Zeolites are the next phase to crystallize and, as described, can form major proportions of the samples on a local scale. Zen (1961) and Thompson (1971) have considered the role of μCO_2 in Ca zeolite-carbonate assemblages and have shown that μCO_2 must be low if zeolite formation is to occur. Ivanov & Gurevich (1975) have demonstrated that lowering of P_{fluid} increases the zone of laumontite stability to higher μCO_2, = 0.02, for $P_f = P_t$ = 1 kb at 260°C and μCO_2 = 0.04 for $P_f = P_t$ = 0.5 kb at 250°C, giving a range of μCO_2 = 0.02 to 0.04 for fluid precipitating laumontite in the Macquarie Island system. Calcite has been observed in many samples containing the lower temperature zeolites (Section 5.4.2) where it forms after crystallization of Na-rich zeolites (analcime and natrolite, sample 157). This suggests that in these samples μCO_2 was high enough for calcite precipitation but that this was suppressed by high μNa initially. Following the lowering of μCO_2 by calcite precipitation, the more calcic low temperature zeolite species (?thomsonite-natrolite and thomsonite) have crystallized.

The progression of zeolites from analcite → natrolite → thomsonite may be represented by the following reactions:

(i) $Na_{16}Al_{16}Si_{32}O_{96}.16H_2O \rightarrow Na_{16}Al_{16}Si_{24}O_{80}.16H_2O + 8SiO_2$

analcite → natrolite + quartz

(ii) $Na_{16}Al_{16}Si_{24}O_{80}.16H_2O + 8Ca^{2+} + 4Al^{3+} + 8H_2O \rightarrow$

natrolite

$Na_4Ca_8Al_{20}O_{80}.24H_2O + 12Na^{+} + 4Si^{4+}$.

thomsonite

Reaction (i) shows that if μCO_2 is high then analcite is favoured with natrolite forming at lower μSiO_2. Quartz has not been observed in the samples indicating that μSiO_2 was never high enough for quartz to form. Reaction (ii) is more complex and indicates that under fluid

conditions of high Ca^{2+}/Na^{+} and Al^{3+}/Si^{4+}, thomsonite will be precipitated. Boles (1977) discussed the heulandite-analcite relations and demonstrated a dependence on Ca^{2+}/Na^{+} of the stability field of analcite which increases with lowering Ca^{2+}/Na^{+} (Figure 5.16) supporting the observations made here. The abundant Na,Ca zeolite which chemically represents a natrolite-thomsonite mixture (Section 5.4.2) and forms prior to the coarse thomsonite reflects steadily increasing Ca^{2+}/Na^{+} ratios. Finally, the occurrence of thomsonite replacing the calcic plagioclase phenocrysts (An_{87-72}) shows that it formed preferentially in a chemical environment where Ca^{2+}/Na^{+} and Al^{3+}/Si^{4+} are both high.

In summary the mineral paragenesis of the zeolite facies assemblages probably formed under low pressure (0.5 to 1 kb = P_{total}) and moderate temperature conditions (50-230°C). μCO_2 was low throughout the sequence. The pore fluid chemistry altered significantly during the formation of these assemblages within amygdules, producing a regular occurrence of smectites → Na-rich zeolites (→ calcite) → Ca-rich zeolites from the rim inwards. The control on phase relations by chemical components such as μCa^{2+} reflects a strong host rock contribution and thus comparable zeolite mineralogies are found in sequences of similar host rocks. Experimental and theoretical studies of this facies must be extended to include Na^{+}, Ca^{2+}, SiO_2 and H_2O before a clear understanding and quantification of the chemistry of the alteration processes will be possible.

Lower greenschist facies

The onset of lower greenschist facies metamorphism is marked by the appearance of chlorite (230°C - Thomasson & Kristmannsdottir, 1972), epidote (230°C - Seki, 1972), albite and sphene, and the disappearance of zeolites (230°C). The presence of actinolite in the most altered lavas at the base of the volcanic sequence indicates a rise in temperature to

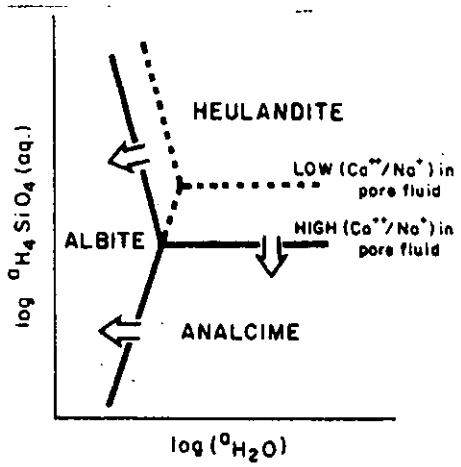

Figure 5.16 Activity diagram at constant temperature, pressure, and activity of H_2O showing phase relations for albite, analcime, and heulandite ($Ca_{3.5}$ $NaAl_8$ $Si_{28}.24H_2O$). Note that equilibrium boundary will shift as a function of varying Ca/Na activity ratios in pore fluids. Arrows show direction of common reactions in low-grade metamorphic rocks. (from Boles, 1977).

~320°C (Keith *et al.*, 1968). Prehnite is sporadically developed through this zone and in underlying higher grade assemblages. This thermal range is in agreement with Rusinov (1965) who concluded that the prehnite-laumontite transition should be at >200°C, and the experimental studies of Liou (1971c).

Liou (1971c) also suggested that substitution of iron may allow expansion of the stability field over considerable ranges of physical conditions. The substitution of iron in prehnites from the Macquarie Island samples is very variable (Section 5.4.3) even on local scales and does not appear to affect or control its stability in this case. The structural formulae of the prehnites show small and variable deficiencies in the Ca^{2+} site and this has been suggested to reflect relatively low fO_2 conditions as some Fe^{2+} is required to fill the Ca^{2+} sites (Liou & Ernst, 1979).

The style of alteration in these rocks is very similar to that of the zeolite facies with Fe-Mg phases (chlorites) lining amygdules and veins, with centre-fills of epidote, albite, sphene and chlorite. Again, the local environment displays a strong control on phase stability and this is demonstrated in sample 38151 where calcite is present in the vein only when the vein cuts amygdules, whereas albite occurs where the veins cut plagioclase. In this case the stability of Na-rich phases under the low Ca^{2+}/Na^{+} conditions observed in the zeolite paragenesis is again indicated, emphasizing a need for this to be investigated experimentally.

Upper greenschist and amphibolite facies

The transition zone from pillow lavas into the dyke swarm sequence also marks a change in metamorphic grade. General features and mineralogy of the metamorphism have been described (Section 5.4.4), the main features being abundant actinolitic amphibole partially or totally replacing the pyroxenes, and the stability of sodic plagioclase (An_{30-36}) rather than albite.

The process of "uralitization" of the dykes, and its timing, requires some discussion. Several lines of evidence are relevant to this problem. Firstly, as discussed earlier (Section 5.4.4), the extent of alteration of the "uralitized" samples is variable, ranging from only minimal alteration albeit with all secondary phases present, to complete alteration of all mafic silicate phases. A hydrothermal process is indicated by the hydrous nature of the secondary phases and the range of alteration suggests a limited fluid supply to the least altered samples.

Secondly, the textures of the samples, particularly in the least altered samples (e.g. 38206), demonstrate the holocrystalline nature of the samples prior to the metamorphic event. Piispanen & Alapieti (1977) reviewed earlier studies of "uralitization" but reached no conclusion as to whether it is a metamorphic event or a late stage magmatic process. Deer *et al.* (1966) considered "uralite" to be derived by the pneumatolytic action of residual water-enriched magmatic fluids on the earlier crystallized pyroxenes. This description is given in reference to uralite as pale green amphibole present as rims on the pyroxene, not where total alteration has occurred. The extent of the alteration amongst the dykes and the continuity of the metamorphism with respect to the overlying sequence strongly suggests that the alteration of the dykes is part of a major hydrothermal process that is defined by secondary assemblages in the volcanic sequence. Late magmatic processes cannot be totally excluded.

Once again local composition exerts strong controls on the secondary phases developed as shown by the restriction of talc-magnetite-tremolite to amygdule sites where these phases are replacing chlorite and more rarely calcite. These replacement textures suggest a complex alteration history with lower temperature phases initially developed. This then requires a reheating event and rules out a late

magmatic origin for the uralitization. It is difficult to envisage a process involving a complete reheating event unless the amygdule assemblages represent the first formed phases in the alteration event and that subsequent reactions were sufficiently exothermic to elevate temperatures past the chlorite stability limit. Zen & Thompson (1974) have considered this question and although their estimates were crude they demonstrated that hydration reactions can produce considerable amounts of heat. This has been supported by Fyfe *et al.* (1978) who noted that essentially anhydrous basalts react with hydrosphere as they move away from ridges on the sea-floor and such processes probably make a substantial contribution to ocean-floor heat flow and submarine heat production (Fyfe, 1973).

The uralitization reaction may be represented in the following simplified form:

$$\underset{\text{augite}}{5Ca_2MgFe(SiO_3)_4} + 2H_2O + 6CO_2 \rightarrow \underset{\text{actinolite}}{Ca_4Mg_5Fe_5(Si_8O_{22})_2(OH)_4} + \underset{\text{calcite}}{6CaCO_3} + \underset{\text{quartz}}{4SiO_2}$$

Thermodynamic data is not available for these components and so an Fe-free reaction has been used, i.e.

$$\underset{\text{diopside}}{5CaMgSi_2O_6} + H_2O + 3CO_2 \rightarrow \underset{\text{tremolite}}{Ca_2Mg_5Si_8O_{22}(OH)_2} + \underset{\text{calcite}}{3CaCO_3} + \underset{\text{quartz}}{2SiO_2}$$

At 25°C, ΔH = -67.4 kcal and at 327°C (600°K), ΔH = -74.6 kcal (using heat of reaction data from Robie & Waldbaum, 1978).

The dykes contain ≃30 vol.% of pyroxene (Ploshko *et al.*, 1970; Joplin, 1971) and in consequence, assuming the previous reaction, for a dyke swarm column 1 km deep and 1 cm^2 in cross-section,

volume of pyroxene = 3×10^4 cm^3

$$\text{number of moles of diopside} = \frac{\text{vol}(3 \times 10^4) \times \text{density}(3.22)}{\text{mol.wt. } (216.553)}$$

$$= 446.1$$

heat produced by conversion to tremolite, etc.

$$= \frac{446.1}{5} \times 74.6$$

$$= 6655.8 \text{ kcal.}$$

Using heat capacity (0.2 cal/gm ^{o}C) and density (2.7 gm/cm) values of water-saturated rock from Fehn *et al.* (1978), this reaction will raise the temperature of the rock column by 123^{o}C. Although these calculations provide only a rough estimate the heat contribution from such hydration reactions is clearly large. The presence of the phases shows that at the time of alteration, i.e. fluid-rock interaction, the temperature was $\simeq$ 300^{o}C near the top of the dyke swarm so this heat generated will encourage fluid circulation and rock reaction. The chlorite may then represent a result of the initial alteration of the rocks, undergoing subsequent reaction as temperatures were elevated beyond the chlorite stability field through the action of exothermic hydration reactions.

Clearly other chemical parameters will change during the alteration of the rocks. The presence of magnetite is evidence for more reducing conditions than higher in the metamorphic sequence where hematite and iron hydroxides are present (zeolite facies). It is not clear where the hematite-magnetite transition occurs specifically but it is within the lower greenschist-upper greenschist zone.

5.7.2 Regional nature of the metamorphism and volcanic stratigraphy

A simplified map showing the distribution of the various grades of metamorphism and the structure of the lavas and dykes is given in Figure 5.17. The metamorphic distribution is based on data from individual sample localities given in Figure 5.1. The salient features shown by Figure 5.17 are firstly, a widespread distribution of each metamorphic grade and the dominance of the higher grade metamorphic assemblages. The latter feature may reflect the complex tectonic evolution of Macquarie Island as well as an erosional effect. In view of the persistence of the little altered lavas throughout the island, however, it seems unlikely that erosion has played a major role.

The simple metamorphic zonation expected from the recognised progression of metamorphic assemblages is not present, but several partial sections may be tentatively recognised. One possible partial section is present west from North Head along the northern coast to Handspike Point. The rocks range from the lavas at North Head through dyke swarms and massive gabbros to the layered gabbro complex at Handspike Point. The North Head lava section (Figure 5.17, section A-B) consists of about 200 m of ocean-floor weathered lavas faulted against lower greenschist metabasalts on the isthmus, which in turn, to the southwest are faulted against dyke swarm rocks. The zeolite facies metabasalts are missing in this section, possibly having been faulted out.

Lavas between Pyramid Peak and Cape Toucher, to the southwest, appear structurally concordant (Figure 5.17, section C-D) and range from zeolite facies assemblages to lower greenschist facies assemblages in the Cape Toucher area. The presence of fresh glasses and the ocean-floor weathered basalts sporadically in the Pyramid Peak area indicate

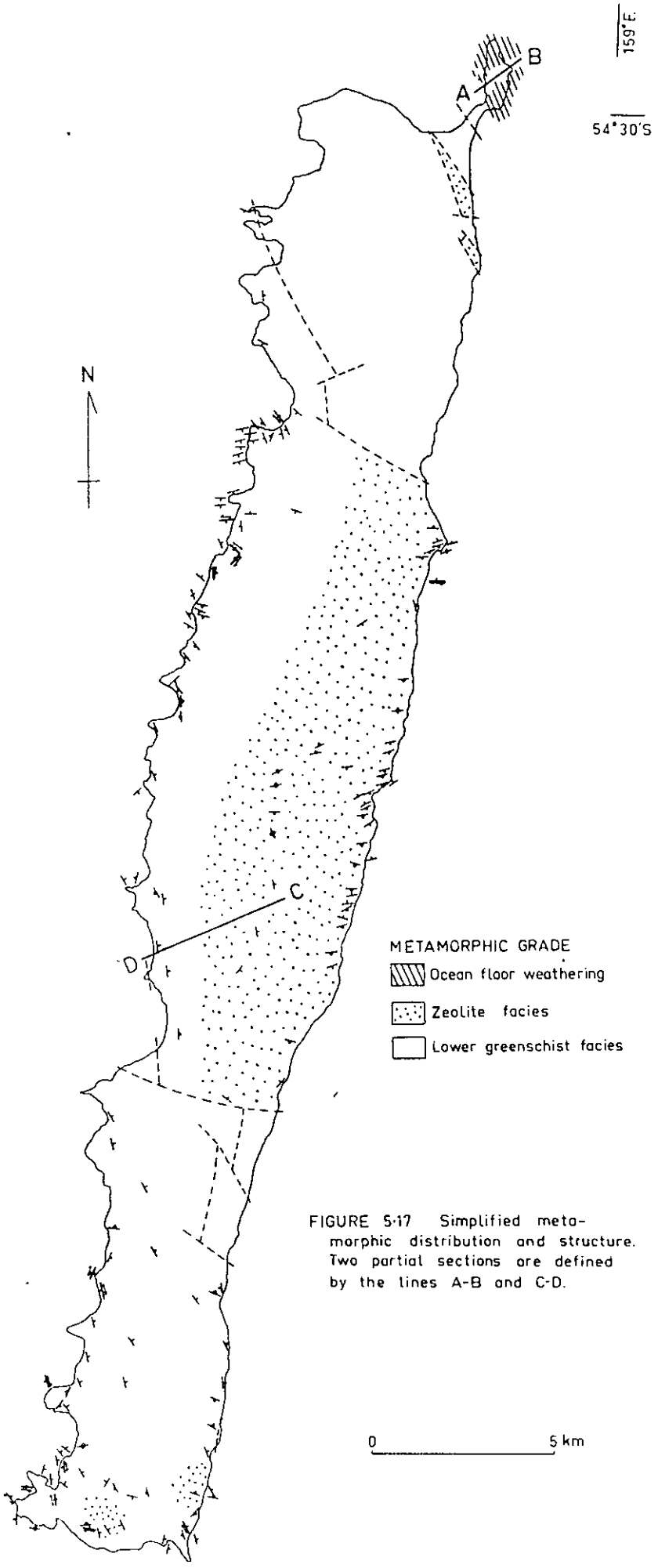

FIGURE 5·17 Simplified metamorphic distribution and structure. Two partial sections are defined by the lines A-B and C-D.

that these rocks may have been near to the upper limit of the zeolite facies metamorphism. Also dykes become very abundant in the Cape Toucher lavas, a feature suggesting these rocks are near the base of the volcanic section. Assuming then that this is an accurate section, a thickness of about 1400 m is suggested for the volcanic section from the top of the zeolite facies zone to the base. In conjunction this gives an estimate of about 1.6 km for the volcanic section and thus a geothermal gradient of about 200°C/km, at the time of metamorphism. These values are comparable to those from other ophiolites (Coleman, 1977).

5.8 A SUMMARY OF OCEAN-FLOOR METAMORPHISM EXPOSED AT MACQUARIE ISLAND

The various secondary assemblages present in the volcanic and dyke swarm sequences on Macquarie Island form a series which is essentially temperature dependent. These assemblages formed under hydrothermal conditions and span a range from very low temperature ocean-floor weathering (0-20°C), through zeolite facies (20-220°C), lower greenschist (220-320°C), upper greenschist and finally lower amphibolite facies (~450°C) grades of metamorphism. Pressure effects are small with the highest pressures at the base of the dyke swarms being up to 1.5 kb.

The assemblages representing the various grades of metamorphism are widely distributed and this regional nature demonstrates the regularity of the ocean-floor metamorphic process. The temperatures indicated by the assemblages define a geothermal gradient of about 200°C/km, a value in agreement with similar studies (Smewing, 1975). The major heat source for this gradient is the area of magma intrusion at the ridge axis but estimates of hydration reaction heat production here and from other studies show that the metamorphic process may, through this mechanism, be able to maintain itself further from the ridge axis than is evident from basic heat loss studies.

The major source of hydrothermal fluid is sea water. This is proved by the sheer volume of secondary hydrous phases present in the rocks, far in excess of any reasonable estimates of magmatic water exsolved from cooling liquids. As discussed, however, magmatic fluids may form some component of the hydrothermal fluid but this will only be small. Other studies have shown the saline nature of fluid phases present in other examples of ocean-floor metamorphism (Spooner & Bray, 1977) in support of this origin. The isotopic studies on secondary phases from the Macquarie Island samples, with the exception of sub-zeolite grade samples, do not give reasonable temperatures for the phases analyzed. This results from the calculations being based in the assumption that the fluid had pristine sea water isotopic values. It is suggested that the isotopic composition of the sea water evolves as it moves through the rocks.

A major feature of the alteration process in all grades is the local variation in the intensity of alteration. It is notable that the intensity of alteration increases and becomes more uniform as the grade of metamorphism increases, reflecting faster reaction rates at the higher temperatures. This intensity variation is obviously another important factor in isotopic equilibration of the secondary phases and the fluid. In cases where only minimal proportions of the rock have been altered it is most unlikely for an "infinite reservoir" system to have existed, resulting in major modification of the fluid isotopic composition.

The pattern of fluid migration in the sequence appears to be variable. The contrast between groundmass alteration and amygdule and vein assemblages is striking at all levels, with local compositional controls being very pronounced away from veins and amygdules. The vein and amygdule assemblages are uniform within the various grades of

alteration, demonstrating a mixing or circulation of the hydrothermal fluids. Thus two levels of fluid activity are recognized, the first on a local scale permeating the samples through the groundmass, and the second a more vigorous activity through amygdules and along veins. This latter activity generates the scatter obtained for the more soluble elements, e.g. K, Rb, and provides a mechanism for enhancing the fluid in base metals, i.e. Cu, Pb, Zn.

5.9 FLUID CONVECTION AND SULPHIDE MINERALIZATION

The occurrence of major sulphate deposits at Nuggets Point, at or near the top of the dyke swarm zone, is extremely interesting. The marked decrease in solubility of $CaSO_4$ with increasing temperature (Blount & Dickson, 1969) has been used to suggest that $CaSO_4$ will precipitate from down-moving fluid. This is demonstrated by the sudden appearance of anhydrite at a depth of 500 metres and a temperature of 200°C in the Reykjanes hydrothermal system (Tomasson & Kristmannsdottir, 1972). On Macquarie Island the sulphate is located at greater depths and with assemblages corresponding to a temperature of $\simeq$300°C. Although the increased pressure ($\simeq$ 1 kb) does increase the sulphate solubility (from 0.005 to 0.016 M/litre H_2O for a 1M NaCl solution at 200°C, Blount & Dickson, 1969) this is not sufficient to explain the temperature difference. The most reasonable model in view of this is that initial temperatures at the top of the dyke swarms were around 200°C and that the heat produced from the hydration reactions (Section 5.5) created an upsurge in fluid temperature and hence sulphate precipitation. This will change the fluid from a slightly alkaline, Na-Mg-SO_4-Cl variety to a reduced, more acid, dominantly Na-Ca-Cl brine (Andrews & Fyfe, 1976).

The sulphide deposits occur mainly within pillow lavas (Section 5.5) and thus are stratigraphically above the Nuggets Point sulphate. As it is necessary to remove the sulphate from solution for sulphides to be precipitated, it may be that these sulphide deposits are formed from cooling solutions moving up through the sequence. The dominance of quartz as the major silicate associated with the sulphides supports this hypothesis as it has not been observed in the other assemblages and the reactions involved in the alteration of the dykes release silica to the fluid.

The gypsum deposits at or near the top of the dyke swarm represent a temperature-induced precipitation from downward moving fluids. Heating from hydration reactions during alteration of the dykes may have prompted this precipitation. The subsequent Cl^- dominated brines are enriched in metals and Si by reaction with the dykes and produce the stockwork sulphide-quartz assemblages present in the volcanic sequence as they move upwards into lower temperature regimes. The dominance of pyrite reflects the inability of the down-going sulphate-rich fluid to carry significant concentrations of the metals at the low te-perature conditions. The upwelling fluids will move along fracture systems where possible causing more intense alteration along the zones. Post-sulphide deposition, these fluids continue up through the sequence producing the anomalously high temperature assemblages, e.g. wairakite patches in zeolite facies assemblages, that occur amongst the Macquarie Island samples. A schematic representation of the alteration process is given in Figure 5.18.

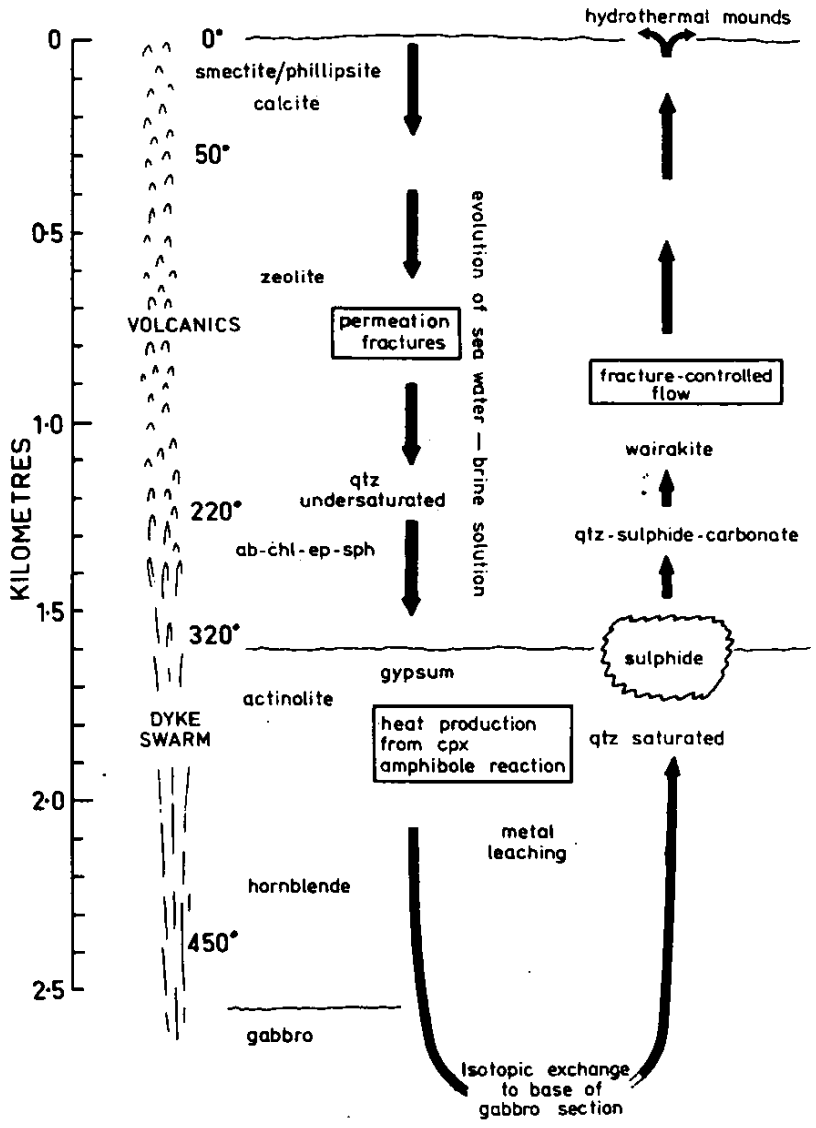

Figure 5.18 Schematic of ocean-floor metamorphism.

Many of the grassland slopes contain small terraces or terracettes (plate 1b). These are commonly misnamed "sheep tracks" throughout rural mainland Australia and on Macquarie Island some workers have similarly misinterpreted these features as due to rabbit tracks or squats. Actually these features are usually a result of creep processes, solifluction and or occasionally small scale slumping.

Wind is another erosive agent on Macquarie Island; during the three month 1975/6 summer the average wind speed was 26 km per hour. However because of the moist surface environment wind deflation effects are drastically reduced relative to those in drier environments. Moist clay has strong interparticle adhesion so that only during the rare dry periods if ever, are the clays deflated. Coarser material is more susceptible and fossil aeolian dunes deposited along the natural wind 'funnel' between Sandy Bay on the east coast and Bauer Bay on the west coast are being eroded through wind deflation. Observations suggest that this was initiated by rabbits burrowing on the windward side of the dunes. Erosion of raised marine ridges on the coastal terraces is probably also a result of similar rabbit activity. These areas are very small relative to the whole island and insignificant in terms of the overall erosion processes.

It has also been suggested that rabbits have increased the incidence of landslips by weakening an area through burrowing. No evidence has been presented on this and a visual comparison of the island today with photographs taken at about the time of introduction of rabbits would suggest that the rate of occurrence has not significantly altered. Furthermore areas of burrowing petrel colonies, which have a higher burrow density than rabbits, are not obviously more eroded than adjacent areas.

In summary, the major processes active on Macquarie Island are various forms of mass movement. Although rabbits may have severe botanical effects on the ecology, they have had little effect on the erosion of Macquarie Island. It is invalid to compare Macquarie Island with mainland Australia because of the major climatic differences and such comparisons are misleading.

ACKNOWLEDGEMENTS

Many people have provided fruitful discussion and advice on this topic, in particular Mr. G. Copson, Dr. E. Colhoun and Dr. J. Jenkins. Mr. G. Copson is thanked for supplying the photographs. The National Parks and Wildlife Service of Tasmania, the Australian Antarctic Division and the University of Tasmania have provided logistic support and funding for two visits to the island and this is gratefully acknowledged.

REFERENCES

Colhoun, E.A., and Goede, A., 1973: Fossil Penguin Bones, ^{14}C Dates and the raised marine terraces of Macquarie Island: some comments. *Search*, 4(11): 499-501.

_____, 1974: A reconnaissance survey of the glaciation of Macquarie Island. *Pap. Proc. R. Soc. Tasm.*, 108: 1-19.

Costin, A.B., and Moore, D.M., 1960: The effects of rabbit grazing on the grasslands of Macquarie Island. *J. Ecol.*, 48: 729-732.

Cumpston, J.S., 1968: Macquarie Island. ANARE *Scientific Reports, Series A*, 93.

Mawson, D., 1943: Macquarie Island: its geography and geology. *Australasian Antarctic expedition 1911-1914 Scientific Reports, Series A*, 5.

Taylor, B.W., 1955: The flora, vegetation and soils of Macquarie Island. *Australian National Antarctic Research Expedition Reports, Series B.*, 11.

Varne, R., and Rubenach, M.S., 1972: Geology of Macquarie Island and its relationship to oceanic crust. *Amer. Geophys. Union, Antarctic Research Series*, 19: 251.